Probabilistic solution of differential equations for Bayesian uncertainty quantification and inference

by

Oksana A. Chkrebtii

M.Sc., Carleton University, 2008

B.Math. (Hons.), Carleton University, 2006

A Thesis submitted in partial fulfillment
of the requirements for the degree of

Doctor of Philosophy

in the
Department of Statistics & Actuarial Science
Faculty of Science

SIMON FRASER UNIVERSITY
Fall 2013

APPROVAL

Name: Oksana A. Chkrebtii

Degree: Doctor of Philosophy

Title of Thesis: Probabilistic solution of differential equations for Bayesian uncertainty quantification and inference

Examining Committee:

Dr. Tim Swartz, Professor
Chair

Dr. David Campbell, Associate Professor
Senior Supervisor

Dr. Derek Bingham, Professor
Supervisor

Dr. Richard Lockhart, Professor
Internal Examiner

Dr. Michael Dowd, Associate Professor
External Examiner, Dalhousie University

Date Approved: December 9th, 2013

Partial Copyright Licence

Abstract

In many areas of applied science the time and space evolution of variables can be naturally described by differential equation models, which define states implicitly as functions of their own rates of change. Inference for differential equation models requires an explicit representation of the states (the solution), which is typically not known in closed form, but can be approximated by a variety of discretization-based numerical methods. However, numerical error analysis is not well-suited for describing functional discretization error in a way that can be propagated through the inverse problem, and is consequently ignored in practice. Because its impact can be substantial, characterizing the effect of discretization uncertainty propagation on inference has been an important open problem.

We develop a probability model for the systematic uncertainty introduced by a finite-dimensional representation of the infinite-dimensional solution of ordinary and partial differential equation problems. The result is a probability distribution over the space of possible state trajectories, describing our belief about the unknown solution given information generated from the model over a discrete grid. Our probabilistic approach provides a useful alternative to deterministic numerical integration techniques in cases when models are chaotic, ill-conditioned, or contain unmodelled functional variability. Based on these results, we develop a fully probabilistic Bayesian approach for the statistical inverse problem of inference and prediction for intractable differential equation models from data, which characterizes and propagates discretization uncertainty in the estimation. Our approach is demonstrated on a number of challenging forward and inverse problems.

To my family and friends, near and far.

"But I have swam through libraries and sailed through oceans..."

—Herman Melville, Moby-Dick, 1851

Acknowledgments

I would like to thank all the people who made this work possible and made my years at Simon Fraser University so wonderful. Many thanks to collaborators Mark Girolami and Ben Calderhead, and also to all the researchers who offered valuable comments and suggestions to the unbelievably many iterations of our paper. Also thank you to Erin Cameron for taking my mind away from differential equations with research on the introduction and spread of invasive earthworms. I am grateful to the Bamfield Marine Sciences Centre for offering the course Models in Ecology with the help of Dr. Mark Lewis, Dr. Marty Krkosek, and Stephanie Peacock, where I met some really great people. I would like to thank very much the Pacific Institute for Mathematical Sciences International Graduate Training Centre in Mathematical Biology for opportunities to connect with many researchers and for organizing some very fun summits in Naramata and Banff. And finally, I gratefully acknowledge the Natural Sciences and Engineering Research Council of Canada whose funding allowed me to spend most of my time learning, asking questions, and exploring my interests.

To all the staff and faculty at the Department of Statistics & Actuarial Science at Simon Fraser University, I want to say thank you for providing the best atmosphere to grow both personally and professionally. I am also grateful to all the people at the School of Mathematics and Statistics at Carleton University, and especially to Dr. Natalia Stepanova for the invaluable guidance and supervision during my undergraduate and M.Sc. studies, and for providing a strong foundation for my research. The office(s) would not have been the same without many amazing officemates. A special mention for making my PhD studies so much fun go to Ryan Lekivetz, Shirin Golchi, Audrey Béliveau, Ruth Joy, Andrew Henrey, Jinny Lim, Zheng Sun, Ararat Harutyunyan, and Krystal Guo, who shared not just the offices, but a passion for unreasonable running on Burnaby Mountain, nights out at the Orpheum, dinner parties, pub nights, hiking adventures, and trips all around Canada. There

are also a group of people without whom this experience would not have been complete: they are my friends, who have become my second family and have stuck with me throughout my years away from home. Thank you to Katrina Rogers-Stewart, Matt Lemire, Phil Munz, Marjolaine Jerry, and Dale Powell, for your friendship.

Most importantly, I want to thank Dave Campbell for being such a great supervisor: for teaching me to understand the subtleties of Bayesian statistics and for being patient when I didn't or when I managed to crash his office computer from a remote research station on Vancouver Island (long story, also involving invasive earthworms); for sending me on many very interesting conferences; and for a summer of research in London, Eindhoven, and Paris, which I will never forget.

To my family: Mom, Dad, Anna, François, I want to say how much your love and support has meant to me throughout these years. Thank you for listening to my whining when my research wasn't going as it should, for the wonderful vacations, for the visits and parties, and by considering my need to run code remotely in choosing resorts with Wi-Fi connection on the beach.

Contents

List of Figures

List of Symbols and Notation

Spaces

$(\Omega, \mathcal{A}, \mu)$	probability triple with sample space Ω, σ-algebra $\mathcal{A}$, and probability measure μ
H	Hilbert space
H^*	dual space of linear functionals of H
$L^2\big(\mathscr{D}\big)$	space of square integrable functions on the domain $\mathscr{D}$
$L^2\big(\mathscr{D}; (\Omega, \mathcal{A}, \mu)\big)$	space of square integrable random functions defined on the domain $\mathscr{D}$ and the probability space $(\Omega, \mathcal{A}, \mu)$
$C^m\big(\mathscr{D}\big)$	space of m-times continuously differentiable functions on the domain $\mathscr{D}$
$M^{r,c}\big(\mathbb{R}\big)$	$r \times c$ matrix space over the real numbers
$M^n\big(\mathbb{R}\big)$	$n \times n$ matrix space over the real numbers

Norms, Vector Products

$\langle \cdot, \cdot \rangle$	vector product
$\|\| \cdot \|\|$	vector norm
$\| \cdot \|$	Euclidian norm

Operators

$\oplus$	direct sum
$\otimes$	tensor product
$\circ$	composition of functions
$\dot{u}$	derivative of u with respect to t
D^{α}	differential operator with multi-index $\|\alpha\| = \alpha_0, \ldots, \alpha_q$
Δ	Laplacian operator
∇	gradient operator
$(\nabla \cdot)$	divergence operator

Other symbols

$\mathcal{B}(\Omega)$	Borel σ-algebra of subsets of Ω
$\mathcal{P}(S)$	power set of the set S
$f = o(g)$	"small oh" notation, $f(x)/g(x) \to 0$ as $x \to a$
$f = O(g)$	"big oh" notation, $\exists C > 0 : \lvert f(x)/g(x) \rvert < C$ as $x \to a$
$\delta_u(\cdot)$	Dirac delta function centered at u
$\lceil q \rceil$	ceiling function: one plus the smallest integer part of q
$\mathcal{N}(m, \mathcal{C})$	Gaussian measure on an infinite-dimensional space with mean function m and covariance operator $\mathcal{C}$
$\mathcal{N}_n(\mathsf{m}, \Lambda)$	Gaussian measure on an n-dimensional space with mean vector m and covariance matrix Λ

Preface

Much of the work presented in this thesis has been summarized in the manuscript *Bayesian Uncertainty Quantification for Differential Equations*, jointly written with David A. Campbell, Mark A. Girolami, and Ben Calderhead. The preprint is available from arXiv at http://arxiv.org/abs/1306.2365. This thesis also contains a variety of unpublished results, extensions, and implementation details that should be of interest to practitioners or those wishing to study this methodology in greater detail.

Complete code for replicating all results presented in this thesis can be downloaded from http://people.stat.sfu.ca/∼ochkrebt/PODES.html.

Chapter 1

Introduction

Variables of interest in many physical, chemical, and biological systems evolve over time and space in a way that is intrinsically linked to their rates of change. Consider, for example, the concentration of a reagent, such as a toxic compound in the liver, metabolized by reacting with enzymes into a product. On a molecular level, the rate at which the toxic substance and the enzymes come into contact depends on their relative concentrations. That is, the instantaneous rate of change of the concentration is a function of the current concentration in the system. Another example might be the velocity of an object, such as a meteorite or re-entering spacecraft, falling in the atmosphere, whose velocity over time is related to its rate of change, or acceleration.

Differential equations (DEs) provide a convenient modelling framework for describing the natural dependence of variables on their derivatives. Such models are widely used in the physical, biological, and social sciences. Frequently, quantities parameterizing DE models are unknown and interest lies in estimating them from measurement data.

Statistical inference for differential equations is made challenging by the fact that the variables of interest, or *system states*, are implicitly defined in terms of their derivatives, while the data is typically only directly measured on the states. In our metabolism example, one can only measure concentrations of each compound, and not their rates of change. Similarly, while acceleration in our physics example can be computed indirectly from the velocity, we can directly only measure the displacement of a falling object.

Therefore, statistical inference about a DE model requires obtaining its equivalent representation in terms of the states alone, also known as the *solution* of the DE. However,

solutions in closed form are typically only available for relatively simple systems, requiring modellers to frequently rely on numerical approximations. Pointwise error bounds on numerical solutions are not well-suited for a probabilistic analysis so that, in practice, discretization error is ignored for the purposes of inference.

1.0.1 Inference for differential equation models

Consider the problem of inferring unknown parameters $\boldsymbol{\theta} \in \Theta$, defining a nonlinear DE model with unknown closed-form solution $\mathbf{u}(t, \boldsymbol{\theta})$, $t \in \mathscr{D}$, from discretely observed data $\mathbf{y}(\mathbf{t})$, $\mathbf{t} \in \mathscr{D}^T$. The likelihood function $\mathcal{L}_{\mathbf{y}(\mathbf{t})}\big(\mathbf{u}(\mathbf{t}, \boldsymbol{\theta})\big)$ provides a measure of distance between the data and the model under a given parameter value. As this likelihood depends on the unknown DE solution, the conventional inference approach substitutes the solution with its N-dimensional numerical approximation $\mathbf{u}^N(\mathbf{t}, \boldsymbol{\theta})$. Inference then proceeds based on the approximation,

$$\mathcal{L}_{\mathbf{y}(\mathbf{t})}\big(\mathbf{u}(\mathbf{t}, \boldsymbol{\theta})\big) \;\approx\; \mathcal{L}_{\mathbf{y}(\mathbf{t})}\big(\mathbf{u}^N(\mathbf{t}, \boldsymbol{\theta})\big).$$

As will be illustrated in this thesis, there are many cases in which the mismatch between the true DE solution and its discrete approximation $\mathbf{u}^N(\mathbf{t}, \boldsymbol{\theta})$ has a well-defined, non-negligible structure, leading to serious inferential bias under the conventional inferential approach. However, this approach remains popular for a number of possible reasons.

1. *A satisfactory probability model of discretization uncertainty has been unavailable.* Numerical error analysis is a well-established field studying the accuracy of numerical techniques (see, for example, Butcher, 2008). However, because error estimates are typically computed pointwise, they are not well-suited for quantifying functional uncertainty in the solution. Moreover, it is unclear how classical numerical error analysis can be considered and propagated forward through the inference methodology to characterize model uncertainty.

2. *Incorrect interpretation of a probabilistic uncertainty model.* A probabilistic description of the discretization unvertainty for an unknown DE solution represents our knowledge about the states given a finite-dimensional discretization grid by a distribution over the space of possible trajectories. This can incorrectly be interpreted as a stochastic model for the deterministic solution itself, which would then be inconsistent

with the theory of deterministic differential equations.

3. *Convenience.* Many statistical procedures rely on approximations. When the approximation error is believed to be negligible and not systematic, it may be difficult to justify adding an additional layer of uncertainty to an already challenging analysis.

The present work develops a probabilistic formalism for describing model uncertainty resulting from discretization of an unknown DE solution, and naturally incorporates the associated functional variability into a fully probabilistic inferential framework. We show that such a probability model can characterize solution uncertainty in a consistent way, and allows us to distinguish discretization uncertainty from other sources of variability. We develop efficient Monte Carlo methods to generate approximate samples from posterior distributions defined by introducing the additional layer of uncertainty associated with model error in the solution.

1.1 Numerical methods and the role of probability

Solving differential equations, either exactly or approximately, is a critical tool for modelling in the natural, applied, and social sciences. Despite the availability of pointwise error bounds for many numerical methods, these are typically assumed negligible for convenience when doing statistical inference. This approach is not limited to differential equation models. Indeed, numerical approximations are commonly used in statistical procedures (see, for example, Lange, 1999), and the associated numerical error is frequently ignored. But should such approximations be considered from a statistical perspective, or should they remain firmly in the area of numerical analysis?

1.1.1 History of probability in numerical analysis

The earliest explicit use of probability to address a numerical problem, pointed out in Diaconis (1988), was due to Poincaré (1896). Poincaré considered the problem of polynomial interpolation of a finite number of function evaluations $\mathbf{g} = [g(t_1), \ldots, g(t_N)]$ based on a power series expansion. Uncertainty about the coefficients of the expansion was modelled through zero-mean Gaussian priors, updated given the function evaluations $\mathbf{g}$. Uncertainty in the coefficients thus induces a distribution over the space of polynomials. This approach

predated Gaussian process (GP) regression, but provided an equivalent estimate of the posterior distribution under a specific covariance specification (e.g., Rasmussen and Williams, 2006).

With advances in computational power and sampling methodology, the Bayesian approach to function estimation became more generally feasible. This led a number of researchers to consider problems of numerical analysis from the point of view of probability theory. O'Hagan (1992) proposed a Gaussian process based approach to contour estimation and function interpolation, and consequently quadrature in low-dimensions exploiting the integrability of GPs. In the last several decades, the Markov chain Monte Carlo (MCMC) approach (Hastings, 1970; Metropolis and Ulam, 1949) has become a standard way to estimate integrals, even in high-dimensional problems when numerical quadrature alone is infeasible. This feature is very useful because many problems reduce to complex integration. For example, Doucet et al. (2010) show how to use two types of Monte Carlo methods to approximate the solution to a class of integral equations. Fredholm equations of the second kind are restated as high-dimensional integrals via their Von Neumann representation and estimated from a sample obtained via sequential or reversible-jump Monte Carlo sampling.

Models defined by differential equations are very flexible and simple to formulate but often difficult to solve. The challenge, as will be illustrated in this thesis, is that the implicit dependence between states and their derivatives is typically nonlinear so that the solution does not reduce to a simple quadrature problem. A very interesting, although not well-known suggestion in Skilling (1991) considered the question of solving ordinary differential equation initial value problems by modelling solutions and their derivatives as convolutions of an underlying latent process that could then be integrated or differentiated as required. The difference with the problem studied by O'Hagan (1992) is that function evaluations must be made sequentially from the updated model because of the implicit dependence of the states on their derivatives.

1.2 Contribution and organization of this thesis

This thesis develops the ideas proposed by Skilling (1991) into a fully usable and widely applicable framework for solving general classes of analytically intractable ordinary and partial differential equation problems. We formalize the model and show that these ideas

can be made computationally feasible, proposing sequential sampling methodologies that capture fast-changing, or even chaotic, dynamics. For these methods, convergence results are obtained under relatively mild conditions. Additionally, we investigate methodologies to make probabilistic solutions more efficient, through the development of recursive algorithm formulations and statistical step size selection techniques.

Using this probabilistic perspective on the forward problem, we then incorporate the model uncertainty into a fully probabilistic inferential framework. We design Monte Carlo algorithms capable of generating samples from posterior distributions for unknown model parameters and state functions, taking into account the additional hierarchical layer introduced by model uncertainty. Our contribution allows us to characterize and separate model uncertainty from other sources of error.

The thesis is organized as follows. Chapter 2 provides a basic review of ordinary and partial differential equations (ODEs and PDEs), defining a number of ODE and PDE problems that often arise in practical applications. We also discuss the types of numerical techniques available to provide approximate solutions to these problems, and point out cases where they fail to reasonably approximate the solution due to model error. Chapter 3 formalizes the Bayesian uncertainty model for unknown univariate ODE solutions, and further extends this framework to multivariate PDE solutions. The stochastic process model for the uncertainty in the system states, which we call the *probabilistic solution*, given a number of model-based derivative evaluations is shown to have a well-defined density with respect to the prior measure under some conditions. Then, Chapter 4 develops sequential sampling strategies that allow us to generate derivative evaluations in a self-consistent model-based way to build up a picture of the implicitly defined DE solution. Furthermore, this chapter provides techniques and algorithms for sampling functional realizations of the probabilistic solution. Next, Chapter 5 considers the statistical inverse problem of estimating model parameters and states from measurement data. We develop a Monte Carlo sampling methodology to obtain realizations of the posterior distribution of the states and the unknown solution. Chapter 6 describes three important kernel functions, two of which were specifically designed to model DE solutions with certain properties. We also compute analytically the pairwise convolutions between each kernel and its integrated version, required for the computational implementation of our probabilistic algorithm. Finally, Chapter 7 discusses adaptive sequential design for discretizing the domain of integration by optimizing an information theoretic criterion.

Chapter 2

Background on Differential Equation Models and Their Solutions

Differential equations are a class of models that describe the relationship, common in nature, between system states and their rates of change with respect to one or several, usually spatio-temporal, variables. In addition to describing the evolution of state variables over time or space, differential equation models also provide some basic constraints on the states, to ensure that a finite number of solutions can exist, and to incorporate any additional information into the model that is known about a particular system.

The versatility of differential equation models, and the variety of dynamics they describe, is best reviewed by examining a number of model types. Therefore, this chapter briefly introduces some commonly used ordinary and partial differential equation (ODE and PDE) problems, and provides examples of their use in modelling real-world phenomena.

The flexibility and intuitive appeal of differential equation models usually comes at a price, stemming from the difficulty in obtaining an explicit representation of the states, or *solution*, that is independent of the derivatives. This chapter gives a broad description of numerical techniques for obtaining approximate solutions given model parameters for each of the ODE and PDE problems presented. We also point out situations in which numerical approximations may give a misleading representation of the true solution.

Throughout this thesis we use examples of differential equation problems which illustrate the systematic nature of discretization error, and showcase the probabilistic posterior solution developed in this work. These models and their interpretation, as well as relevant references, are provided in this section. We shall refer to the task of solving these systems, given any parameters or inputs, as the *forward problem*, which will then be applied in Chapter 5 to the *inverse problem* of inferring unknown parameters from data.

2.1 Ordinary differential equation models

Ordinary differential equations (ODEs) describe the relationship between the *states* (or *dependent variables*), $\mathbf{u}(\,\cdot\,, \boldsymbol{\theta}) : [a, b] \to \mathbb{R}^P$, and their derivatives, $\dot{\mathbf{u}}(\,\cdot\,, \boldsymbol{\theta}) : [a, b] \to \mathbb{R}^P$, with respect to a single indexing variable (or *independent variable*), $t \in [a, b] \subset \mathbb{R}$, which we shall call "time" for convenience. We refer to P as the *dimension* of the system. The *order* of the system refers to the highest-order derivative in the expression. Nevertheless, ODEs of order greater than one can be reformulated by defining derivatives as additional states. Therefore, without loss of generality, we shall consider first order ODE systems, written in the *explicit* form:

$$\dot{\mathbf{u}}(t, \boldsymbol{\theta}) = f_{\boldsymbol{\theta}}\big(t, \mathbf{u}(t, \boldsymbol{\theta})\big), \quad t \in [a, b],$$

where the *vector field* function, $f_{\boldsymbol{\theta}} : [a, b] \times \mathbb{R}^P \to \mathbb{R}^P$, is fully specified given the *inputs* (or *model parameters*), $\boldsymbol{\theta} \in \Theta$. The space containing all possible state trajectories is called the *phase space*.

For the purposes of modelling real systems, and in order to obtain a finite number of solutions satisfying the system dynamics, some constraints on the states or derivatives must be imposed. Broadly speaking, the type of constraints and their relationship to the model define different classes of ODE problems discussed below.

2.1.1 Initial value problems

Initial value problems (IVPs) are well suited for describing systems that begin at known initial conditions and evolve according to the dynamics described by the ODE model. Many problems in the natural sciences are formulated as IVPs, such as the trajectory of a single object orbiting a large stationary body; the movement of a simple pendulum; atmospheric

convection; chemical kinetics; and the interaction of animal populations in a predator-prey system.

Definition 1. *A P-dimensional, first-order initial value problem (IVP) in explicit form is given by:*

$$\begin{cases} \dot{\mathbf{u}}(t, \boldsymbol{\theta}) &= f_{\boldsymbol{\theta}}\big(t, \mathbf{u}(t, \boldsymbol{\theta})\big), \qquad t \in [a, b], \\ \mathbf{u}(a, \boldsymbol{\theta}) &= \mathbf{u}_a, \end{cases} \tag{2.1}$$

on the interval $[a, b]$, where $\mathbf{u}(\,\cdot\,, \boldsymbol{\theta}) : [a, b] \to \mathbb{R}^P$, and $f_{\boldsymbol{\theta}} : [a, b] \times \mathbb{R}^P \to \mathbb{R}^P$.

A unique solution for this system exists under a relatively mild assumption on the vector field, known as the *Lipschitz condition.*

Definition 2. *Let $|\cdot|$ denote the Euclidian vector norm. A function $f : [a, b] \times \mathbb{R}^P \to \mathbb{R}^P$ is Lipschitz continuous with respect to the second variable if there exists a constant $L < \infty$ such that, for any $t \in [a, b]$ and $\mathbf{u}, \mathbf{v} \in \mathbb{R}^P$, the inequality:*

$$|f\,(t, \mathbf{u}) - f\,(t, \mathbf{v})\,| \leq L|\mathbf{u} - \mathbf{v}|,$$

holds.

Roughly, this condition ensures that small deviations between trajectories do not propagate into disproportionately large differences in their respective vector field evaluations. This allows the use of a result known as the contraction mapping lemma on metric spaces (e.g. Butcher, 2008, p. 22) to show that a unique solution satisfying (2.1) exists. We refer the reader to Butcher (2008, p.23) for the proof of the following well-known result.

Theorem 2.1.1. *If $f_{\boldsymbol{\theta}} : [a, b] \times \mathbb{R}^P \to \mathbb{R}^P$ is Lipschitz continuous in the second argument, then there exists a unique solution, $\mathbf{u}(\cdot, \boldsymbol{\theta}) : [a, b] \to \mathbb{R}^P$, satisfying the initial value problem (2.1).*

Although a unique solution for (2.1) exists under this relatively mild condition, it is typically not available in closed form. In such cases, modellers rely on *numerical integration* (or *numerical solution*) techniques to provide an approximation to the ODE solution, based on discretizing the time domain by an ordered partition $\mathbf{s} = [s_1, \cdots, s_N] \in [a, b]^N$, where

each point s_n is called a *knot*. Many widely-used numerical methods are variants of the approximation obtained by replacing the integrals in the equations:

$$\begin{cases} \mathbf{u}(s_{n+1}, \boldsymbol{\theta}) &= \mathbf{u}(s_{n+1-k}, \boldsymbol{\theta}) + \int_{s_{n+1-k}}^{s_{n+1}} f_{\boldsymbol{\theta}}\big(t, \mathbf{u}(t, \boldsymbol{\theta})\big) \mathrm{d}t, \quad k-1 \leq n \leq N, \\ \mathbf{u}(s_1, \boldsymbol{\theta}) &= \mathbf{u}_a, \end{cases} \tag{2.2}$$

with a quadrature rule defined by *quadrature weights*, $\{w_j\}_{j=1}^J$, intermediate *quadrature nodes*, $t_j \in [s_{n-k+1}, s_{n+1}], 1 \leq j \leq J$, and *step number*, k. The result is a set of nonlinear algebraic equations:

$$\begin{cases} \mathbf{u}(s_{n+1}, \boldsymbol{\theta}) &= \mathbf{u}(s_{n+1-k}, \boldsymbol{\theta}) + \sum_{j=1}^J w_j \, f_{\boldsymbol{\theta}}\big(t_j, \mathbf{u}(t_j, \boldsymbol{\theta})\big), \quad k-1 \leq n \leq N, \\ \mathbf{u}(s_1, \boldsymbol{\theta}) &= \mathbf{u}_a. \end{cases} \tag{2.3}$$

The difficulty in solving system (2.3) lies in the implicit dependence of the vector field, $f_{\boldsymbol{\theta}}$, on the state, $\mathbf{u}$. For this reason, each subsequent state, $\mathbf{u}(s_{n+1}, \boldsymbol{\theta})$, must either be approximated recursively, or via deterministic nonlinear optimization techniques. By their nature, such numerical solutions, are *deterministic*, in the sense that a numerical solver algorithm, implemented under the same conditions, will always yield the same solution for a given ODE system.

Algorithms defined with $k = 1$ steps have no evaluation points within each interval of integration, $[s_n, s_{n+1}]$, so a temporary approximation for $\mathbf{u}(t)$ is used to evaluate $f_{\boldsymbol{\theta}}$ at the J quadrature nodes within each interval. After the approximation for $\mathbf{u}(s_{n+1}, \boldsymbol{\theta})$ is computed, these temporary values are discarded. Such methods are called one-step quadrature schemes, and include the well-known *Euler* and *Runge-Kutta* algorithms. Multistep methods allow a step number of $k > 1$, so that approximation of $\mathbf{u}(s_{n+1}, \boldsymbol{\theta})$ can be based on evaluations of the vector field, $f_{\boldsymbol{\theta}}$, at k previously computed states, $\mathbf{u}(s_{n-k+1}, \boldsymbol{\theta}), \ldots, \mathbf{u}(s_n, \boldsymbol{\theta})$. Examples of multistep algorithms include the k-step *Adams-Bashforth* and *Adams-Moulton* solvers.

For a given discretization grid, $\mathbf{s}$, the quality of the approximation is related to the choice of quadrature method. Error propagation through the solver occurs largely as a result of replacing the true solution evaluations with approximations, $\tilde{\mathbf{u}}(s_2, \boldsymbol{\theta}), \ldots, \tilde{\mathbf{u}}(s_n, \boldsymbol{\theta})$, and using these to estimate the solution, $\mathbf{u}(s_{n+1}, \boldsymbol{\theta})$, at the subsequent grid point. Although this sequential loss of precision may seem alarming, standard assumptions about the smoothness

of the vector field typically result in an upper bound on such error propagation.

Collocation approaches are based on a solution approximation via truncated basis expansion at each grid knot:

$$\tilde{\mathbf{u}}(s_{n+1}, \boldsymbol{\theta}) = \sum_{j=1}^{J} c_j \, \psi_j(s_{n+1}), \quad 1 \leq n \leq N,$$

with continuously differentiable basis functions, $\psi_j \in \big(C^1\big([a,b]\big)\big)^P$, and unknown coefficients, $c_j \in \mathbb{R}^P$. The coefficients are then obtained by solving the system of N nonlinear algebraic equations:

$$\begin{cases} \sum_{j=1}^{J} c_j \, \dot{\psi}_j(s_{n+1}) &= f_{\boldsymbol{\theta}}\big(s_{n+1}, \tilde{\mathbf{u}}(s_{n+1}, \boldsymbol{\theta})\big), \quad 1 \leq n \leq N, \\ \mathbf{u}(s_1, \boldsymbol{\theta}) &= \mathbf{u}_a, \end{cases}$$

usually, by means of a sequential optimization procedure. When bases have a bounded support on the scale of the discretization size, we have *local collocation schemes*. A well-known *global collocation scheme* (Shu et al., 2003) uses radially symmetric basis functions, $\psi_j(t_k) = \psi_j\big(|t_k - t_j|\big)$. The formalism presented in this thesis has some similarities with collocation methods constructed using a basis system of eigenfunctions of a covariance operator.

Understanding the performance of numerical methods is crucial for practitioners and modellers. This is called *error analysis*, and includes statements about the convergence of a particular method to a true unknown ODE solution under some assumptions, as well as asymptotic rates of convergence. The theorems apply to a sequence of partitions of the range $[a, b]$ into N intervals, $(s_{n-1}, s_n], 2 < n \leq N$. The dependence on N of the knots is supressed in what follows.

Definition 3. *A numerical approximation, $\tilde{\mathbf{u}}_n(t, \boldsymbol{\theta})$, of the true unknown ODE solution, $\mathbf{u}(t, \boldsymbol{\theta})$, is convergent if it satisfies,*

$$\sup_{t \in [a,b]} |\tilde{\mathbf{u}}_n(t, \boldsymbol{\theta}) - \mathbf{u}(t, \boldsymbol{\theta})| \to 0, \quad \textit{as} \max_{n=2,\ldots,N} \big(s_n - s_{n-1}\big) \to 0,$$

where $|\cdot|$ is the Euclidian vector norm.

Proving that this global error tends to zero requires some assumptions about the smoothness of the true solution, typically that it is continuously differentiable on each interval (s_{n-1}, s_n). For linear multistep methods, convergence arguments hold the step number fixed, but consider the step length (related to the size of the discretization grid) in the limit.

Chaotic systems

The deterministic nature and apparent simplicity of many nonlinear dynamical systems can nevertheless lead to unpredictable behaviour in the solution. This phenomenon, known as *deterministic chaos*, lacks a formal definition but has many characteristic features. Chaotic systems have time-evolution trajectories that diverge exponentially fast with time following any small perturbation in the phase space. This feature was first noted in Poincaré (1913, p. 397), who suggested that prediction for such systems appears to be impossible. The detailed study of chaos is a recent undertaking, which became possible with computational advances that allowed for numerical simulation of chaotic systems, starting with the work of Lorenz (1963) on atmospheric convection using an early computer.

When systems of nonlinear differential equations describe chaotic trajectories, numerical solutions inherit their extreme sensitivity to perturbations. Hence, numerical methods produce solutions that can vary immensely with small changes in the discretization grid or in the choice of numerical solver. As a result, the deterministic solution approximation does not capture, even on average, the true long-range behaviour of the system. Crucially, this uncertainty in solving the forward problem leads to challenges for the inverse problem.

Presently, the study of chaos is extremely relevant for modelling a large variety of physical systems, including laser cavities, chemical reactions, fluid motion, crystal growth, weather prediction, earthquake dynamics (Baker and Gollub, 1996, chapter 7). In this thesis, we provide a probabilistic framework for addressing existing issues for such systems. We will provide examples ranging from the canonical Lorenz system to a model of reaction-diffusion dynamics, and the classical Navier-Stokes model of turbulent fluid flow.

Lorenz chaotic system

The Lorenz system (Lorenz, 1963) is a canonical example of a chaotic ODE model of greatly simplified, three-state fluid convection between two moving surfaces of different temperatures. States u, v, and w describe, respectively, the streamflow (a feature of the fluid flow),

the temperature difference between rising and descending currents, and the nonlinearity in the temperature difference between surfaces. The model is formulated as a first-order nonlinear IVP,

$$\begin{cases} \dot{u}(t,\boldsymbol{\theta}) &= -\theta_1\, u(t,\boldsymbol{\theta}) + \theta_1\, v(t,\boldsymbol{\theta}), & t \in [a,b], \\ \dot{v}(t,\boldsymbol{\theta}) &= -\theta_2\, u(t,\boldsymbol{\theta}) - v(t,\boldsymbol{\theta}) - u(t,\boldsymbol{\theta})\, w(t,\boldsymbol{\theta}), & t \in [a,b], \\ \dot{w}(t,\boldsymbol{\theta}) &= u(t,\boldsymbol{\theta})\, v(t,\boldsymbol{\theta}) - \theta_3\, w(t,\boldsymbol{\theta}), & t \in [a,b], \\ (u(a,\boldsymbol{\theta}), v(a,\boldsymbol{\theta}), w(a,\boldsymbol{\theta})) &= (u_a, v_a, w_a), \end{cases} \tag{2.4}$$

with dimensionless parameters, $\boldsymbol{\theta} = (\theta_1, \theta_2, \theta_3) \in \mathbb{R}^3$, that represent fluid properties and the experimental and temperature configuration. We consider the standard choice of parameters $\boldsymbol{\theta} = (10, 8/3, 28)$ in the chaotic regime. In such cases, the flow (state trajectory) becomes restricted around a three-dimensional bounded region called a *strange attractor* (this was shown independently by Afraimovich et al., 1977; Guckenheimer and Williams, 1979; Williams, 1979). Trajectories travel around one of two unstable fixed points, at times traversing the attractor to the other fixed point. Moreover, neighbouring trajectories diverge exponentially fast from one another.

The Lorenz IVP has a unique solution whose trajectory lies on a bounded region of the phase space (e.g., Robinson, 2001, pp. 271-272). However, the solution is not known in closed form and must be approximated numerically. Although numerical solutions are by their nature deterministic, qualitative dynamics of the system are nevertheless studied statistically by introducing artificial perturbations on the numerical solution. For example, the rate of exponential growth (the *Lyapunov exponent*) between nearby trajectories can be estimated statistically using numerical techniques while introducing small changes to the trajectory over a grid defined along the domain.

As with all chaotic systems, numerical methods fail to capture the long-range effect of error propagation on the system dynamics due to the severe amplification of truncation error (e.g., Foias and Temam (2001); Sauer et al. (1997); and, as illustrated in Figure 2.2). Nevertheless, the importance of computing numerical solutions to such systems lies in the, often qualitative, study of the dynamics at larger scales of resolution.

Despite the extreme effects of truncation error, numerical solutions of the Lorenz system

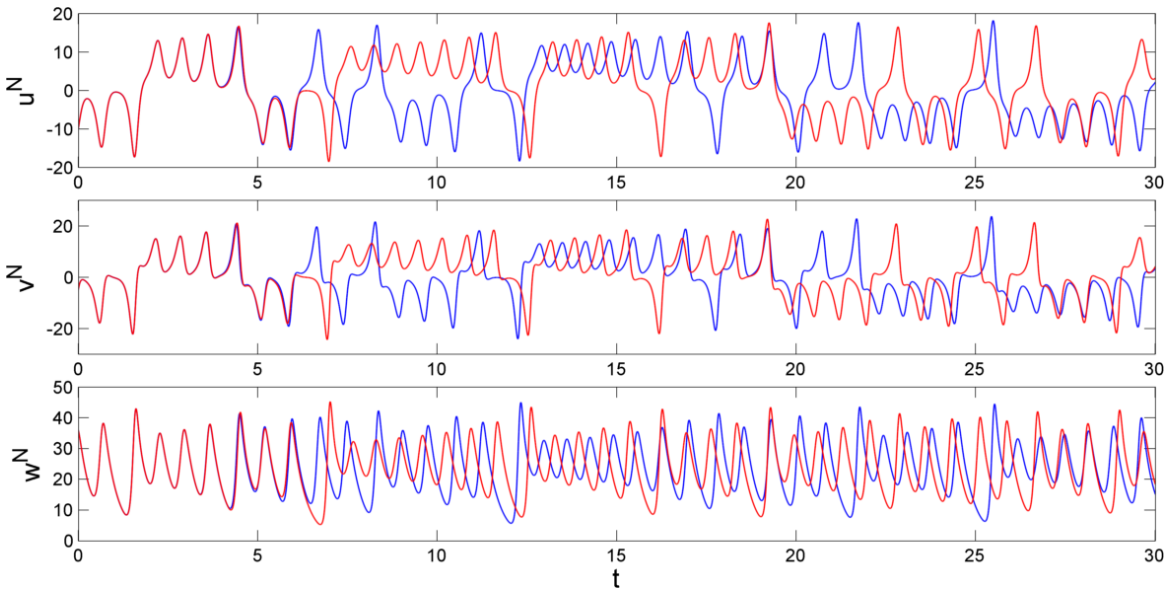

Figure 2.1: *Two numerical solutions to the Lorenz IVP (2.4), for each state in the system (top, middle, bottom rows), computed under almost identical initial conditions. The trajectories correspond to the initial function* $(-10, -5, 36)$ *(red), and the initial function perturbed by adding* 10^{-3} *(blue). Numerical solutions were obtained via the ode45 (MATLAB) numerical solver with an error tolerance of* 10^{-4}.

have played a central role in the mathematical study of deterministic chaos (e.g., Mischaikow and Mrozek, 1995). In particular, the existence of a strange attractor for this system was shown by Tucker (1999) using a computer-assisted proof. Roughly speaking, the proof required constructing a specialized numerical solver for the Lorenz system that would provide exact upper bounds on the numerical error at each solver iteration, particularly within phase space regions where the trajectories are most sensitive to perturbations. However, computation of error bounds for general chaotic systems is still an active area of research (see review in Mrozek and Srzednicki, 2010).

2.1.2 Multi-point boundary value problems

The boundary value problem (BVP) imposes constraints on the states at one or more locations, $\mathbf{c} = [c_1, \cdots, c_D] \in [a, b]^D$, on the time domain. The method of solution for these systems varies depending on the form of the constraints. Here we examine two categories of BVP, depending on whether constraints are specified at the same time locations for some subset of the system states. It is important to note that BVP constraints often have the form

of algebraic equations, which we limit in our exposition to the case where each boundary value is given an explicit value.

Definition 4. *The P-dimensional, first-order, multi-point boundary value problem (MP-BVP) in explicit form is given by:*

$$\begin{cases} \dot{\mathbf{u}}(t, \boldsymbol{\theta}) & = & f_{\boldsymbol{\theta}}\big(t, \mathbf{u}(t, \boldsymbol{\theta})\big), & t \in [a, b] \\ \big(\mathbf{u}^{(\boldsymbol{\alpha})}(c_1, \boldsymbol{\theta}), \ldots, \mathbf{u}^{(\boldsymbol{\alpha})}(c_D, \boldsymbol{\theta})\big) & = & \big(\mathbf{u}_{c_1}^{(\boldsymbol{\alpha})}, \ldots, \mathbf{u}_{c_D}^{(\boldsymbol{\alpha})}\big), & \boldsymbol{\alpha} \in \{1, \ldots, P\} \setminus \emptyset, \end{cases} \tag{2.5}$$

on the interval $[a, b]$, where $\mathbf{u}(\,\cdot\,, \boldsymbol{\theta}) : [a, b] \to \mathbb{R}^P$, and $f_{\boldsymbol{\theta}} : [a, b] \times \mathbb{R}^P \to \mathbb{R}^P$. The notation $\mathbf{u}^{(\boldsymbol{\alpha})}$ represents some non-empty subset of the P states.

Mixed, or separated, boundary value problems do not have all constraints applied at the same set of time points across states.

Definition 5. *The P-dimensional, first-order mixed boundary value problem (MBVP) with two constraints is given in explicit form by:*

$$\begin{cases} \dot{\mathbf{u}}(t, \boldsymbol{\theta}) & = & f_{\boldsymbol{\theta}}\big(t, \mathbf{u}(t, \boldsymbol{\theta})\big), & t \in [a, b], \\ \big(\mathbf{u}^{(\boldsymbol{\alpha}_1)}(a, \boldsymbol{\theta}), \mathbf{u}^{(\boldsymbol{\alpha}_2)}(b, \boldsymbol{\theta})\big) & = & \big(\mathbf{u}_a^{(\boldsymbol{\alpha}_2)}, \mathbf{u}_b^{(\boldsymbol{\alpha}_2)}\big), & \boldsymbol{\alpha}_i \in \{1, \ldots, P\} \setminus \emptyset,\ \boldsymbol{\alpha}_1 \neq \boldsymbol{\alpha}_2, \end{cases} \tag{2.6}$$

on the interval $[a, b]$, where $\mathbf{u}(\,\cdot\,, \boldsymbol{\theta}) : [a, b] \to \mathbb{R}^P$, and $f_{\boldsymbol{\theta}} : [a, b] \times \mathbb{R}^P \to \mathbb{R}^P$.

In contrast to IVPs, which require relatively mild conditions for existence of a unique solution, the multiple constraints imposed by BVPs can result in no solutions or multiple solutions under the same conditions (e.g. Keller, 1968).

Approaches for numerically solving multi-point BVPs fall within two categories: *shooting* (or *initial value*) methods, and the *finite differences* method. Both approaches begin by discretizing the time domain over a finite grid. The finite difference method attempts to solve the fully constrained algebraic equations (2.3) simultaneously. The more popular shooting methods ignore all the constraints in the system except for the known initial states, propose values for the unknown initial states, and solve the resulting IVP numerically. Each proposed initial value is then given a weight corresponding to how well the associated IVP solution satisfies the remaining boundary conditions. The resulting objective function in

the unknown state is then optimized numerically (see, for example Keller, 1968), yielding a single deterministic approximation of the solution, without any indication that additional solutions may exist. For this reason, the presence of multiple solutions introduces severe challenges for parameter estimation methods based on deterministic numerical BVP solvers if the data is inconsistent with the single solution found in the optimization step.

Lane-Emden mixed boundary value problem

It may be difficult to imagine a dynamic system that imposes constraints on the states at multiple locations along the domain. Indeed, BVPs do not often directly arise in models of a specific phenomenon, but instead occur when higher-order IVPs are translated to first-order, or when PDE boundary value problems are reduced to ODE problems via spectral projection techniques.

As an example, we consider a special case of the Lane-Emden equation, a second-order IVP which appears in models of gaseous spherical objects, such as stars (Shampine, 2003), relating pressure scaled relative to central density to its rate of change over distance from the centre of the object. The Lane-Emden equation is solved by rewriting it as a first order mixed boundary value problem,

$$\begin{cases} \dot{u}(t,\boldsymbol{\theta}) &= v(t,\boldsymbol{\theta}), & t \in [a,b], \\ \dot{v}(t,\boldsymbol{\theta}) &= -\theta_1 \frac{v(t,\boldsymbol{\theta})}{t} - \theta_2\, u^5(t,\boldsymbol{\theta}), & t \in [a,b], \\ \big(u(b,\boldsymbol{\theta}), v(a,\boldsymbol{\theta})\big) &= \big(u_b, v_a\big), \end{cases} \tag{2.7}$$

where $\boldsymbol{\theta} = (\theta_1, \theta_2) \in \mathbb{R}^2$. When θ_2 is a constant with respect to time, this system has a unique analytical solution on the interval $t \in [0,1]$. However, multiple solutions may be possible on a restricted domain of integration. Indeed, numerical approximations of the solution to the Lane-Emden MBVP on the interval $t \in [0.5,1]$, given parameter values $\boldsymbol{\theta} = (2,1)$, and boundary conditions $\big(u_b, v_a\big) = \Big(\frac{\sqrt{3}}{2}, -\frac{288}{2197}\Big)$, appear to suggest the presence of two solutions. Each of the numerical solutions shown in Figure 2.2 is obtained using the bvp4c solver in MATLAB, which employs a shooting technique starting from a user-specified *initial guess* for the optimization routine. In the case that multiple solutions approximately satisfy the system dynamics, the objective function of the shooting algorithm is multimodal

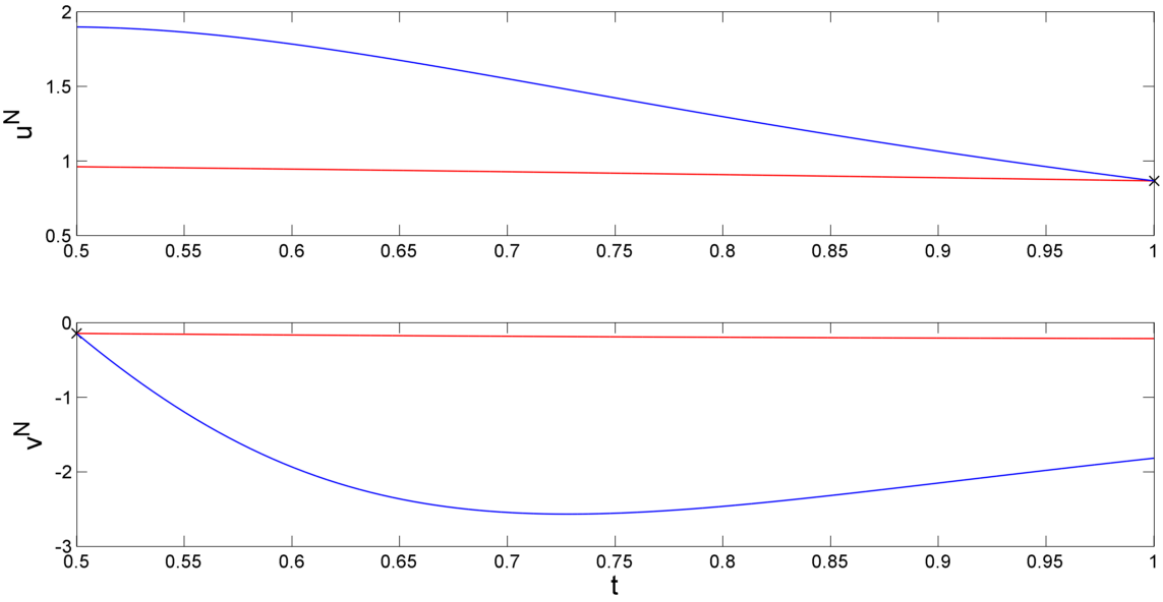

Figure 2.2: *Numerical solutions to the Lane-Emden MBVP with parameters* $\boldsymbol{\theta} = (2, 1)$ *and boundary conditions* $(u_b, v_a) = \left(\frac{\sqrt{3}}{2}, -\frac{288}{2197}\right)$. *The bvp4c (MATLAB) numerical solver was used with two different starting points:* $u_a \in \{1, 2\}$. *Two distinct solutions were obtained (red, blue).*

in the unknown initial value. Moreover, modes are extremely highly peaked (converging to removable discontinuities as the step size tends to zero), and may be located relatively far apart from one another. The optimizer is thus capable of detecting only one mode, and corresponding single solution, at a time for a given initial guess.

2.1.3 Delay initial function problems

Incorporating time lags into ODE models allows the description of a large class of systems, such as mechanisms governing gene transcription (Bernard et al., 2006; Lewis, 2003), signalling pathways (Swameye et al., 2003), and cell kinetics (Busenberg and Tang, 1994). ODE delay initial function problems (DIFPs) relate state derivatives to both present and past states, with fixed delays $\tau_j \in [0, \infty)$.

Definition 6. *The P-dimensional, first-order delay initial function probelm (DIFP) is given in explicit form by:*

$$\begin{cases} \dot{\mathbf{u}}(t,\boldsymbol{\theta}) &= f_{\boldsymbol{\theta}}\big(t, \mathbf{u}(t,\boldsymbol{\theta}), \mathbf{u}(t-\tau_1,\boldsymbol{\theta}), \ldots, \mathbf{u}(t-\tau_d,\boldsymbol{\theta})\big), \quad t \in [a,b], \\ \mathbf{u}(t,\boldsymbol{\theta}) &= \boldsymbol{\phi}(t), \qquad\qquad\qquad\qquad\qquad\qquad\quad t \in [a - \max_{1\le j\le d}\tau_j, a]\,, \end{cases} \tag{2.8}$$

where $\mathbf{u}(\,\cdot\,,\boldsymbol{\theta}) : [a,b] \to \mathbb{R}^P$, $f_{\boldsymbol{\theta}} : [a,b] \times \mathbb{R}^P \to \mathbb{R}^P$, *and* $\boldsymbol{\phi} : [a - \max_{1\le j\le d}\tau_j, a] \to \mathbb{R}^P$.

DIFP trajectories depend on an infinite-dimensional *input function*, or *history*, $\boldsymbol{\phi}$, instead of a finite-dimensional initial state. For this reason, DIFPs are considered transitional models between ODEs, which provide vector-valued constraints, and PDEs, which impose function-valued constraints at the boundaries of the domain. DIFPs are well-suited to describing biological and physical dynamics that take time to propagate through systems. Time delayed components are often used to proxy unmodelled or poorly-understood mechanisms that introduce a time lag in the dynamics. Such models can contain additional functional inputs and yield solutions with periodic discontinuities in the derivative.

We refer the interested reader to Bellen and Zennaro (2003) for an overview of the conditions required for the existence and uniqueness of DIFP solutions, and for a discussion of how numerical methods approach the variety of challenges associated with such problems. Although numerical DIFP solvers are available, they are sometimes considered unsatisfactory in applications, as illustrated in Figure 2.3 for a simple system of time-delayed oscillatory decay. Additional problems arise when the history function is not fully specified, but only available at a finite number of nodes. In this case, numerical methods rely on interpolation of the initial nodes, and ignore the uncertainty introduced by replacing $\boldsymbol{\phi}$ with an approximation. This has potential for impacting the system dynamics even over the short term, changing the structure of the solution. The following simple example illustrates how this situation affects the numerical approach.

Delayed oscillatory decay model

As an example, let us consider the simple one-dimensional DIFP,

$$\begin{cases} \dot{u}(t,\boldsymbol{\theta}) &= -\theta_1\, u(t-\tau,\boldsymbol{\theta}), & t \in [a,b] \\ u(t,\boldsymbol{\theta}) &= \phi(t), & t \in [a-\tau,a], \end{cases} \tag{2.9}$$

and consider the model parameters $\boldsymbol{\theta} = (\theta_1, \tau) = (1,1)$. The analytical solution for this DIFP is obtained by a recursion implemented using the symbolic toolbox in MATLAB. Let us examine, for comparison, a numerical solution obtained via the dde23 software in MATLAB when the initial function is only available at a selected number of nodes.

The first row of Figure 2.3 shows the analytical solution to problem (2.9) with fully known initial function, $\phi(t) = 1,\ t \in [-1,0]$. In this case, the numerical solution undersmooths the function starting at $t = 1$ on the domain, although the oscillatory decay dynamics of the system are such that the solution eventually settles into a trajectory that matches the true solution well. In the second row of Figure 2.3, we consider the history function, $\phi(t) = 1 + \frac{\sin(4\pi t)}{4},\ t \in [-1,0]$, that is only partially specified, without error, over a set of six nodes. An approximation to the initial function is taken to be the mean of an interpolating Gaussian process with square exponential covariance structure. Uncertainty associated with the interpolation is discarded, and the dde23 algorithm is applied to solve the problem numerically. This results in severe deviations from the true solution, even for this very stable system.

2.2 Partial differential equation models

Partial differential equation (PDE) models describe the evolution of a variable implicitly as a function of its rates of change with respect to multiple indexing variables. PDE models are ubiquitous in the applied sciences, where they are used to study a variety of phenomena, from animal movement, to the propagation pattern of a pollutant in the atmosphere.

2.2.1 Initial boundary value problems

PDE boundary value problems (PDE BVPs) relate the state to its rates of change with respect to multiple variables, under a constraint imposed at the boundary of the domain $\mathscr{D} \subset \mathbb{R}^{q+1}$.

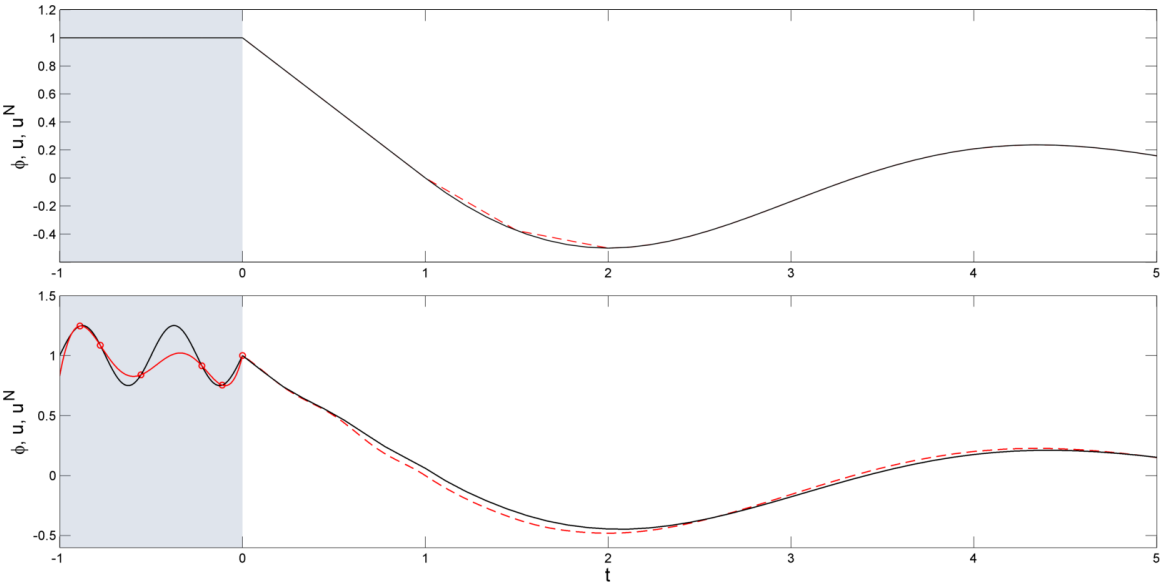

Figure 2.3: *Top: analytical (black) and numerical (red) solution to the DIFP (2.9) with fully-specified initial function* $\phi(t) = 1,\ t \in [-1, 0]$. *Bottom: analytical (black) solution to the DIFP (2.9) with initial function* $\phi(t) = 1 + \frac{\sin(4\pi t)}{4},\ t \in [-1, 0]$. *The numerical solution (red) is obtained for the same system with only a partially specified initial function, given without error at a set of six knots (circled in red).*

Definition 7. *The P-dimensional PDE boundary value problem (PDE BVP) in implicit form is given by:*

$$\begin{cases} F_{\boldsymbol{\theta}}\left(x, t, D\mathbf{u}(x,t,\boldsymbol{\theta}), D^2\mathbf{u}(x,t,\boldsymbol{\theta}), \ldots, D^k\mathbf{u}(x,t,\boldsymbol{\theta})\right) &= 0, & (x,t) \in \mathscr{D}, \\ \mathbf{u}(x,t,\boldsymbol{\theta}) &= \mathbf{u}_B(x,t), & (x,t) \in \partial\mathscr{D}, \end{cases} \tag{2.10}$$

where $\mathscr{D} \subset \mathbb{R}^{q+1}$ is the domain with boundary $\partial\mathscr{D}$, $x \in \mathbb{R}^q$ is a vector of spatial coordinates, and $\mathbf{u}(\,\cdot\,, \boldsymbol{\theta}) : \mathscr{D} \to \mathbb{R}^P$ is the state. The operator D is defined as:

$$D^\alpha \mathbf{u}(x,t,\boldsymbol{\theta}) = \frac{\partial^{|\alpha|}\mathbf{u}(x,t,\boldsymbol{\theta})}{\partial t^{\alpha_0}\, \partial x^{(1)^{\alpha_1}} \ldots\, \partial x^{(q)^{\alpha_q}}} = \partial t^{\alpha_0}\, \partial x^{(1)^{\alpha_1}} \ldots\, \partial x^{(q)^{\alpha_q}}\, \mathbf{u}(x,t,\boldsymbol{\theta}),$$

using the multi-index notation, $|\alpha| = \alpha_0, \ldots, \alpha_q$.

Existence of solutions for PDE boundary value problems is a vast area, and we refer the reader to Jost (2012) for an introduction to this topic. Methods for numerically solving PDE BVPs of this type typically begin by discretizing the spatial derivatives using algebraic approximations. *Finite difference approximations* for the partial derivatives relate the state of the PDE at neighbouring spatial discretization nodes to one another. The more precise *spectral methods* project the functions defining the PDE onto a finite-dimensional subspace of the space of solution trajectories. More precisely, spectral methods provide a global approximation in terms of basis functions $\psi_k \in \left(C^1\left([a,b]\right)\right)^P$:

$$\tilde{\mathbf{u}}^m(x_m, t, \boldsymbol{\theta}) = \sum_{j=1}^{N_t} b_j\, \psi_j(x_m, t), \quad 1 \le m \le N_x,$$

with coefficients $b_j \in \mathbb{R}^P$. Substituting this representation into the PDE, and projecting on the bases, yields a system of $N_t \times N_x$ coupled ODEs which, given associated constraints, can then be solved by one of a number of numerical methods, such as those described in the previous section.

Kuramoto-Sivashinsky nonlinear PDE

The Kuramoto-Sivashinsky (KS) PDE is a model of reaction-diffusion systems (Kuramoto and Tsuzuki, 1976; Sivashinsky and Michelson, 1980), originally used to describe phenomena, such as laminar flame fronts, driven far from equilibrium by instabilities. This model is also of mathematical interest because it exhibits temporal chaotic dynamics. Just as with the Lorenz system, we point out that numerical solutions do not provide a sensible approximation of this system's long-range behaviour.

The KS system is a one-dimensional, nonlinear PDE BVP describing the time evolution of the intensity of a flame front, u, by,

$$\begin{cases} \frac{\partial}{\partial t}u(x,t,\boldsymbol{\theta}) &= -u(x,t,\boldsymbol{\theta})\,\frac{\partial}{\partial x}u(x,t,\boldsymbol{\theta}) - \frac{\partial^2}{\partial x^2}u(x,t,\boldsymbol{\theta}) - \frac{\partial^4}{\partial x^4}u(x,t,\boldsymbol{\theta}), & (x,t)\in\mathscr{D} \\ u(x,a,\boldsymbol{\theta}) &= u_B(x) & (x,t)\in\partial\mathscr{D}. \end{cases} \tag{2.11}$$

Following Kassam and Trefethen (2005), we consider the spatio-temporal domain $\mathscr{D} = [0, 32\pi] \times [0, 150]$. Figure 2.4 shows two numerical solutions of the Kuramoto-Sivashinsky BVP under two nearly identical initial functions: $u_B(x) = \cos\left(\frac{x}{16}\right)\left\{1+\sin\left(\frac{x}{16}\right)\right\}$, and $u_B(x) = \cos\left(\frac{x}{16}\right)\left\{1+\sin\left(\frac{x}{16}\right)\right\} + 10^{-2}$. Numerical trajectories were obtained by transforming (2.11) to a 128-dimensional system of ODEs via spectral projection on the Fourier space. The resulting stiff ODE initial value problem was solved numerically with a fourth-order Runge-Kutta scheme while using an exponential time-differencing transformation at each algorithm iteration (see, for example, Kassam and Trefethen, 2005). Figure 2.4 illustrates that small differences in the initial function become amplified over time, resulting in substantially different dynamics over the second half of the domain. Discretization uncertainty along the domain likely has a similarly disruptive effect on the solution, which however cannot be studied using a deterministic numerical solution approximation.

Navier-Stokes model of fluid dynamics

The Navier-Stokes system is a fundamental model of fluid dynamics, incorporating laws of conservation of mass, energy and linear momentum, as well as physical properties of the fluid over a domain under constraints imposed along the boundaries. It is used to describe

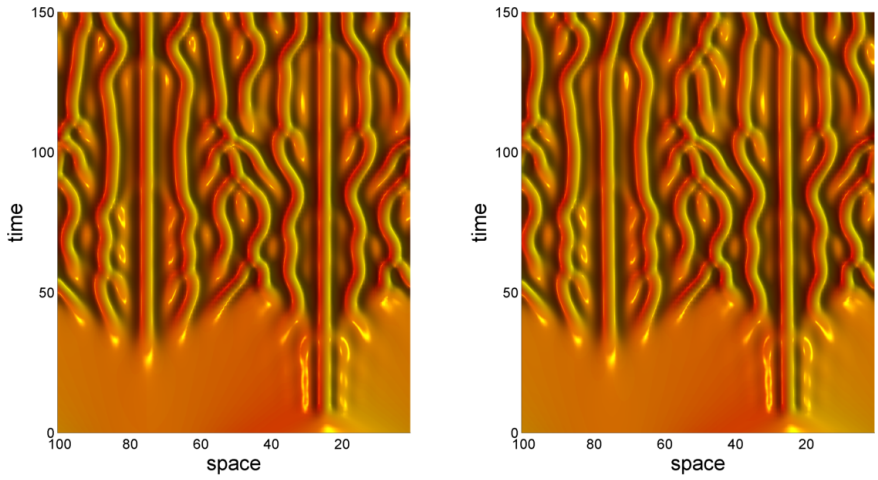

Figure 2.4: *Top view of a numerical solution of the Kuramoto-Sivashinsky PDE boundary value problem on the domain* $\mathscr{D} = [0, 32\pi] \times [0, 150]$. *The numerical solution on the left was obtained under the initial function* $u_B(x) = \cos\left(\frac{x}{16}\right)\left\{1 + \sin\left(\frac{x}{16}\right)\right\}$, *while the numerical solution on the right was obtained under the initial function* $u_B(x) = \cos\left(\frac{x}{16}\right)\left\{1 + \sin\left(\frac{x}{16}\right)\right\} + 10^{-2}$.

a variety of phenomena from the flow of water around a bridge beam to the movement of air around the wing of an aircraft. Therefore it is an important component of complex models in oceanography, weather, atmospheric pollution, and glacier movement. Despite its extensive use, the dynamics of Navier-Stokes models are poorly understood at small time-scales, where they can give rise to *turbulence* (chaotic dynamics).

The Navier-Stokes PDEs models the time evolution of P components of the velocity, $\mathbf{u} : \mathscr{D} \to \mathcal{R}^P$, of an incompressible fluid on a spatial domain $\mathcal{X}$. The Navier-Stokes BVP on the spatio-temporal domain $\mathscr{D} = \mathcal{X} \times \mathcal{T}$ is defined by:

$$\begin{cases} \frac{\partial}{\partial t}\mathbf{u} - \theta_1 \Delta\mathbf{u} + \big(\mathbf{u} \cdot \nabla\big)\mathbf{u} &= \mathsf{f} - \nabla\mathsf{p}, & (x,t) \in \mathscr{D}, \\ \nabla \cdot \mathbf{u} &= 0, & (x,t) \in \mathscr{D}, \\ \int \mathbf{u}^{(j)}\, \mathrm{d}x &= 0, & (x,t) \in \mathscr{D},\ j = 1, 2, \\ \mathbf{u} &= \mathbf{u}_B, & (x,t) \in \mathcal{X} \times \{0\}. \end{cases} \tag{2.12}$$

The model is parameterized by the viscosity of the fluid, $\theta_1 > 0$; the pressure function

$\mathsf{p} : \mathscr{D} \to \mathbb{R}$, and the external time-homogeneous forcing function $\mathsf{f} : \mathcal{X} \to \mathbb{R}$. We consider a domain defined by a 2-dimensional torus $\mathcal{X} = [0, 2\pi) \times [0, 2\pi)$, expressed in spherical coordinates. We further assume periodic boundary conditions, and viscosity $\theta_1 = 1 \times 10^{-3}$ in the turbulent regime.

Often, the quantity of interest is the local spinning motion of the incompressible fluid, called *vorticity*, which we will define as,

$$\varpi(x, t, \boldsymbol{\theta}) = -\nabla \times \mathbf{u}(x, t, \boldsymbol{\theta}),$$

where clockwise rotation corresponds to positive vorticity. This variable will be used to better visualize the solution of the Navier-Stokes system by reducing the two components of velocity to a one-dimensional function.

Chapter 3

A Probability Model for the Unknown Solution and its Derivative

This chapter introduces a probability model for the functional uncertainty associated with estimating an unknown DE solution from a finite number of model evaluations. Such an idea was first considered informally by Skilling (1991), although with little practical success. In this chapter we translate this insight into a formal framework, and show that the resulting probability model is well-defined under standard assumptions for general univariate and multivariate solutions.

Section 3.1 reviews some fundamental notions required for defining measures on general Hilbert spaces (our focus in this thesis will be the $L^2(\mathscr{D})$ Hilbert space of square integrable functions). In Section 3.2, we introduce the proposed probabilistic model for the uncertainty in the unknown DE solution. We first define a prior measure on the space of solutions and then provide an informal derivation of the posterior measure given a set of noisy derivative realizations. In Section 3.3 we show that this probability measure is indeed well-defined and absolutely continuous with respect to the prior measure.

3.1 Review of selected measure theoretic concepts

A model of functional uncertainty in the solution of differential equations requires defining convenient measures on (infinite-dimensional) spaces of functions of specified smoothness. In this section, we provide a selected review of some relevant measure theoretic concepts and define the probability measures that we will work with in this thesis. For an in-depth overview of this subject, we refer the reader to Lifshits (1995), Stuart (2010), and references therein. This section assumes familiarity with the basics of function space theory, for which we refer the reader to Megginson (1998).

3.1.1 Radon measures on Hilbert spaces

We restrict[1] our attention specifically to measures defined on *Hilbert spaces*.

Definition 8. *A Hilbert space $(H, ||\cdot||)$ is a complete vector space, whose norm, $||\cdot||$, is defined by its inner product $\langle\cdot,\cdot\rangle$. Moreover, a Hilbert space that admits a countable orthonormal basis is called separable.*

We will hereafter refer to this space simply as H and omit the vector norm from the notation. A useful separable Hilbert space that we will work with is the $L^2(\mathscr{D})$ space of square integrable functions on the compact closed set $\mathscr{D} \subset \mathbb{R}^{q+1}$.

Definition 9. *The space $L^2(\mathscr{D})$ includes all functions $f : \mathscr{D} \to \mathbb{R}$ such that $\int_{\mathscr{D}} f^2(x)\,dx < \infty$, and has inner product:*

$$\langle f, g\rangle = \int_{\mathscr{D}} f(x)\, g(x)\, dx, \quad f, g \in L^2(\mathscr{D}).$$

The above definition applies to real functions. There are corresponding definitions of Hilbert spaces in which the scalar field is the set of complex numbers. We will use them without further comment.

Throughout this thesis we will consider the underlying *probability space*, $(H, \mathcal{A}, \mu_0)$, where H is a Hilbert space with associated norm $||\cdot||$; $\mathcal{A}$ is a σ-algebra of subsets of H; and μ_0 is a probability measure defined on the *measure space* $(H, \mathcal{A})$. We further restrict our

[1] Results for more general Banach spaces are sometimes required. We refer the reader to Stuart (2010) for a more general review in the Banach space setting.

attention to the class of *Radon measures*, which have desirable topological properties, and avoid certain pathologies (e.g., Lifshits, 1995).

Definition 10. *A Radon measure on H is a measure μ such that,*

$$\mu(A) = \sup\left\{\mu(B) | B \subset A, B \text{ compact}\right\}, \quad A \in \mathcal{A}.$$

These include Gaussian measures on finite and infinite-dimensional Hilbert spaces (Billingsley, 1968). We will also use the notions of *absolute continuity* and the *Radon-Nikodym Theorem*:

Definition 11. *Let μ and μ_0 be two measures defined on the same measure space, $(H, \mathcal{A})$. Then μ is absolutely continuous with respect to μ_0 if $\mu_0(A) = 0$ implies $\mu(A) = 0$ for $A \in \mathcal{A}$.*

Theorem 3.1.1 (Radon-Nikodym Theorem)**.** *Let μ and μ_0 be two measures defined on the same measure space, $(H, \mathcal{A})$. If μ is absolutely continuous with respect to μ_0 and μ_0 is σ-finite, then there exists an A-measurable function $f : H \to [0, \infty]$ such that,*

$$\mu(A) = \int_A f(x)\, d\mu_0(x), \quad \forall A \in \mathcal{A}.$$

The function $f(x)$ is denoted by $\frac{\mathrm{d}\mu}{\mathrm{d}\mu_0}(x)$ and is called the *Radon-Nikodym derivative* of μ with respect to the reference measure μ_0, or informally, the *density*. When H is finite-dimensional, the Lebesgue measure is a useful standard reference measure. However, the Lebesgue measure is not defined when H is infinite-dimensional (see, for example, Kuo, 1975). In these cases, the Gaussian measure, which exists on infinite-dimensional spaces, is a convenient choice.

3.1.2 Preliminaries

Appropriate choice of positive definite covariance functions for our model will require consideration of their properties, including stationarity and isotropy.

Definition 12. *A function $K : \mathscr{D} \times \mathscr{D} \to \mathbb{R}$ that induces an operator on a Hilbert space H of functions defined on $\mathscr{D}$ via $Kg(t) = \int K(t, \tilde{t}) g(\tilde{t}) d\tilde{t}$, $g \in H$, is called positive semidefinite if $\langle g, Kg \rangle \geq 0$. Moreover, if the function also satisfies the condition that $\langle g, Kg \rangle = 0$ iff $g = 0$, it is called positive definite.*

Note for the space of interest $L^2(\mathscr{D})$, the (necessary and sufficient) condition for positive semidefiniteness can be written as,

$$\int_{\mathscr{D}} \int_{\mathscr{D}} K(t,\tilde{t})\, g(t)\, g(\tilde{t})\, \mathrm{d}\mu(t)\, \mathrm{d}\mu(\tilde{t}) \quad \geq 0, \quad \forall\, g \in L^2(\mathscr{D}),$$

with respect to the measure μ. For positive definiteness, this integral must also equal zero iff $g = 0$.

Definition 13. *A function $K : \mathscr{D} \times \mathscr{D} \to \mathbb{R}$ is called stationary if it can be written as a function of the difference between its arguments:*

$$K(t,\tilde{t}) = g(t - \tilde{t}).$$

Furthermore K is isotropic if it can be written as function of the normed difference between its arguments,

$$K(t,\tilde{t}) = g(|t - \tilde{t}|).$$

3.1.3 The Gaussian measure

In this thesis, we will consider *continuously-indexed* Gaussian processes, where the indexing variable can be any element of an uncountable set $\mathscr{D} \subset \mathbb{R}^{q+1}$.

Definition 14. *A Gaussian process $\{h(d,\omega) : d \in \mathscr{D}, \omega \in \Omega\}$ is a mapping $\mathscr{D} \times \big(\Omega, \mathcal{A}, P\big) \to \mathbb{R}$ such that $h(\cdot,\omega) \in H$, distributed according to a Gaussian measure on $\big(H, \mathcal{B}(H)\big)$, where $\mathcal{B}(H)$ is the Borel sigma algebra of subsets of H.*

Therefore, we will sometimes refer to the Gaussian process $\{h(d) : d \in \mathscr{D}\}$, omitting dependence on ω, as a *random function* with samples $h : \mathscr{D} \to \mathbb{R} \in H$, having Gaussian measure. The Gaussian measure on an infinite-dimensional Hilbert space is characterized by the joint distribution of any finite-dimensional realization.

Definition 15. *A measure μ defined on $\big(H, \mathcal{B}(H)\big)$ is Gaussian if for any finite set of indices, $\mathbf{d} = [d_1, \cdots, d_N] \in \mathscr{D}^N$, the vector $\mathsf{h} = [h(d_1), \cdots, h(d_N)] \in \big(H^*\big)^N$, where H^* is the dual space of linear functionals of H, is distributed according to a multivariate Gaussian measure, $\mathcal{N}_N\big(\mathsf{m}, C\big)$, where $\mathsf{m} \in \mathbb{R}^N$ is the mean vector and $C \in M^N(\mathbb{R})$ is a positive definite covariance matrix.*

The mean and covariance of a measure on H are defined as follows.

Definition 16. *Let H be a Hilbert space of functions. The mean of a measure μ on $(H, \mathcal{A})$ is a function $m \in H$ such that for all $h \in H$,*

$$m = \int_H h(x) d\mu(x),$$

which we denote by Eh. The covariance of μ is a linear operator $\mathcal{C} : H \to H$ such that for all $k, \ell \in H$

$$\mathcal{C} = E(k - m) \otimes (\ell - m),$$

where $\otimes$ is the tensor product.

Importantly, given a mean and covariance operator, we can uniquely describe a Gaussian process.

Theorem 3.1.2. *A Gaussian process is uniquely defined by its mean and covariance operator.*

Next, we present an important theorem that will allow us to show that the conditional unknown DE solution and its derivative, as defined in the next section, exist and are distributed according to a Gaussian measure.

Theorem 3.1.3 (e.g., Stuart, 2010)**.** *Let $H = H_1 \oplus H_2$ be a separable Hilbert space, and let $\big(h_1, h_2\big) \in H_1 \oplus H_2$ be a Gaussian random variable with mean $m = \big(m_1, m_2\big)$ and positive definite covariance operator $\mathcal{C}$. Then the conditional distribution of h_1 given h_2 is well-defined, Gaussian with mean and covariance operator:*

$$m = m_1 + \mathcal{C}_{12}\mathcal{C}_{22}^{-1}\left(h_2 - m_2\right),$$
$$\mathcal{C} = \mathcal{C}_{11} - \mathcal{C}_{12}\mathcal{C}_{22}^{-1}\mathcal{C}_{21},$$

where the cross-covariances are defined as $\mathcal{C}_{ij} = E\left(h_i - m_i\right) \otimes \left(h_j - m_j\right)$.

3.2 Model for the probabilistic solution and its derivative

We wish to construct a probability model describing our uncertainty about an unknown infinite-dimensional solution of a differential equation problem reconstructed from a finite-dimensional vector of evaluations generated from the model. Such a probabilistic representation requires modelling solution uncertainty as a measure defined on a suitable probability space. From a modelling perspective, care must be taken in describing this as a model of our *knowledge* about the system given available information, rather than of any stochasticity inherent in the deterministic DE model. This characteristic is a familiar one in the field of Bayesian statistics, where distributions on unknown quantities are used to describe their uncertainty relative to the observer.

We begin by considering a univariate ODE solution $\mathbf{u} \in H$ on the domain $\mathscr{D} \subset \mathbb{R}$, and then extend the result for multivariate PDE solutions. We restrict our attention to solutions on the space $H = \left(L^2(\mathscr{D})\right)^P$, noting that the model can be extended to more general Hilbert spaces. Employing Gaussian distributional assumptions throughout allows us to obtain a closed form expression for the posterior distribution of the solution and its derivative. It is certainly possible to make alternative distributional assumptions, which will introduce the need for an additional layer of Monte Carlo draws from the posterior distribution, as we will see in Chapter 4.

3.2.1 Univariate solution model

Suppose that there exists an unknown function, or functions, $\mathbf{u}(\cdot, \boldsymbol{\theta}) : \mathscr{D} \to \mathbb{R}^P$ satisfying a general ODE problem (e.g., 2.1, 2.5, 2.6, or 2.8). The vector field $f_{\boldsymbol{\theta}}$ and parameters $\boldsymbol{\theta}$ are fully specified, and any constraints, such as initial or boundary conditions, are provided without error. From this we can usually obtain full or partial a priori information about the smoothness of the solution. We can also make a judgement about whether multiple solutions are possible, such as in the case of mixed boundary value problems, and, in some cases, the exact number of solutions. This information will be encoded in the prior measures on the solution and its derivative, which will then be updated based on a set of derivative realizations generated from the model.

For exposition, we have made the simplifying assumption that the P solution states are mutually independent, so that cross-covariances between states in our model may be set to zero and the analysis can proceed sequentially over each dimension. Indeed, an analogous

assumption commonly underlies classical numerical methods. However, our probabilistic approach can straightforwardly incorporate dependence between states by modelling the derivatives via dependent Gaussian process priors (see, for example, Boyle and Frean, 2005).

Derivative realizations

Let us consider a discrete grid, or *mesh*, defined by the partition $\mathbf{s}_{1:n} = [s_1, \cdots, s_n]^\intercal \in \mathscr{D}^n$ of the domain $\mathscr{D} = [a, b] \subset \mathbb{R}$. Suppose also that we are able to obtain n realizations, $\mathbf{f}_{1:n} = [\mathbf{f}_1, \cdots, \mathbf{f}_n]^\intercal \in M^{n,P}\big(\mathbb{R}\big)$, of the random function describing our knowledge of the derivative. Assume the following Gaussian error model:

$$\mathbf{f}_{1:n} \,|\, \dot{\mathbf{u}}(s_1, \boldsymbol{\theta}), \ldots, \dot{\mathbf{u}}(s_n, \boldsymbol{\theta}) \sim \mathcal{N}_n\big([\dot{\mathbf{u}}(s_1, \boldsymbol{\theta}), \ldots, \dot{\mathbf{u}}(s_n, \boldsymbol{\theta})]^\intercal, \boldsymbol{\Lambda}_n\big), \tag{3.1}$$

where $\boldsymbol{\Lambda}_n \in \big(\mathrm{M}^n(\mathbb{R})\big)^P$ is a positive definite covariance matrix.

Solution derivative

Next, define a Gaussian prior measure for the time derivative of the solution function,

$$\dot{\mathbf{u}}(\cdot, \boldsymbol{\theta}) \sim \mu_0^f = \mathcal{N}(\mathbf{m}_0^f, \mathcal{C}_0^f), \tag{3.2}$$

on the measure space $\big(L^2\big([a, b]\big)^P, \mathcal{A}\big)$ with mean function and covariance:

$$\mathbf{m}_0^f(t) = \boldsymbol{\ell}(t), \tag{3.3}$$

$$\mathcal{C}_0^f(t, \tilde{t}) = \alpha^{-1} \textstyle\int_{\mathbb{R}} \mathrm{R}_\lambda(t, z)\mathrm{R}_\lambda(\tilde{t}, z)\mathrm{d}z \equiv \mathrm{RR}(t, \tilde{t}). \tag{3.4}$$

The prior mean function, $\boldsymbol{\ell} : [a, b] \to \mathbb{R}^P$, contains any information about the shape of the derivative that is known a priori[2]. The covariance operator, $\mathcal{C}_0^f$, is defined in terms of a *kernel function*, $\mathrm{R}_\lambda : \mathscr{D} \times \mathbb{R} \to \mathbb{R}^P$, chosen in such a way that the eigenfunctions of $\mathcal{C}_0^f$ form a basis for the space containing the derivative of the true solution. The function R_λ is positive definite and square integrable in each input, and scaled by the *length-scale hyperparameter*, $\lambda \in (0, \infty)^P$, and the *prior precision hyperparameter*, $\alpha \in (0, \infty)^P$. We use the notation $\mathrm{RR} = R\mathcal{K}R^*$ to denote the operator obtained by a convolution of R with its

[2]Practically speaking, if we have some prior knowledge of the derivative dynamics, encoding them in the prior mean function will, in general, require using fewer model evaluations than would otherwise be necessary to obtain a reliable estimate of the solution.

adjoint, R^* weighted by $\mathcal{K} = \alpha^{-1}$. For convenience, we will often omit from the notation the dependence on *auxiliary parameters*, $\Psi_n = [\alpha, \lambda, R, \mathbf{s}_{1:n}]$, associated with the derivative model.

Let us use the subscript n to indicate an update based on n derivative realizations, $\mathbf{f}_{1:n}$. Informally, updating the prior derivative measure (3.2) using model derivative realizations distributed according to (3.1) yields the Gaussian predictive posterior measure,

$$\dot{\mathbf{u}}(\cdot, \boldsymbol{\theta}) \,|\, \mathbf{f}_{1:n}, \mathbf{u}_a \;\sim\; \mu_n^f = \mathcal{N}\big(\mathbf{m}_n^f, \mathcal{C}_n^f\big), \tag{3.5}$$

on the probability space $\big(L^2\big([a,b]\big)^P, \mathcal{A}, \mu_0^f\big)$ with mean and covariance:

$$\mathbf{m}_n^f(t) = \mathbf{m}_0^f(t) + \mathrm{RR}(t, \mathbf{s}_{1:n})\big(\boldsymbol{\Lambda}_n + \mathrm{RR}(\mathbf{s}_{1:n}, \mathbf{s}_{1:n})\big)^{-1}\big(\mathbf{f}_{1:n} - \mathbf{m}_0^f(\mathbf{s})\big), \tag{3.6}$$

$$\mathcal{C}_n^f(t, \tilde{t}) = \mathrm{RR}(t, \tilde{t}) - \mathrm{RR}(t, \mathbf{s}_{1:n})\big(\boldsymbol{\Lambda}_n + \mathrm{RR}(\mathbf{s}_{1:n}, \mathbf{s}_{1:n})\big)^{-1}\mathrm{RR}(\mathbf{s}_{1:n}, \tilde{t}). \tag{3.7}$$

This notation will be convenient when we consider a sequential algorithm for sampling derivative realizations in the next chapter.

It is useful to note here that the posterior distribution (3.5) in the derivative space takes the form of the well-known Gaussian process regression model (see, for example, Rasmussen and Williams, 2006).

Solution state

We can now obtain a model of the solution, $\mathbf{u}(\cdot, \boldsymbol{\theta}) : \mathscr{D} \to \mathbb{R}^P$, by taking the corresponding integrated Gaussian prior measure:

$$\mathbf{u}(\cdot, \boldsymbol{\theta}) \sim \mu_0 = \mathcal{N}(\mathbf{m}_0, \mathcal{C}_0), \tag{3.8}$$

on the measure space $\big(L^2\big([a,b]\big)^P, \mathcal{A}\big)$ with mean and covariance:

$$\mathbf{m}_0(t) = \mathbf{u}_a + \textstyle\int_a^t \boldsymbol{\ell}(z)\mathrm{d}z, \tag{3.9}$$

$$\mathcal{C}_0(t, \tilde{t}) = \alpha^{-1} \textstyle\int_{\mathbb{R}} \mathrm{Q}_\lambda(t, z)\mathrm{Q}_\lambda(\tilde{t}, z)\mathrm{d}z \equiv \mathrm{QQ}(t, \tilde{t}), \tag{3.10}$$

where $Q_\lambda(t, z) = \int_a^t R_\lambda(x, z)\mathrm{d}x$ is the integrated scaled kernel, and $\mathbf{u}_a$ is the initial condition of the differential equation. The mean function $\mathbf{m}_0$ can be used to enforce boundary conditions and constraints, as will be shown in Chapter 4. Informally, the resulting posterior

measure for the solution of the differential equation follows as,

$$\mathbf{u}(\cdot,\boldsymbol{\theta})\,|\,\mathbf{f}_{1:n},\mathbf{u}_a \;\sim\; \mu_n = \mathcal{N}\big(\mathbf{m}_n,\mathcal{C}_n\big), \tag{3.11}$$

on the probability space $\big(L^2\big([a,b]\big)^P,\mathcal{A},\mu_0\big)$ with mean function and covariance:

$$\mathbf{m}_n(t) = \mathbf{m}_0(t) + \mathrm{QR}(t,\mathbf{s}_{1:n})\big(\boldsymbol{\Lambda}_n + \mathrm{RR}(\mathbf{s}_{1:n},\mathbf{s}_{1:n})\big)^{-1}\big(\mathbf{f}_{1:n} - \mathbf{m}_0^f(\mathbf{s}_{1:n})\big), \tag{3.12}$$

$$\mathcal{C}_n(t,\tilde{t}) = \mathrm{QQ}(t,\tilde{t}) - \mathrm{QR}(t,\mathbf{s}_{1:n})\big(\boldsymbol{\Lambda}_n + \mathrm{RR}(\mathbf{s}_{1:n},\mathbf{s}_{1:n})\big)^{-1}\mathrm{RQ}(\mathbf{s}_{1:n},\tilde{t}). \tag{3.13}$$

Hence, under the Gaussian prior specification and Gaussian error model, we have a closed form representation of the posterior distribution of the solution state and of its derivative. All that remains for conveniently evaluating their realizations is a closed form representation of $\mathrm{RR},\mathrm{RQ},\mathrm{QR},\mathrm{QQ} : [a,b]\times[a,b]\to\mathbb{R}^P$. These are provided in Chapter 6 for three illustrative types of kernel function.

3.2.2 Multivariate solutions

Having defined a probability model for the uncertainty in an unknown ODE solution, we can now examine the case of PDE solutions of the form $\mathbf{u}(\cdot,\boldsymbol{\theta}) : \mathscr{D}\to\mathbb{R}^P$ on the domain $\mathscr{D}\subset\mathbb{R}^{q+1}$, $q>0$. We will consider Gaussian processes indexed by a spatio-temporal variable $d=[x,t]^{\mathsf{T}}\in\mathbb{R}^{q+1}$ with partition defined by the mesh with vertices $\mathbf{s}_{1:n}\in\mathscr{D}^n$. As before, we define a Gaussian prior distribution on the derivative function $\dot{\mathbf{u}}(\cdot,\boldsymbol{\theta})$ and update it given derivative realizations $\mathbf{f}_{1:n}$. We define the mean function as before, but assume tensor product (multiplicative) kernel functions in each dimension,

$$\mathrm{R}_\lambda(d,\tilde{d}) = \prod_{i=1}^{q+1}\mathrm{R}_{\lambda^{(i)}}(d^{(i)},\tilde{d}^{(i)}),$$

where $\lambda\in\mathbb{R}^{q+1}$ is a vector of length-scales, and the notation, $d^{(i)}$, denotes the ith element of the vector d. Indeed, a multiplicative kernel greatly simplifies the analysis, as we are able to compute the required convolutions exactly as follows:

$$\begin{aligned}\mathrm{RR}(d,\tilde{d}) &= \alpha^{-1}\textstyle\int_{\mathbb{R}^{q+1}}\mathrm{R}_\lambda(d,z)\mathrm{R}_\lambda(\tilde{d},z)\mathrm{d}z\\ &= \alpha^{-1}\int_{\mathbb{R}^{q+1}}\prod_{i=1}^{q+1}\mathrm{R}_{\lambda^{(i)}}(d^{(i)},z^{(i)})\prod_{i=1}^{q+1}\mathrm{R}_{\lambda^{(i)}}(\tilde{d}^{(i)},z^{(i)})\;\mathrm{d}z^{(i)}\end{aligned}$$

$$= \alpha^{-1} \prod_{i=1}^{q+1} \int_{\mathbb{R}} \mathrm{R}_{\lambda^{(i)}}(d^{(i)}, z^{(i)})\, \mathrm{R}_{\lambda^{(i)}}(\tilde{d}^{(i)}, z^{(i)})\, \mathrm{d}z$$
$$= \alpha^{-1} \prod_{i=1}^{q+1} \mathrm{RR}_{\lambda^{(i)}}(d^{(i)}, \tilde{d}^{(i)}),$$

and, similarly,

$$\mathrm{RQ}(d, \tilde{d}) = \alpha^{-1} \prod_{i=1}^{q+1} \mathrm{RQ}_{\lambda^{(i)}}(d^{(i)}, \tilde{d}^{(i)}),$$
$$\mathrm{QR}(d, \tilde{d}) = \alpha^{-1} \prod_{i=1}^{q+1} \mathrm{QR}_{\lambda^{(i)}}(d^{(i)}, \tilde{d}^{(i)}),$$
$$\mathrm{QQ}(d, \tilde{d}) = \alpha^{-1} \prod_{i=1}^{q+1} \mathrm{QQ}_{\lambda^{(i)}}(d^{(i)}, \tilde{d}^{(i)}).$$

One important requirement for obtaining the correct covariances is to properly parameterize the domain $\mathscr{D}$ in order to evaluate each of the bivariate convolutions involving $Q_{\lambda^{(i)}}$ over the correct intervals $\mathscr{D}^{(1)}, \ldots, \mathscr{D}^{(q+1)}$.

Probabilistic Posterior Solution

We will hereafter use the term *probabilistic solution* to refer to the random function distributed according to the posterior measure (3.11) defining our belief about the unknown differential equation solution given a set of noisy realizations of the derivative.

Definition 17. *The probabilistic solution of a PDE problem, given n realizations of the derivative, refers to the random function,*

$$\mathbf{u}(\cdot, \boldsymbol{\theta}) \,|\, \boldsymbol{\theta}, \mathbf{f}_{1:n}, \mathbf{u}_a, \Psi_n \in \left(L^2\big(\mathscr{D}; (\Omega, \mathcal{A}, P)\big)\right)^P, \tag{3.14}$$

distributed according to (3.11). For notational convenience, we shall sometimes denote the probabilistic solution by $\mathbf{u}_n(\cdot, \boldsymbol{\theta})$*, and its derivative by* $\dot{\mathbf{u}}_n(\cdot, \boldsymbol{\theta})$*.*

Therefore, we now have a probability statement describing DE solution uncertainty at

any finite set of time points, $\mathbf{d} = [\mathbf{x}, \mathbf{t}]^\mathsf{T} \in \mathbb{R}^{(q+1)\times T}$, conditioned on an approximate finite-dimensional solution estimated using an n-dimensional mesh $\mathbf{s}$:

$$p\big(\mathbf{u}(\mathbf{d}, \boldsymbol{\theta}) \,\big|\, \boldsymbol{\theta}, \mathbf{f}_{1:n}, \mathbf{u}_a, \Psi_n\big) = \mathcal{N}_T\big(\mathbf{m}_n(\mathbf{d}), \mathcal{C}_n(\mathbf{d}, \mathbf{d})\big). \tag{3.15}$$

The next section provides technical details about the above informal derivation, and shows that the posterior measures presented above are indeed well-defined.

3.3 The probabilistic solution is well-defined

In this section, we justify the claim that the conditional distribution of the DE solution given n derivative evaluations is well-defined, and that it has density $\mathrm{d}\mu_n/\mathrm{d}\mu_0$ with respect to the prior measure μ_0.

Theorem 3.3.1. *Consider the model presented in Section 3.2 and let $\boldsymbol{\ell} : \mathscr{D} \to \mathbb{R}^P$ and $R_\lambda : \mathbb{R}^{q+1} \times \mathbb{R}^{q+1} \to \mathbb{R}^P$ be deterministic, square integrable functions. The probabilistic solution $\mathbf{u}_n(\cdot, \boldsymbol{\theta})$ and its derivative $\dot{\mathbf{u}}_n(\cdot, \boldsymbol{\theta})$ are well-defined and distributed according to (3.11) and (3.5), respectively.*

Proof. Without loss of generality, we restrict our attention to solutions of dimension $P = 1$ on a univariate domain, $\mathscr{D} = [a, b] \subset \mathcal{R}$. Consider the space $\mathcal{F} = L^2(\mathbb{R}; (H, \mathcal{A}, \mu_0))$ and let $\mathcal{F}^*$ denote the dual space of linear functionals of $\mathcal{F}$. Define, for all $u \in \mathcal{F}$ and $v \in \mathcal{F}^*$, the following linear continuous operators. Define $\mathrm{R} : \mathcal{F} \to \mathcal{F}^*$ to be the integral transform, $\mathrm{R}u(t) = \int_{-\infty}^{\infty} R_\lambda(t, z)u(z)\mathrm{d}z$, and let $\mathrm{R}^* : \mathcal{F}^* \to \mathcal{F}$ be its adjoint, $\mathrm{R}^*v(t) = \int_{-\infty}^{\infty} R_\lambda(z, t)v(z)\mathrm{d}z$. Similarly, define $\mathrm{Q} : \mathcal{F} \to \mathcal{F}^*$ to be the integral transform, $\mathrm{Q}u(t) = \int_{-\infty}^{\infty} Q_\lambda(t, z)u(z)\mathrm{d}z$, and let $\mathrm{Q}^* : \mathcal{F}^* \to \mathcal{F}$ denote its adjoint, $\mathrm{Q}^*v(t) = \int_{-\infty}^{\infty} Q_\lambda(z, t)v(z)\mathrm{d}z$.

Consider the white noise process $\zeta(t) \in \mathcal{F}$, distributed as,

$$\zeta \sim \mathcal{N}(0, \mathcal{K}),$$

with mean 0 and covariance $\mathcal{K}(t, \tilde{t}) = \delta_t(\tilde{t})\ \alpha^{-1}$. Next, model the derivative of the solution by the integral transform:

$$\dot{u}(t, \boldsymbol{\theta}) = m_0^f(t) + \mathrm{R}\zeta(t), \tag{3.16}$$

defined for all $\zeta \in \mathcal{F}$ and $t \in [a, b]$. Then, the differential equation solution model is obtained by integrating $\dot{u}(t, \boldsymbol{\theta})$ with respect to t:

$$u(t, \boldsymbol{\theta}) = m_0(t) + \mathrm{Q}\zeta(t). \tag{3.17}$$

We are interested in the conditional distribution of the state $u(\cdot, \boldsymbol{\theta}) - m_0 \in \mathcal{F}^*$ and derivative $\dot{u}(\cdot, \boldsymbol{\theta}) - m_0^f \in \mathcal{F}^*$ given a vector of n noisy derivative evaluations, $\mathrm{f}_{1:n} - m_0^f(\mathbf{s}_{1:n}) \in \mathbb{R}^n$, on a grid defined by $\mathbf{s}_{1:n} \in [a, b]^n$ under the Gaussian error model:

$$\mathrm{f}_{1:n} - m_0^f(\mathbf{s}_{1:n}) = \mathrm{R}\zeta(\mathbf{s}_{1:n}) + \eta(\mathbf{s}_{1:n}),$$

where $\eta(\mathbf{s}_{1:n}) \sim \mathcal{N}_n(\mathbf{0}, \Lambda_n)$ is independent of ζ, and $\Lambda_n \in \mathrm{M}^n(\mathbb{R})$ is a positive definite matrix.

Now consider the vector $[\dot{u}(\cdot, \boldsymbol{\theta}) - m_0^f, \mathrm{f}_{1:n} - m_0^f(\mathbf{s}_{1:n})] = [\mathrm{R}\zeta, \mathrm{R}\zeta(\mathbf{s}_{1:n}) + \eta(\mathbf{s}_{1:n})] \in \mathcal{F}^* \oplus \mathbb{R}^n$, where the first element is function-valued and the second element is a vector-valued. This vector is jointly Gaussian with mean $M = (0, \mathbf{0})$ and covariance operator C with positive definite (see Chapter 6) cross-covariance operators:

$$\begin{aligned} C_{11} &= \mathrm{R}\mathcal{K}\mathrm{R}^* \qquad & C_{12} &= \mathrm{R}\mathcal{K}\mathrm{R}^* \\ C_{21} &= \mathrm{R}\mathcal{K}\mathrm{R}^* \qquad & C_{22} &= \mathrm{R}\mathcal{K}\mathrm{R}^* + \Lambda_n. \end{aligned} \tag{3.18}$$

Since both $\mathcal{F}^*$ and $\mathbb{R}^n$ are separable Hilbert spaces, it follows from Theorem 3.1.3 that the random variable $[\dot{u}(\cdot, \boldsymbol{\theta}) - m_0^f | \mathrm{f}_{1:n} - m_0^f(\mathbf{s}_{1:n})]$ is well-defined and distributed according to a Gaussian measure with mean and covariance:

$$\begin{aligned} \mathrm{E}\big(\dot{u}(\cdot, \boldsymbol{\theta}) - m_0^f \,\big|\, \mathrm{f}_{1:n} - m_0^f(\mathbf{s}_{1:n})\big) &= C_{12}C_{22}^{-1}(\mathrm{f}_{1:n} - m_0^f(\mathbf{s}_{1:n})), \\ \mathrm{Cov}\big(\dot{u}(\cdot, \boldsymbol{\theta}) - m_0^f \,\big|\, \mathrm{f}_{1:n} - m_0^f(\mathbf{s}_{1:n})\big) &= C_{11} - C_{12}C_{22}^{-1}C_{21}. \end{aligned}$$

Similarly, we consider the vector $[u(\cdot, \boldsymbol{\theta}) - m_0, \mathrm{f}_{1:n} - m_0^f(\mathbf{s}_{1:n})] = [\mathrm{Q}\zeta, \mathrm{R}\zeta(\mathbf{s}_{1:n}) + \eta(\mathbf{s}_{1:n})] \in \mathcal{F}^* \oplus \mathbb{R}^n$, with mean $M = (0, \mathbf{0})$ and cross-covariances:

$$\begin{aligned} C_{11} &= \mathrm{Q}\mathcal{K}\mathrm{Q}^* \qquad & C_{12} &= \mathrm{Q}\mathcal{K}\mathrm{R}^* \\ C_{21} &= \mathrm{R}\mathcal{K}\mathrm{Q}^* \qquad & C_{22} &= \mathrm{R}\mathcal{K}\mathrm{R}^* + \Lambda_n. \end{aligned}$$

By Theorem 3.1.3, the conditional distribution of $[\dot{u}(\cdot,\boldsymbol{\theta}) - m_0^f | \mathrm{f}_{1:n} - m_0^f(\mathbf{s}_{1:n})]$ is a well-defined Gaussian distribution with mean and covariance:

$$\begin{aligned}\mathrm{E}\big(u(\cdot,\boldsymbol{\theta}) - m_0 \,\big|\, \mathrm{f}_{1:n} - m_0^f(\mathbf{s}_{1:n})\big) &= C_{12}C_{22}^{-1}(\mathrm{f}_{1:n} - m_0^f(\mathbf{s}_{1:n})),\\ \mathrm{Cov}\big(u(\cdot,\boldsymbol{\theta}) - m_0 \,\big|\, \mathrm{f}_{1:n} - m_0^f(\mathbf{s}_{1:n})\big) &= C_{11} - C_{12}C_{22}^{-1}C_{21}.\end{aligned}$$

Furthermore, μ_n and $\dot{\mu}_n$ are absolutely continuous with respect to the corresponding prior Gaussian measures μ_0 and μ_0^f, and therefore the Radon-Nikodym derivatives $\mathrm{d}\mu_n/\mathrm{d}\mu_0$ and $\mathrm{d}\mu_n^f/\mathrm{d}\mu_0^f$ exist.

Extension to multivariate solutions follows straightforwardly under tensor product kernels, defined in Section 3.2.2. Extension to solutions of dimension $P > 1$ is immediate for mutually independent states. Dependence between states can be incorporated through dependent Gaussian priors, and requires more cumbersome notation. □

The posterior distribution of the derivative function is a Gaussian process, and the posterior distribution of the state is its integrated version. Therefore, we can obtain the distribution of any finite number T of sample evaluations on $\mathbf{d} \in \mathscr{D}^T$ by Definition 15. The conditional density of the state evaluated at $\mathbf{d}$ is jointly Gaussian,

$$p\big(\mathbf{u}(\mathbf{d},\boldsymbol{\theta}) \,\big|\, \mathbf{f}_{1:n} - \mathbf{m}_0^f(\mathbf{s}_{1:n}), \mathbf{u}_a, \Psi_n\big) = \mathcal{N}_T\left(\mathbf{m}_n(\mathbf{t}), \mathcal{C}_n(\mathbf{d},\mathbf{d})\right),$$

where $\mathbf{m}_n$ and $\mathcal{C}_n$ are defined in (3.13). Similarly, the conditional density of the derivative computed at $\mathbf{d}$ becomes,

$$p\big(\dot{\mathbf{u}}(\mathbf{d},\boldsymbol{\theta}) \,\big|\, \mathbf{f}_{1:n} - \mathbf{m}_0^f(\mathbf{s}_{1:n}), \mathbf{u}_a, \Psi_n\big) = \mathcal{N}_T\left(\mathbf{m}_n^f(\mathbf{d}), \mathcal{C}_n^f(\mathbf{d},\mathbf{d})\right).$$

where $\mathbf{m}_n^f$ and $\mathcal{C}_n^f$ are defined in (3.7). As a consequence, estimation only requires a finite number of matrix operations if the convolutions RR, QR, RQ, and QQ can be obtained analytically (see Chapter 6).

Equation (3.15) suggests the probabilistic solution can be utilized as an alternative to a numerical solution approximation and associated error analysis, with prediction replacing deterministic interpolation. There just remains the question of how to obtain noisy evaluations of the derivative. In the following chapter we provide a detailed description of a suitable probabilistic algorithm and show that it has desirable properties.

Chapter 4

Probabilistic Solution of Differential Equations

In Chapter 3, we presented a Gaussian process model for the DE solution given a finite-dimensional set of realizations, $\mathbf{f}_{1:n} = [\mathbf{f}_1, \cdots, \mathbf{f}_n]^\mathsf{T} \in M^{n,P}(\mathbb{R})$, of the derivative process over the discrete mesh with vertices $\mathbf{s}_{1:n} = [s_1, \cdots, s_n]^\mathsf{T} \in \mathscr{D}^n$. In this chapter we show how to generate realizations, $\mathbf{f}_{1:n}$, from the model when the solution and its derivative are unknown. Based on this sequential approach, we develop probabilistic solutions for P-dimensional ODE problems (2.1), (2.5), (2.6), and (2.8), as well as the P-dimensional PDE boundary value problem (2.10). For each case, we outline a sampling algorithm for generating realizations from the joint density of the predicted state, $\mathbf{u}(\mathbf{t}, \boldsymbol{\theta})$, $\mathbf{t} \in \mathscr{D}^T$ and vector field evaluations, $\mathbf{f}_{1:N}$,

$$p\big(\mathbf{u}(\mathbf{t}, \boldsymbol{\theta}), \mathbf{f}_{1:N} \big| \boldsymbol{\theta}, \mathbf{u}_a, \boldsymbol{\Psi}_N\big) = p\big(\mathbf{u}(\mathbf{t}, \boldsymbol{\theta}) \big| \mathbf{f}_{1:N}, \boldsymbol{\theta}, \mathbf{u}_a, \boldsymbol{\Psi}_N\big)\, p\big(\mathbf{f}_{1:N} \big| \boldsymbol{\theta}, \mathbf{u}_a, \boldsymbol{\Psi}_N\big), \tag{4.1}$$

where the two terms on the right hand side represent the probability density of the probabilistic solution and the auxiliary vector of field evaluations, respectively. We also suggest a recursive formulation of the proposed algorithms, which introduces computational efficiencies, provides intuitive insight about iterative updating, and is used to show that the probabilistic solution of a Lipschitz-continuous ODE initial value problem is consistent for the unique solution satisfying the system under standard regularity conditions. Finally, we illustrate our methodology through a number of challenging forward problems described in

Chapter 2.

4.1 Solving ODE initial value problems

Our goal is to generate a sequence of derivative realizations, $\mathbf{f}_{1:N}$, upon which we may condition our inference of the solution of a system of differential equations. Moreover, we must generate $\mathbf{f}_{1:N}$ in a completely model-based way, without the availability of any experimental measurements of the states, or any prior knowledge of the true solution or suitable approximation. As hinted in the introduction, we may consider these realizations to be auxiliary variables that extract information from the model sequentially.

4.1.1 Generating derivative realizations from the model

Suppose that at time step $(n+1), 1 \leq n < N$, we have access to n derivative realizations, $\mathbf{f}_{1:n}$, corresponding to the ordered knots $\mathbf{s}_{1:n}$. Conditioned on these, and according to the model presented in Chapter 3, we can obtain a closed form predictive distribution μ_n for the solution that admits sampling. We then generate a realization, $\tilde{\mathbf{u}}_n\big(s_{n+1}, \boldsymbol{\theta}\big)$, of the solution state at the next defined knot s_{n+1} and map the realization to the derivative space by using the vector field transformation,

$$\mathbf{f}_{n+1} = f_{\boldsymbol{\theta}}\big(s_{n+1}, \tilde{\mathbf{u}}(s_{n+1}, \boldsymbol{\theta})\big).$$

In a fundamental difference with numerical solvers, our model accounts for the fact that the derivative realization $\mathbf{f}_{n+1}$ is measured with error (arising from using a previously estimated state). Indeed, we are able to incorporate this uncertainty into each subsequent posterior solution by parameterizing the error model (3.1) for $\mathbf{f}_{n+1}$ using the variance $\mathcal{C}_n^f(s_{n+1}, s_{n+1})$. We can now update the estimated state given the newly generated derivative observation, $\mathbf{f}_{n+1}$, and update the covariance of the error model (3.1) as follows:

$$\Lambda_{n+1} = \operatorname{diag}\big(\mathcal{C}_0^f(s_1, s_1), \ldots, \mathcal{C}_n^f(s_{n+1}, s_{n+1})\big). \tag{4.2}$$

Once all N derivative realizations are obtained, we can make predictions about any of the P solution states at an arbitrary collection of evaluation points, $\mathbf{t} \in \mathscr{D}^T$. This procedure is described in Algorithm 1 for the ODE initial value problem (2.1), using the notation

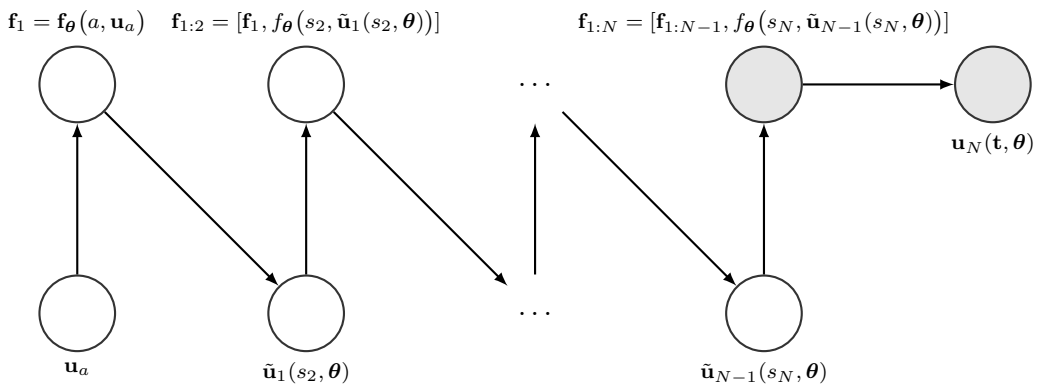

Figure 4.1: *Directed acyclic graph diagram for Algorithm 1, producing a sample from the probability density* $p\big(\mathbf{u}_N(\mathbf{t}, \boldsymbol{\theta}), \mathbf{f}_{1:N} \big| \boldsymbol{\theta}, \mathbf{u}_a, \Psi_N\big)$. *The grey nodes represent values that are returned by the algorithm, and all others are discarded.*

$\mathbf{m}_n$ and $\mathcal{C}_n$ defined in (3.12, 3.13). We characterize the error in the derivative realizations by defining the covariance matrix Λ_n in terms of the variance of the step-ahead predictive posterior density for the derivatives as shown in (4.2). This algorithm is also illustrated graphically in Figure 4.1.

In Section 4.1.4 we will show that the sequential probabilistic solution generated via Algorithm 1 is consistent for the unique solution satisfying the IVP (2.1). The recursive formulation used in the proof, which allows efficient implementation of Algorithm 1, is developed in Section 4.1.3.

Probabilistic solution of the Lorenz system

Figure 4.2 shows 100 realizations from the probabilistic solution of the Lorenz system with model parameters $\boldsymbol{\theta} = (10, 8/3, 28)$ and initial states $\mathbf{u}_a = (-11, -5, 38)$. The probabilistic solution is obtained by discretizing the interval $t \in [0, 30]$ by an equally-spaced grid of size $N = 3000$. The squared exponential covariance is chosen for this application based on our assumption that the solution is infinitely-differentiable. We set the length-scale in each dimension to twice the step size, effectively giving largest weight to the latest generated derivative realization. The prior precision is set to the low value of $\alpha = 10^{-2}\,[1, 1, 1]^\mathsf{T}$ units, reflecting our prior knowledge that the system exhibits chaotic dynamics.

Algorithm 1 Sample a probabilistic IVP solution from $p\big(\mathbf{u}(\mathbf{t},\boldsymbol{\theta}),\mathbf{f}_{1:N}\big|\boldsymbol{\theta},\mathbf{u}_a,\Psi_n\big)$

Initialize $\mathbf{f}_1 = f_{\boldsymbol{\theta}}(a,\mathbf{u}_a)$ and $\mathcal{C}_0(s_1,s_1)=0$;

for step number $n = 1 : N-1$ **do**

for state $p = 1 : P$ **do**

Sample step-ahead realization $\tilde{\mathbf{u}}^{(p)}(s_{n+1},\boldsymbol{\theta})$ from the predictive distribution for state p,

$$\tilde{\mathbf{u}}^{(p)}(s_{n+1}) \sim p\big(\mathbf{u}^{(p)}(s_{n+1},\boldsymbol{\theta})\big|\boldsymbol{\theta},\mathbf{f}^{(p)}_{1:n},\mathbf{u}_a,\Psi_n\big) = \mathcal{N}\big(\mathbf{m}^{(p)}_n(s_{n+1}),\mathcal{C}^{(p)}_n(s_{n+1},s_{n+1})\big);$$

end for

Compute next derivative observation with mean $\mathbf{f}_{n+1} = f_{\boldsymbol{\theta}}(s_{n+1},\tilde{\mathbf{u}}(s_{n+1},\boldsymbol{\theta}))$ and variance $\mathcal{C}^{f(p)}_n(s_{n+1},s_{n+1})$;

end for

for state $p = 1 : P$ **do**

Sample a realization, $\mathbf{u}^{(p)}(\mathbf{t},\boldsymbol{\theta})$, of the solution from the conditional distribution for state p at the chosen points $\mathbf{t} \in [a,b]^T$,

$$\mathbf{u}^{(p)}(\mathbf{t},\boldsymbol{\theta}) \sim p\big(\mathbf{u}^{(p)}(\mathbf{t},\boldsymbol{\theta})\big|\boldsymbol{\theta},\mathbf{f}^{(p)}_{1:N},\mathbf{u}_a,\Psi_n\big) = \mathcal{N}\big(\mathbf{m}^{(p)}_N(\mathbf{t}),\mathcal{C}^{(p)}_N(\mathbf{t},\mathbf{t})\big);$$

end for

Return $\mathbf{u}(\mathbf{t},\boldsymbol{\theta}),\mathbf{f}_{1:N}$.

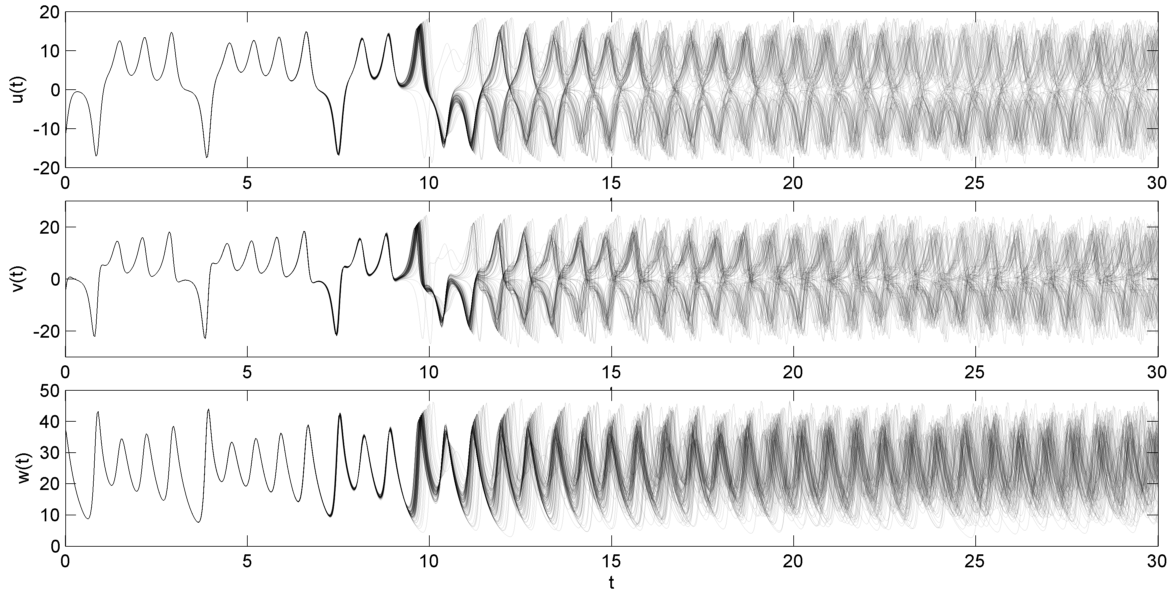

Figure 4.2: *Sample of 100 realizations from the probabilistic solution for the Lorenz system under a fixed initial state.*

4.1.2 Relationship with numerical solvers

Interestingly, many classical numerical solvers can be interpreted from this probabilistic perspective. Instead of providing a probability measure on the a space of functions, they instead yield a functional point estimate of the DE solution. This can be achieved by Rao-Blackwellizing the probabilistic solution at each step of Algorithm 1,

$$\mathbf{u}_n(s_{n+1}) = \mathrm{E}\big(\mathbf{u}(\cdot, \boldsymbol{\theta}) \,|\, \boldsymbol{\theta}, \mathbf{f}_{1:n}, \mathbf{u}_a, \Psi_n\big),$$

while assuming noise-free derivative realizations $\mathbf{f}_{1:n}$, by letting $\boldsymbol{\Lambda}_n = 0$ for all $1 \leq n \leq N$. Under these assumptions, the probabilistic solver becomes a k-step numerical radial basis function quadrature method with bases given by the eigenfunctions of the covariance $\mathcal{C}_0$. The number of steps is determined by the length-scale[1]. Using covariance functions with unbounded support results in a more general multi-step solver, which gives positive weight to all past derivative realizations, with weights decaying towards zero at rates that depend

[1]for example, under a covariance function with bounded support of length 2λ and fixed step size h, the number of steps in the algorithm becomes $k = \lceil \lambda / h \rceil$.

on the choice of covariance.

4.1.3 Recursive formulation of probabilistic solution

In this section we introduce two results. Lemma 4.1.1 provides a recursive formulation for the probabilistic solution of the IVP (2.1) generated via Algorithm 1. This lemma is an important part of the proof of consistency in Section 4.1.4. The related result in Lemma 4.1.2 allows us to avoid computationally expensive matrix inversions in the algorithmic implementation.

We denote the probabilistic solution and its derivative obtained after n solver iterations by $\mathbf{u}_n(t, \boldsymbol{\theta})$ and $\dot{\mathbf{u}}_n(t, \boldsymbol{\theta})$ respectively, and derivative realizations by:

$$\mathbf{f}_{1:n} = \left[f_{\boldsymbol{\theta}}\big(a, \mathbf{u}_a\big), f_{\boldsymbol{\theta}}\big(s_2, \tilde{\mathbf{u}}_1(s_2, \boldsymbol{\theta})\big), \cdots, f_{\boldsymbol{\theta}}\big(s_n, \tilde{\mathbf{u}}_{n-1}(s_n, \boldsymbol{\theta})\big)\right]^{\mathsf{T}},$$

where $\tilde{\mathbf{u}}_n(t, \boldsymbol{\theta})$ denotes a realization of the probabilistic solution $\mathbf{u}_n(t, \boldsymbol{\theta})$ at time $t \in \mathscr{D}$.

Lemma 4.1.1. *The probabilistic IVP solution and its derivative at the nth iteration of Algorithm 1 can be expressed in terms of the mean and covariance computed in the $(n-1)$st iteration. They are related by the expressions:*

$$\begin{aligned}
\mathbf{m}_n(t) &= \mathbf{m}_0(t) + \mathbf{m}_{n-1}(t) + (\mathbf{f}_n - \mathbf{m}_0^f(s_n) - \mathbf{m}_{n-1}^f(s_n)) \textstyle\int_a^t \mathcal{C}_{n-1}^f(x, s_n)dx / 2\mathcal{C}_{n-1}^f(s_n, s_n) \\
\mathbf{m}_n^f(t) &= \mathbf{m}_0^f(t) + \mathbf{m}_{n-1}^f(t) + (\mathbf{f}_n - \mathbf{m}_0^f(s_n) - \mathbf{m}_{n-1}^f(s_n))\, \mathcal{C}_{n-1}^f(t, s_n) / 2\mathcal{C}_{n-1}^f(s_n, s_n) \\
\mathcal{C}_n(t, v) &= \mathcal{C}_{n-1}(t, v) - \mathcal{C}_{n-1}(t, s_n)\, \mathcal{C}_{n-1}(s_n, v) / 2\mathcal{C}_{n-1}^f(s_n, s_n) \\
\mathcal{C}_n^f(t, v) &= \mathcal{C}_{n-1}^f(t, v) - \mathcal{C}_{n-1}^f(t, s_n)\, \mathcal{C}_{n-1}^f(s_n, v) / 2\mathcal{C}_{n-1}^f(s_n, s_n).
\end{aligned}$$

Furthermore, the matrix $B_n^{-1} = (\Lambda_n + RR(\mathbf{s}_{1:n}, \mathbf{s}_{1:n}))^{-1}$ can be written in block form in terms of B_{n-1}^{-1} (row and column indices are denoted in brackets),

$$\begin{aligned}
B^{-1}_{n_{(1:n-1,1:n-1)}} &= B_{n-1}^{-1}\left(2\mathcal{C}_{n-1}^f(s_n, s_n) + RR(\mathbf{s}_{1:n-1}, s_n) RR(s_n, \mathbf{s}_{1:n-1}) B_{n-1}^{-1}\right) / 2\mathcal{C}_{n-1}^f(s_n, s_n) \\
B^{-1}_{n_{(1:n-1,n)}} &= -B_{n-1}^{-1} RR(\mathbf{s}_{1:n-1}, s_n) / 2\mathcal{C}_{n-1}^f(s_n, s_n) \\
B^{-1}_{n_{(n,1:n-1)}} &= -RR(s_n, \mathbf{s}_{1:n-1}) B_{n-1}^{-1} / 2\mathcal{C}_{n-1}^f(s_n, s_n) \\
B^{-1}_{n_{(n,n)}} &= 1 / 2\mathcal{C}_{n-1}^f(s_n, s_n),
\end{aligned}$$

starting from $B_1^{-1} = 1/RR(s_1, s_1)$ and $\mathcal{C}_0^f(s_1, s_1) = 0$.

Proof. We use the fact that B_n is a non-negative symmetric partitioned matrix to write its inverse in the block form:

$$\mathrm{B}_n^{-1} \equiv (\Lambda_n + \mathrm{RR}(\mathbf{s}_{1:n}, \mathbf{s}_{1:n}))^{-1} = \begin{bmatrix} \mathrm{B}_{n-1} & \mathrm{RR}(\mathbf{s}_{1:n-1}, s_n) \\ \mathrm{RR}(s_n, \mathbf{s}_{1:n-1}) & \mathcal{C}_{n-1}^f(s_n, s_n) + \mathrm{B}_1 \end{bmatrix}^{-1}$$

$$= \frac{1}{2\mathcal{C}_{n-1}^f(s_n, s_n)} \begin{bmatrix} \mathrm{B}_{n-1}^{-1}\left(2\mathcal{C}_{n-1}^f(s_n, s_n) + \mathrm{RR}(\mathbf{s}_{1:n-1}, s_n)\mathrm{RR}(s_n, \mathbf{s}_{1:n-1})\mathrm{B}_{n-1}^{-1}\right) & -\mathrm{B}_{n-1}^{-1}\mathrm{RR}(\mathbf{s}_{1:n-1}, s_n) \\ -\mathrm{RR}(s_n, \mathbf{s}_{1:n-1})\mathrm{B}_{n-1}^{-1} & 1 \end{bmatrix},$$

(see for example, Rohde, 1965), starting with the base case:

$$\mathrm{B}_1^{-1} = \left(\mathcal{C}_0^f(s_1, s_1) + \mathrm{RR}(s_1, s_1)\right)^{-1} = 1/\mathrm{RR}(s_1, s_1).$$

Using this and the definition of the mean and covariance of the probabilistic solution and its derivative obtained in Section 3.2, we obtain the expressions,

$$\begin{aligned}
\mathbf{m}_n(t) &= \mathbf{m}_0(t) + \mathrm{QR}(t, \mathbf{s}_{1:n-1})\mathrm{B}_{n-1}^{-1}(\mathbf{f}_{1:n-1} - \mathbf{m}_0^f(\mathbf{s}_{1:n-1})) \\
&\quad + \big\{\mathrm{QR}(t, \mathbf{s}_{1:n-1})\mathrm{B}_{n-1}^{-1}\mathrm{RR}(\mathbf{s}_{1:n-1}, s_n)\mathrm{RR}(s_n, \mathbf{s}_{1:n-1})\mathrm{B}_{n-1}^{-1}(\mathbf{f}_{1:n-1} - \mathbf{m}_0^f(\mathbf{s}_{1:n-1})) \\
&\quad - \mathrm{QR}(t, s_n)\mathrm{RR}(s_n, \mathbf{s}_{1:n-1})\mathrm{B}_{n-1}^{-1}(\mathbf{f}_{1:n-1} - \mathbf{m}_0^f(\mathbf{s}_{1:n-1})) \\
&\quad - \mathrm{QR}(t, \mathbf{s}_{1:n-1})\mathrm{B}_{n-1}^{-1}\mathrm{RR}(\mathbf{s}_{1:n-1}, s_n)(\mathbf{f}_n - \mathbf{m}_0^f(s_n)) \\
&\quad + \mathrm{QR}(t, s_n)(\mathbf{f}_n - \mathbf{m}_0^f(s_n))\big\}/2\mathcal{C}_{n-1}^f(s_n, s_n) \\
&= \mathbf{m}_{n-1}(t) + (\mathbf{f}_n - \mathbf{m}_0^f(s_n) - \mathbf{m}_{n-1}^f(s_n)) \int_a^t \mathcal{C}_{n-1}^f(x, s_n)\mathrm{d}x/2\mathcal{C}_{n-1}^f(s_n, s_n),
\end{aligned}$$

$$\begin{aligned}
\mathbf{m}_n^f(t) &= \mathbf{m}_0(t) + \mathrm{RR}(t, \mathbf{s}_{1:n-1})\mathrm{B}_{n-1}^{-1}(\mathbf{f}_{1:n-1} - \mathbf{m}_0^f(\mathbf{s}_{1:n-1})) \\
&\quad + \big\{\mathrm{RR}(t, \mathbf{s}_{1:n-1})\mathrm{B}_{n-1}^{-1}\mathrm{RR}(\mathbf{s}_{1:n-1}, s_n)\mathrm{RR}(s_n, \mathbf{s}_{1:n-1})\mathrm{B}_{n-1}^{-1}(\mathbf{f}_{1:n-1} - \mathbf{m}_0^f(\mathbf{s}_{1:n-1})) \\
&\quad - \mathrm{RR}(t, s_n)\mathrm{RR}(s_n, \mathbf{s}_{1:n-1})\mathrm{B}_{n-1}^{-1}(\mathbf{f}_{1:n-1} - \mathbf{m}_0^f(\mathbf{s}_{1:n-1})) \\
&\quad - \mathrm{RR}(t, \mathbf{s}_{1:n-1})\mathrm{B}_{n-1}^{-1}\mathrm{RR}(\mathbf{s}_{1:n-1}, s_n)(\mathbf{f}_n - \mathbf{m}_0^f(s_n)) \\
&\quad + \mathrm{RR}(t, s_n)(\mathbf{f}_n - \mathbf{m}_0^f(s_n))\big\}/2\mathcal{C}_{n-1}^f(s_n, s_n) \\
&= \mathbf{m}_{n-1}^f(t) + (\mathbf{f}_n - \mathbf{m}_0^f(s_n) - \mathbf{m}_{n-1}^f(s_n))\, \mathcal{C}_{n-1}^f(t, s_n)/2\mathcal{C}_{n-1}^f(s_n, s_n),
\end{aligned}$$

$$
\begin{aligned}
\mathcal{C}_n^f(t,v) &= \mathrm{RR}(t,v) - \mathrm{RR}(t,\mathbf{s}_{1:n-1})\mathrm{B}_{n-1}^{-1}\mathrm{RR}(\mathbf{s}_{1:n-1},v) \\
&\quad - \mathrm{RR}(t,\mathbf{s}_{1:n-1})\mathrm{B}_{n-1}^{-1}\mathrm{RR}(\mathbf{s}_{1:n-1},s_n)\mathrm{RR}(s_n,\mathbf{s}_{1:n-1})\mathrm{B}_{n-1}^{-1}\mathrm{RR}(\mathbf{s}_{1:n-1},v)/2\mathcal{C}_{n-1}^f(s_n,s_n) \\
&\quad + \mathrm{RR}(t,s_n)\mathrm{RR}(s_n,\mathbf{s}_{1:n-1})\mathrm{B}_{n-1}^{-1}\mathrm{RR}(\mathbf{s}_{1:n-1},v)/2\mathcal{C}_{n-1}^f(s_n,s_n) \\
&\quad + 2\mathcal{C}_{n-1}^f(s_n,s_n)\mathrm{RR}(t,\mathbf{s}_{1:n-1})\mathrm{B}_{n-1}^{-1}\mathrm{RR}(\mathbf{s}_{1:n-1},s_n)\mathrm{RR}(s_n,v)/2\mathcal{C}_{n-1}^f(s_n,s_n) \\
&\quad - \mathrm{RR}(t,s_n)\mathrm{RR}(s_n,v)/2\mathcal{C}_{n-1}^f(s_n,s_n) \\
&= \mathcal{C}_{n-1}^f(t,v) - \mathcal{C}_{n-1}^f(t,s_n)\ \mathcal{C}_{n-1}^f(s_n,v)/2\mathcal{C}_{n-1}^f(s_n,s_n),
\end{aligned}
$$

$$
\begin{aligned}
\mathcal{C}_n(t,v) &= \mathrm{QQ}(t,v) - \mathrm{QR}(t,\mathbf{s}_{1:n-1})\mathrm{B}_{n-1}^{-1}\mathrm{RQ}(\mathbf{s}_{1:n-1},v) \\
&\quad - \mathrm{QR}(t,\mathbf{s}_{1:n-1})\mathrm{B}_{n-1}^{-1}\mathrm{RR}(\mathbf{s}_{1:n-1},s_n)\mathrm{RR}(s_n,\mathbf{s}_{1:n-1})\mathrm{B}_{n-1}^{-1}\mathrm{RQ}(\mathbf{s}_{1:n-1},v)/2\mathcal{C}_{n-1}^f(s_n,s_n) \\
&\quad + \mathrm{QR}(t,s_n)\mathrm{RR}(s_n,\mathbf{s}_{1:n-1})\mathrm{B}_{n-1}^{-1}\mathrm{RQ}(\mathbf{s}_{1:n-1},v)/2\mathcal{C}_{n-1}^f(s_n,s_n) \\
&\quad + \mathrm{QR}(t,\mathbf{s}_{1:n-1})\mathrm{B}_{n-1}^{-1}\mathrm{RR}(\mathbf{s}_{1:n-1},s_n)\mathrm{RQ}(s_n,v)/2\mathcal{C}_{n-1}^f(s_n,s_n) \\
&\quad - \mathrm{QR}(t,s_n)\mathrm{RQ}(s_n,v)/2\mathcal{C}_{n-1}^f(s_n,s_n) \\
&= \mathcal{C}_{n-1}(t,v) - \mathcal{C}_{n-1}(t,s_n)\ \mathcal{C}_{n-1}(s_n,v)/2\mathcal{C}_{n-1}^f(s_n,s_n).
\end{aligned}
$$

□

Lemma 4.1.2. *The step-ahead predictive probabilistic solution at the nth step can be obtained by using the recursion,*

$$
\begin{aligned}
\mathbf{m}_n(\mathbf{s}_{n+1}) &= \mathbf{m}_0(\mathbf{s}_{n+1}) + \mathbf{m}_{n-1}(\mathbf{s}_{n+1}) \\
&\quad + (\mathbf{f}_n - \mathbf{m}_0^f(s_n) - \mathbf{m}_{n-1}^f(s_n)) \textstyle\int_a^{s_{n+1}} \mathcal{C}_{n-1}^f(x,s_n)dx/2\mathcal{C}_{n-1}^f(s_n,s_n) \\
\mathcal{C}_n^f(s_{n+1},s_{n+1}) &= \mathcal{C}_{n-1}^f(s_{n+1},s_{n+1}) - (\mathcal{C}_{n-1}^f(s_{n+1},s_n))^2/2\mathcal{C}_{n-1}^f(s_n,s_n),
\end{aligned}
$$

starting with the base case:

$$
\begin{aligned}
B_1^{-1} &= 1/RR(s_1,s_1), \\
\mathcal{C}_1^f(s_2,s_2) &= RR(s_2,s_2) - RR(s_2,s_1)\ B_1^{-1}RR(s_1,s_2), \\
\mathbf{m}_1(s_2) &= \mathbf{m}_0(s_2) + QR(s_2,s_1)\ B_1^{-1}(f(s_1,\mathbf{u}_a) - \mathbf{m}_0^f(s_1)).
\end{aligned}
$$

Proof. The proof follows by directly applying Lemma 4.1.1 and using the fact that the Gaussian measure is uniquely defined by its mean and covariance (see Theorem 3.1.2).

□

Computational considerations

The iterative smoothing step in Algorithm 1 requires inverting the $n \times n$ matrix, B_n, for every $1 \leq n \leq N$, which quickly becomes computationally expensive. Therefore we recommend avoiding costly matrix inversions by instead updating the matrix inverse, B_n^{-1}, at each iteration via Lemmas 4.1.1 and 4.1.2 using output obtained in the previous algorithm iteration. Additionally, computational efficiency can further be increased by using bounded support kernel functions, which render the Toeplitz matrix $\mathrm{RR}(\mathbf{s}_{1:n}, \mathbf{s}_{1:n})$ sparse, reducing the number of matrix operations required for the inversion of B_n.

For a fixed grid $\mathbf{s}$ and given hyperparameters, α and λ, the inverse matrix B_n^{-1} and the derivative covariance matrix $\mathcal{C}_n^f(s_{n+1}, s_{n+1})$ may be stored and reused when many evaluations of Algorithm 1 are required[2] (e.g., when evaluating the posterior distribution of model parameters θ from observed data).

4.1.4 Posterior consistency

We have described how to infer the unknown solution to the initial value problem (2.1) with Lipschitz-continuous vector field $f_{\boldsymbol{\theta}} : [a, b] \times \mathbb{R}^P \to \mathbb{R}^P$, based on derivative information generated sequentially from the model. We now show that the resulting probabilistic solution converges in L^1 to the true solution satisfying (2.1). The result is obtained for the case of IVPs, but also extends to the probabilistic solutions of ODE and PDE problems that are based on Algorithm 1, which will be presented in the following sections.

Theorem 4.1.3. *The probabilistic solution obtained using Algorithm 1 for the initial value problem (2.1) on $[a, b]$ with Lipschitz continuous vector field $f_{\boldsymbol{\theta}} : [a, b] \times \mathbb{R}^p \to \mathbb{R}^p$, converges in L^1 to the unique solution satisfying (2.1) if the solution is continuously differentiable and its derivative lies in the function space spanned by the eigenfunctions of the covariance operator $\mathcal{C}_0^f$.*

[2]The reader is also referred to the related discussion of ensemble MCMC in Neal (2011) for sampling from mixture distributions while viewing function evaluations as "fast" parameters.

Proof. For clarity of exposition, we assume that $\mathbf{m}_0(t) = 0$ for all $t \in [a, b]$, and define $h = \max_{n=2,\ldots,N} \left(s_n - s_{n-1}\right)$ to be the maximum step length. We would like to show that the integrated Gaussian process $\{\mathbf{u}_n(t, \boldsymbol{\theta}), t \in [a, b]\}$, or probabilistic solution, is a consistent estimator of the solution when the vector $\mathbf{f}_{1:n}$ is built up sequentially using Algorithm 1 as $h \to 0$ and $\lambda, \alpha^{-1} = \big(o(h)\big)^P$. Solution updates are constructed using the recurrence derived in Lemma 4.1.1, where the mean update is the expected difference between the forward predicted derivative at the nth knot and the corresponding vector field evaluation, multiplied by the scaled cross-covariance $\frac{\mathcal{C}^f_{n-1}(t,s_n)}{2\mathcal{C}^f_{n-1}(s_n,s_n)}$. If we further consider the case of interpolation, the scaled cross-covariance becomes $\frac{\mathcal{C}^f_{n-1}(t,s_n)}{\mathcal{C}^f_{n-1}(s_n,s_n)}$.

Assume that the true solution $\mathbf{u}(\cdot, \boldsymbol{\theta})$ is continuously differentiable on [a,b]. Then, if the probabilistic solution $\mathbf{u}_{n-1}(\cdot, \boldsymbol{\theta})$ is mean-square differentiable on [a,b], we can write the difference between the expected probabilistic solution and the true solution in terms of their Taylor expansions around s_n (assuming bounded remainders):

$$
\begin{aligned}
&\mathrm{E}\left(\mathbf{u}_n(t, \boldsymbol{\theta}) - \mathbf{u}(t, \boldsymbol{\theta})\right) \\
&= \mathrm{E}\Big[\big\{\mathbf{u}_n(s_n, \boldsymbol{\theta}) - \mathbf{u}(s_n, \boldsymbol{\theta})\big\} + (t - s_n) \cdot \big\{\dot{\mathbf{u}}_n(s_n, \boldsymbol{\theta}) - f_{\boldsymbol{\theta}}\big(s_n, \mathbf{u}(s_n, \boldsymbol{\theta})\big)\big\} + O(h^2)\Big] \\
&= \mathrm{E}\Big[\mathbf{u}_{n-1}(s_n, \boldsymbol{\theta}) + \big\{f_{\boldsymbol{\theta}}\big(s_n, \mathbf{u}_{n-1}(s_n, \boldsymbol{\theta})\big) - \dot{\mathbf{u}}_{n-1}(s_n, \boldsymbol{\theta})\big\} \frac{\mathcal{C}_{n-1}(s_n, s_n)}{\mathcal{C}^f_{n-1}(s_n, s_n)} - \mathbf{u}(s_n, \boldsymbol{\theta}) \\
&\quad + (t - s_n) \cdot \big[\dot{\mathbf{u}}_{n-1}(s_n, \boldsymbol{\theta}) + \big\{f_{\boldsymbol{\theta}}\big(s_n, \mathbf{u}_{n-1}(s_n, \boldsymbol{\theta})\big) - \dot{\mathbf{u}}_{n-1}(s_n, \boldsymbol{\theta})\big\} \frac{\mathcal{C}^f_{n-1}(s_n, s_n)}{\mathcal{C}^f_{n-1}(s_n, s_n)} \\
&\quad - f_{\boldsymbol{\theta}}\big(s_n, \mathbf{u}(s_n, \boldsymbol{\theta})\big)\big] + O(h^2)\Big] \\
&= \mathrm{E}\Big[\mathbf{u}_{n-1}(s_n, \boldsymbol{\theta}) - \mathbf{u}(s_n, \boldsymbol{\theta}) + \big\{f_{\boldsymbol{\theta}}\big(s_n, \mathbf{u}_{n-1}(s_n, \boldsymbol{\theta})\big) - \dot{\mathbf{u}}_{n-1}(s_n, \boldsymbol{\theta})\big\} \frac{\mathcal{C}_{n-1}(s_n, s_n)}{\mathcal{C}^f_{n-1}(s_n, s_n)} \\
&\quad + (t - s_n) \cdot \big[f_{\boldsymbol{\theta}}\big(s_n, \mathbf{u}_{n-1}(s_n, \boldsymbol{\theta})\big) - f_{\boldsymbol{\theta}}\big(s_n, \mathbf{u}(s_n, \boldsymbol{\theta})\big)\big] + O(h^2)\Big], \qquad (4.3)
\end{aligned}
$$

where we have used the recursion from Lemma 4.1.1 to rewrite $\mathbf{u}_n(s_n, \boldsymbol{\theta})$ and $\dot{\mathbf{u}}(s_n, \boldsymbol{\theta})$. Since $(\mathbf{u}_n(t, \boldsymbol{\theta}) - \mathbf{u}(t, \boldsymbol{\theta}))$ is a normal random variable, its absolute value follows a folded normal distribution (see, for example, Leone et al., 1961) with mean,

$$
\mathrm{E}\big|\mathbf{u}_n(t, \boldsymbol{\theta}) - \mathbf{u}(t, \boldsymbol{\theta})\big| \qquad (4.4)
$$

$$= \mathrm{E}\big(\mathbf{u}_n(t) - \mathbf{u}(t,\boldsymbol{\theta})\big)\left\{1 + 2\Phi\left(\frac{\mathrm{E}(\mathbf{u}_n(t) - \mathbf{u}(t,\boldsymbol{\theta}))}{\sqrt{\mathcal{C}_n(t,t)}}\right)\right\} + \sqrt{\frac{2}{\pi}\,\mathcal{C}_n(t,t)}\exp\left\{-\frac{\mathrm{E}(\mathbf{u}_n(t,\boldsymbol{\theta}) - \mathbf{u}(t,\boldsymbol{\theta}))^2}{2\mathcal{C}_n(t,t)}\right\},$$

where Φ is the cdf of the standard normal distribution. Then we can bound the expected absolute difference as follows:

$$\begin{aligned}
\beta_n(t) &\equiv \mathrm{E}\big|\mathbf{u}_n(t,\boldsymbol{\theta}) - \mathbf{u}(t,\boldsymbol{\theta})\big| \\
&\leq |\mathrm{E}(\mathbf{u}_n(t,\boldsymbol{\theta}) - \mathbf{u}(t,\boldsymbol{\theta}))| + \sqrt{2\mathcal{C}_1(t,t)} \\
&\leq \beta_{n-1}(s_n) + |t - s_n| \cdot \mathrm{E}\big|f_{\boldsymbol{\theta}}\big(s_n, \mathbf{u}_{n-1}(s_n,\boldsymbol{\theta})\big) - f_{\boldsymbol{\theta}}\big(s_n, \mathbf{u}(s_n,\boldsymbol{\theta})\big)\big| \\
&\quad + \mathrm{E}\big|f_{\boldsymbol{\theta}}\big(s_n, \mathbf{u}_{n-1}(s_n,\boldsymbol{\theta})\big) - \dot{\mathbf{u}}_{n-1}(s_n,\boldsymbol{\theta})\big|\frac{\mathcal{C}_{n-1}(s_n,s_n)}{\mathcal{C}^f_{n-1}(s_n,s_n)} + \sqrt{2\mathcal{C}_1(t,t)},
\end{aligned}$$

where we have used equation (4.4), then equation (4.3) together with Jensen's inequality. The Lipschitz continuity of f and the fact that the expected value of $\big|f_{\boldsymbol{\theta}}\big(s_n, \mathbf{u}_{n-1}(s_n,\boldsymbol{\theta})\big) - \dot{\mathbf{u}}_{n-1}(s_n,\boldsymbol{\theta})\big|$ is bounded then implies:

$$\begin{aligned}
\beta_n(t) &\leq \beta_{n-1}(s_n) + L|t - s_n|\beta_{n-1}(s_n) + O\left(\frac{\mathcal{C}_{n-1}(s_n,s_n)}{2\mathcal{C}^f_{n-1}(s_n,s_n)}\right) + O(\sqrt{\mathcal{C}_1(t,t)}) \\
&= \beta_{n-1}(s_n)\,(1 + L|t - s_n|) + O(h^2),
\end{aligned}$$

Now we apply the Gronwall Lemma and the standard transformation used in the proofs of convergence for one-step methods (see, for example, Butcher, 2008, p.67-68) to obtain the inequality:

$$\beta_n(t) \leq \begin{cases} \beta_0(s_1) + hB(t-a), & L = 0, \\ \exp\{(t-a)L\}\beta_0(s_1) + \exp\{(t-a)L - 1\}hB/L, & L > 0, \end{cases}$$

where B is the constant upper bound on all the remainders. This expression tends to 0 as $\alpha^{-1}, \lambda, h \to 0$, since $\beta_0(s_1) = 0$. Then, taking the expectation of $\beta_n(t)$ with respect to the vector of derivative realizations, we obtain:

$$\mathrm{E}_{\mathbf{f}}\big|\mathbf{u}_n(t,\boldsymbol{\theta}) - \mathbf{u}(t,\boldsymbol{\theta})\big| = \mathrm{E}_{\mathbf{f}}\big[\mathrm{E}\{|\mathbf{u}_n(t,\boldsymbol{\theta}) - \mathbf{u}(t,\boldsymbol{\theta})|\}\big] \to 0, \quad \text{as } \alpha^{-1}, \lambda, h \to 0,$$

and the probabilistic solution $\mathbf{u}_n(\cdot,\boldsymbol{\theta})$ is consistent for $\mathbf{u}(\cdot,\boldsymbol{\theta})$.

□

To those who are familiar with the convergence arguments used in numerical analysis, the assumption that auxiliary parameters, λ and α^{-1}, associated with the solver should tend to zero with the step size may seem unclear. However, this assumption is analogous to maintaining a constant number of steps in a k-step numerical method regardless of the step size.

4.2 Solving ODE Boundary value problems

We begin this section by describing our probability model for the unknown solution of the mixed boundary value problem (2.6). We then use a variant of this method to obtain and sample from the probabilistic solution of the two-point boundary value problem (2.5).

Mixed boundary value problems require a different probabilistic solver formulation from the probabilistic IVP, as well as some care about the sampling algorithm. For the purpose of exposition, we restrict our attention to the MBVP (2.6) with $P = 2$ states, and boundary values $\big(\mathbf{u}^{(2)}(b, \boldsymbol{\theta}), \mathbf{u}^{(1)}(a, \boldsymbol{\theta})\big) = \big(\mathbf{u}_b^{(2)}, \mathbf{u}_a^{(1)}\big)$. Estimating the solution for this problem can be reduced to (i) estimation of the initial value for the second state, $\mathbf{u}^{(2)}(a, \boldsymbol{\theta})$, followed by (ii) estimation of the system solution given $\tilde{\mathbf{u}}^{(2)}(a, \boldsymbol{\theta})$. We note that the second stage is equivalent to solving an IVP with initial condition, $\mathbf{u}(a, \boldsymbol{\theta}) = \big(\mathbf{u}_a^{(1)}, \tilde{\mathbf{u}}^{(2)}(a, \boldsymbol{\theta})\big)$, where we again make the simplifying assumption that the states, $\mathbf{u}^{(i)}(\cdot, \boldsymbol{\theta})$, $i = 1, 2$, are conditionally independent given vector field evaluations, to write,

$$\mathbf{u}(\cdot, \boldsymbol{\theta}) \;\big|\; \mathbf{f}_{1:N}, [\mathbf{u}_a^{(1)}, \tilde{\mathbf{u}}^{(2)}(a, \boldsymbol{\theta})], \Psi_n \;\sim\; \mathcal{N}_1\big(\mathbf{m}_n, \mathcal{C}_n\big),$$

where $\mathbf{m}_n$ and $\mathcal{C}_n$ are defined in (3.12, 3.13), and the derivative realizations are,

$$\mathbf{f}_{1:n} = \big[f_{\boldsymbol{\theta}}\big(a, [\mathbf{u}_a^{(1)}, \tilde{\mathbf{u}}^{(2)}(a, \boldsymbol{\theta})]^{\mathsf{T}}\big), f_{\boldsymbol{\theta}}\big(s_2, \tilde{\mathbf{u}}_1(s_2, \boldsymbol{\theta})\big), \cdots, f_{\boldsymbol{\theta}}\big(s_n, \tilde{\mathbf{u}}_{n-1}(s_n, \boldsymbol{\theta})\big)\big]^{\mathsf{T}},$$

where $\tilde{\mathbf{u}}_n(t, \boldsymbol{\theta})$ denotes a sampled realization of the probabilistic solution, $\mathbf{u}_n(t, \boldsymbol{\theta})$, of the IVP obtained by setting $\mathbf{u}(a, \boldsymbol{\theta}) = [\mathbf{u}_a^{(1)}, \tilde{\mathbf{u}}^{(2)}(a, \boldsymbol{\theta})]$, while ignoring the endpoint constraint, $\mathbf{u}^{(2)}(b, \boldsymbol{\theta}) = \mathbf{u}_b^{(2)}$.

We propose to address the first part of the problem by treating the known boundary value, $\mathbf{u}_b^{(2)}$, of the second state, as a data point obtained from the model, with the following

likelihood:

$$\mathbf{u}_b^{(2)} \,|\, \mathbf{f}_{1:N}, [\mathbf{u}_a^{(1)}, \tilde{\mathbf{u}}^{(2)}(a, \boldsymbol{\theta})], \Psi_n \sim \mathcal{N}_1\big(\mathbf{m}_n(b), \mathcal{C}_n(b, b)\big), \tag{4.5}$$

where the predictive variance of the probabilistic solution at the endpoint boundary, $\mathcal{C}_n(b, b)$, is interpreted analogously to an endpoint mismatch tolerance in the numerical setting. The prior measure on the unknown second initial state, $\mathbf{u}^{(2)}(a, \boldsymbol{\theta})$, depends on our knowledge about the system[3].

We can now write the posterior distribution of the states, based on a mesh of size N, as follows:

$$\begin{aligned}
&\big[\mathbf{u}(\cdot, \boldsymbol{\theta}) \;\big|\; \mathbf{f}_{1:N}, [\mathbf{u}_b^{(2)}, \mathbf{u}_a^{(1)}], \Psi_N\big] \\
&\propto \big[\mathbf{u}_b^{(2)} \,|\, \mathbf{f}_{1:N}, [\mathbf{u}_a^{(1)}, \tilde{\mathbf{u}}^{(2)}(a, \boldsymbol{\theta})], \Psi_N\big] \;\big[\mathbf{u}(\cdot, \boldsymbol{\theta}) \;\big|\; \mathbf{f}_{1:N}, [\mathbf{u}_a^{(1)}, \tilde{\mathbf{u}}^{(2)}(a, \boldsymbol{\theta})], \Psi_N\big] \\
&\qquad \big[\mathbf{f}_{1:N} \;\big|\; [\mathbf{u}_a^{(1)}, \tilde{\mathbf{u}}^{(2)}(a, \boldsymbol{\theta})], \Psi_N\big] \;\big[\tilde{\mathbf{u}}^{(2)}(a, \boldsymbol{\theta})\big].
\end{aligned} \tag{4.6}$$

In contrast to the case of IVPs, the MBVP probabilistic solution distributed according to (4.6) will typically not be available analytically. However, any number of samples from it may be obtained via Monte Carlo. In fact, we can easily evaluate the likelihood (4.5) of the endpoint constraint of the first state, and the prior distribution on the unknown second initial state, while the second and third factors of the expression (4.6) can be obtained by forward-simulation from Algorithm 1.

Algorithm 2 describes the basic Metropolis-Hastings procedure for sampling from the probabilistic solution (4.6). An important consideration for solving MBVPs probabilistically is to sample efficiently from possibly multimodal posteriors in the initial value. In fact, MBVPs often have multiple solutions, whose number may not be known a priori. In such cases, there may be several disjoint regions of the state space where functions obey the DE model dynamics approximately. This multimodality in (4.5) translates into a multimodal posterior probabilistic solution, as shown on the left side of Figure 4.3. Therefore, we recommend using a population MCMC scheme, such as parallel tempering (Geyer, 1991), which can quickly identify and explore disjoint regions of high posterior probability.

[3]For example, if we know that the endpoint is equally likely to lie within a certain interval, we may use a uniform prior on that interval. Otherwise, a prior distribution with unbounded support should be used.

Algorithm 2 Draw K realizations from the probabilistic mixed BVP solution $p\big(\mathbf{u}(\mathbf{t},\boldsymbol{\theta}), \mathbf{f}_{1:N} \mid \boldsymbol{\theta}, \big(\mathbf{u}_b^{(2)}, \mathbf{u}_a^{(1)}\big), \Psi_N\big)$

Initialize $\tilde{\mathbf{u}}^{(2)}(a,\boldsymbol{\theta}), \mathbf{u}(\mathbf{t},\boldsymbol{\theta}), \mathbf{f}_{1:N}$;

for iteration $k = 1 : K$ **do**

Propose $\tilde{\mathbf{u}}^{(2)\star}(a,\boldsymbol{\theta}) \sim q(\tilde{\mathbf{u}}^{(2)\star}(a,\boldsymbol{\theta}) | \tilde{\mathbf{u}}^{(2)}(a,\boldsymbol{\theta}))$;

Conditionally simulate solution $\mathbf{u}^\star(\mathbf{t},\boldsymbol{\theta})$ and vector field realizations $\mathbf{f}_{1:N}^\star$ from the density $p\big(\mathbf{u}^\star(\mathbf{t},\boldsymbol{\theta}), \mathbf{f}_{1:N}^\star \mid \boldsymbol{\theta}, \big(\mathbf{u}_a^{(1)}, \tilde{\mathbf{u}}^{(2)\star}(a,\boldsymbol{\theta})\big), \Psi_N\big)$ via Algorithm 1;

Compute:

$$\rho\big(\tilde{\mathbf{u}}^{(2)}(a,\boldsymbol{\theta}), \mathbf{u}(\mathbf{t},\boldsymbol{\theta}), \mathbf{f}_{1:N} \to \tilde{\mathbf{u}}^{(2)\star}(a,\boldsymbol{\theta}), \mathbf{u}^\star(\mathbf{t},\boldsymbol{\theta}), \mathbf{f}_{1:N}^\star\big)$$
$$= \frac{q(\tilde{\mathbf{u}}^{(2)\star}(a,\boldsymbol{\theta}) | \tilde{\mathbf{u}}^{(2)}(a,\boldsymbol{\theta}))}{q(\tilde{\mathbf{u}}^{(2)}(a,\boldsymbol{\theta}) | \tilde{\mathbf{u}}^{(2)\star}(a,\boldsymbol{\theta}))} \frac{p(\tilde{\mathbf{u}}^{(2)\star}(a,\boldsymbol{\theta}))}{p(\tilde{\mathbf{u}}^{(2)}(a,\boldsymbol{\theta}))} \frac{p\big(\mathbf{u}_b^{(2)} \,|\, \mathbf{f}_{1:N}^\star, [\mathbf{u}_a^{(1)}, \tilde{\mathbf{u}}^{(2)\star}(a,\boldsymbol{\theta})], \Psi_N\big)}{p\big(\mathbf{u}_b^{(2)} \,|\, \mathbf{f}_{1:N}, [\mathbf{u}_a^{(1)}, \tilde{\mathbf{u}}^{(2)}(a,\boldsymbol{\theta})], \Psi_N\big)};$$

if $\min\big\{1, \rho\big\} > \mathrm{U}[0,1]$ **then**

Update $\tilde{\mathbf{u}}^{(2)}(a,\boldsymbol{\theta}) = \tilde{\mathbf{u}}^{(2)\star}(a,\boldsymbol{\theta})$;

Update $\mathbf{u}(\mathbf{t},\boldsymbol{\theta}) = \mathbf{u}^\star(\mathbf{t},\boldsymbol{\theta})$;

Update $\mathbf{f}_{1:N} = \mathbf{f}_{1:N}^\star$;

end if

Return $\mathbf{u}(\mathbf{t},\boldsymbol{\theta}), \mathbf{f}_{1:N}$.

end for

Next, let us consider the related question of solving a two-point boundary value problem (2.5) on the domain $\mathscr{D} = [a, b]$. For expositional simplicity, we consider a boundary value problem with one constraint located at each boundary of the domain for each of at most $M < P$ states, $\big(\mathbf{u}^{(i)}(a, \boldsymbol{\theta}), \mathbf{u}^{(i)}(b, \boldsymbol{\theta})\big) = \big(\mathbf{u}_a^{(i)}, \mathbf{u}_b^{(i)}\big)$, $i = 1, \ldots, M$[4].

We again treat the known boundary values, $\mathbf{u}_b^{(1)}, \ldots, \mathbf{u}_b^{(M)}$, as data points obtained from the model, assumed independent with likelihood,

$$\begin{aligned}
\mathbf{u}_b^{(1)} \,|\, \mathbf{f}_{1:N}, [\mathbf{u}_a^{(1)}, \ldots, \mathbf{u}_a^{(M)}, \tilde{\mathbf{u}}^{(M+1)}(a, \boldsymbol{\theta}), \ldots, \tilde{\mathbf{u}}^{(P)}(a, \boldsymbol{\theta})], \Psi_N &\sim \mathcal{N}_1\big(\mathbf{m}_N^{(1)}(b), \mathcal{C}_N^{(1)}(b, b)\big), \\
&\vdots \\
\mathbf{u}_b^{(M)} \,|\, \mathbf{f}_{1:N}, [\mathbf{u}_a^{(1)}, \ldots, \mathbf{u}_a^{(M)}, \tilde{\mathbf{u}}^{(M+1)}(a, \boldsymbol{\theta}), \ldots, \tilde{\mathbf{u}}^{(P)}(a, \boldsymbol{\theta})], \Psi_N &\sim \mathcal{N}_1\big(\mathbf{m}_N^{(M)}(b), \mathcal{C}_N^{(M)}(b, b)\big),
\end{aligned}$$

The posterior distribution of the states, based on a mesh of size N, differs from (4.6) and has the form:

$$\begin{aligned}
&\big[\mathbf{u}(\cdot, \boldsymbol{\theta}) \,\big|\, \mathbf{f}_{1:N}, \{\mathbf{u}_a^{(i)}, \mathbf{u}_b^{(i)}\}_{i=1,\ldots,M}, \Psi_N\big] \\
&\propto \big[\mathbf{u}_b^{(2)} \,|\, \mathbf{f}_{1:N}, [\mathbf{u}_a^{(1)}, \ldots, \mathbf{u}_a^{(M)}, \tilde{\mathbf{u}}^{(M+1)}(a, \boldsymbol{\theta}), \ldots, \tilde{\mathbf{u}}^{(P)}(a, \boldsymbol{\theta})], \Psi_N\big] \\
&\quad \big[\mathbf{u}(\cdot, \boldsymbol{\theta}) \,\big|\, \mathbf{f}_{1:N}, [\mathbf{u}_a^{(1)}, \ldots, \mathbf{u}_a^{(M)}, \tilde{\mathbf{u}}^{(M+1)}(a, \boldsymbol{\theta}), \ldots, \tilde{\mathbf{u}}^{(P)}(a, \boldsymbol{\theta})], \Psi_N\big] \\
&\quad \big[\mathbf{f}_{1:N} \,\big|\, [\mathbf{u}_a^{(1)}, \ldots, \mathbf{u}_a^{(M)}, \tilde{\mathbf{u}}^{(M+1)}(a, \boldsymbol{\theta}), \ldots, \tilde{\mathbf{u}}^{(P)}(a, \boldsymbol{\theta})], \Psi_N\big] \,\big[\tilde{\mathbf{u}}^{(2)}(a, \boldsymbol{\theta})\big]. \qquad (4.7)
\end{aligned}$$

Realizations from this posterior distribution can be obtained via Algorithm 3.

Probabilistic solution of the Lane-Emden mixed boundary value problem

We illustrate the probabilistic solution of a MBVP by solving the Lane-Emden model described in the introduction. Our goal is to obtain a Monte Carlo estimate of the unknown initial state $u(a, \boldsymbol{\theta})$ and the associated probabilistic solution for the system (2.7). As explained above, we treat the given boundary value u_b as a single data sample, with Gaussian observation error centered at the mean of probabilistic solution on $t = b$. The unknown initial state $\tilde{u}(a, \boldsymbol{\theta})$ is assigned a Gaussian prior with a mean of 1.5 and a standard deviation of $2\big|u_b - v_a\big|$. The probabilistic solver in this example uses a squared exponential covariance

[4]Note that the order of the states can be permuted without loss of generality.

Algorithm 3 Draw K realizations from the probabilistic two-point BVP solution $p\big(\mathbf{u}(\mathbf{t},\boldsymbol{\theta}), \mathbf{f}_{1:N} \mid \boldsymbol{\theta}, \{\mathbf{u}_a^{(i)}, \mathbf{u}_b^{(i)}\}_{i=1,\ldots,M}, \Psi_N\big)$

Initialize $\{\tilde{\mathbf{u}}^{(i)}(a,\boldsymbol{\theta})\}_{i=M+1,\ldots,P}, \mathbf{u}(\mathbf{t},\boldsymbol{\theta}), \mathbf{f}_{1:N}$;

for iteration $k = 1 : K$ **do**

Propose $\tilde{\mathbf{u}}^{(i)\star}(a,\boldsymbol{\theta}) \sim q(\tilde{\mathbf{u}}^{(i)\star}(a,\boldsymbol{\theta})|\tilde{\mathbf{u}}^{(i)}(a,\boldsymbol{\theta})), i = M+1,\ldots,P$;

Conditionally simulate $\mathbf{u}^\star(\mathbf{t},\boldsymbol{\theta})$ and vector field realizations $\mathbf{f}_{1:N}^\star$ from the density $p\big(\mathbf{u}^\star(\mathbf{t},\boldsymbol{\theta}), \mathbf{f}_{1:N}^\star \mid \boldsymbol{\theta}, [\mathbf{u}_a^{(1)},\ldots,\mathbf{u}_a^{(M)}, \tilde{\mathbf{u}}^{(M+1)}(a,\boldsymbol{\theta}),\ldots,\tilde{\mathbf{u}}^{(P)}(a,\boldsymbol{\theta})], \Psi_N\big)$ via Algorithm 1;

Compute:

$$\rho\big(\{\tilde{\mathbf{u}}^{(i)}(a,\boldsymbol{\theta})\}_{i=M+1,\ldots,P}, \mathbf{u}(\mathbf{t},\boldsymbol{\theta}), \mathbf{f}_{1:N} \to \{\tilde{\mathbf{u}}^{(i)\star}(a,\boldsymbol{\theta})\}_{i=M+1,\ldots,P}, \mathbf{u}^\star(\mathbf{t},\boldsymbol{\theta}), \mathbf{f}_{1:N}^\star\big)$$
$$= \prod_{i=M+1}^{P} \frac{q(\tilde{\mathbf{u}}^{(i)\star}(a,\boldsymbol{\theta})|\tilde{\mathbf{u}}^{(i)}(a,\boldsymbol{\theta}))}{q(\tilde{\mathbf{u}}^{(i)}(a,\boldsymbol{\theta})|\tilde{\mathbf{u}}^{(i)\star}(a,\boldsymbol{\theta}))} \frac{p(\tilde{\mathbf{u}}^{(i)\star}(a,\boldsymbol{\theta}))}{p(\tilde{\mathbf{u}}^{(i)}(a,\boldsymbol{\theta}))}$$
$$\frac{p\big(\mathbf{u}_b^{(i)} \,|\, \mathbf{f}_{1:N}^\star, [\mathbf{u}_a^{(1)},\ldots,\mathbf{u}_a^{(M)}, \tilde{\mathbf{u}}^{(M+1)\star}(a,\boldsymbol{\theta}),\ldots,\tilde{\mathbf{u}}^{(P)\star}(a,\boldsymbol{\theta})], \Psi_N\big)}{p\big(\mathbf{u}_b^{(i)} \,|\, \mathbf{f}_{1:N}, [\mathbf{u}_a^{(1)},\ldots,\mathbf{u}_a^{(M)}, \tilde{\mathbf{u}}^{(M+1)}(a,\boldsymbol{\theta}),\ldots,\tilde{\mathbf{u}}^{(P)}(a,\boldsymbol{\theta})], \Psi_N\big)};$$

if $\min\big\{1,\rho\big\} > \mathrm{U}[0,1]$ **then**

Update $\tilde{\mathbf{u}}^{(i)}(a,\boldsymbol{\theta}) = \tilde{\mathbf{u}}^{(i)\star}(a,\boldsymbol{\theta}), i = M+1,\ldots,P$;

Update $\mathbf{u}(\mathbf{t},\boldsymbol{\theta}) = \mathbf{u}^\star(\mathbf{t},\boldsymbol{\theta})$;

Update $\mathbf{f}_{1:N} = \mathbf{f}_{1:N}^\star$;

end if

Return $\mathbf{u}(\mathbf{t},\boldsymbol{\theta}), \mathbf{f}_{1:N}$.

end for

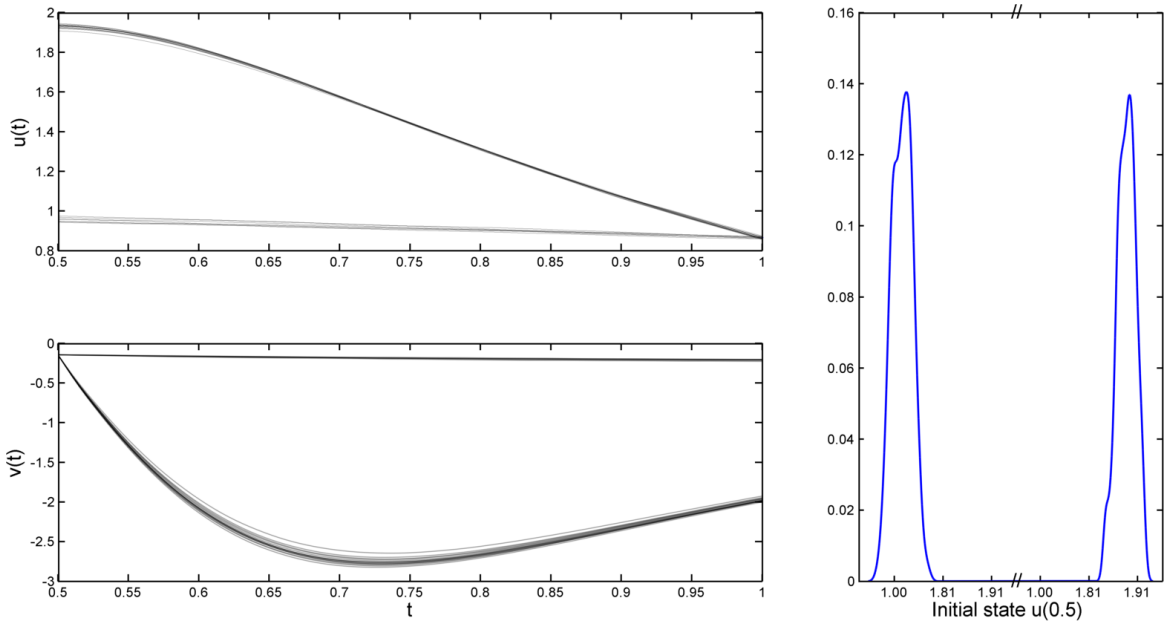

Figure 4.3: *Sample of 100 probabilistic solution realizations for states $u(\cdot, \boldsymbol{\theta})$ (left, above) and $v(\cdot, \boldsymbol{\theta})$ (left, below); the estimated marginal unnormalized log-density of the unknown initial state u_a (right).*

to model the solution on a grid of $N = 100$ equally-spaced solver knots. The length-scale is set to twice the step size and the prior precision is 1 unit. The left side of Figure 4.3 shows a sample from the probabilistic solution and identifies two high-density regions corresponding to distinct solutions. The right side of Figure 4.3 shows the estimated marginal unnormalized log-density of the unknown initial state u_a, highlighting two distinct regions of the state space where solutions may exist.

4.3 Solving ODE delay initial function problems

In this section, we outline a probabilistic solution method for the fixed delay initial function problem (2.8). For notational clarity, we consider a delay initial function problem with a single non-zero delay τ. We begin by partitioning the domain of integration, $\mathscr{D} = [a, b]$, into $I = \lceil (b-a)/\tau \rceil$ intervals of length τ and define the mesh,

$$\mathbf{s}^i = \left[s_1^i, \cdots, s_N^i\right], \quad i = 0, \ldots, I,$$

$$s_1^i = a + \tau(i-1),\ s_N^i = a + \tau i, \quad i = 0, \ldots, I,$$

with $\mathbf{s} = \left[\mathbf{s}^1, \cdots, \mathbf{s}^I\right]$. Again for notational simplicity, we use the same number, N, of mesh points over each interval (this can be generalized straightforwardly to any number $N_i > 2$ of mesh points per interval). Any variable pertaining to the ith interval, where $1 \leq i \leq I$, will be represented with the superscript i.

In the case where the initial function $\boldsymbol{\phi} : [a - \tau, a] \to \mathbb{R}^P$ in (2.8) is fully specified, we may obtain the initial value, $\mathbf{u}(a) = \boldsymbol{\phi}(a)$, directly from the initial function. If the initial function is known only at a finite set of nodes, $\mathbf{s}_{1:J}^0$, we first fit an interpolating Gaussian process to the initial function evaluations,

$$\boldsymbol{\phi} \,|\, \boldsymbol{\phi}(s_1^0), \ldots, \boldsymbol{\phi}(s_J^0), \Psi_J^0 \sim \mathcal{N}\big(\mathbf{m}_J^0, \mathcal{C}_J^0\big)$$

using auxiliary parameters $\Psi_J^0 = [\alpha^0, \lambda^0, R^0, \mathbf{s}_{1:J}^0]$ (see for example, Rasmussen and Williams, 2006). We then take the initial state, $\mathbf{u}(a) = \tilde{\boldsymbol{\phi}}(a)$, to be a realization of the estimated initial function. The uncertainty in the initial function generates uncertainty in the initial condition, which we encode in the state and derivative covariances by,

$$\mathcal{C}_0^1(a, a) = \mathcal{C}_N^0(a, a) + \mathcal{C}_N^0(a - \tau, a - \tau) + 2\mathcal{C}_N^0(a, a - \tau) \tag{4.8}$$

$$\mathcal{C}_0^{f1}(a, a) = \mathcal{C}_N^{f0}(a, a) + \mathcal{C}_N^{f0}(a - \tau, a - \tau) + 2\mathcal{C}_N^{f0}(a, a - \tau). \tag{4.9}$$

Given n interval i derivative realizations,

$$\mathbf{f}_{1:n}^i = \left[f_{\boldsymbol{\theta}}\big(s_1^i, \tilde{\mathbf{u}}_0^i(s_1^i, \boldsymbol{\theta}), \tilde{\mathbf{u}}_N^{i-1}(s_1^i - \tau, \boldsymbol{\theta})\big), \cdots, f_{\boldsymbol{\theta}}\big(s_n^i, \tilde{\mathbf{u}}_{n-1}^i(s_n^i, \boldsymbol{\theta}), \tilde{\mathbf{u}}_N^{i-1}(s_n^i - \tau, \boldsymbol{\theta})\big)\right]^{\mathsf{T}}$$

the predictive distribution also depends on the states evaluated on the preceding interval through the following probabilistic solution:

$$\mathbf{u}^i(\cdot, \boldsymbol{\theta}) \;\big|\; \mathbf{f}_{1:n}^i, \boldsymbol{\phi}, \Psi_n^i \;\sim\; \mathcal{N}\big(\mathbf{m}_k^i, \mathcal{C}_n^i\big)$$

where, $\Psi_n^i = [\alpha, \lambda, R, \mathbf{s}_{1:n}^i]$, and,

$$\mathbf{m}_n^i(t) = \mathbf{m}_N^{i-1}(s_1^i) + \mathrm{QR}(t, \mathbf{s}_{1:n}^i)\big(\boldsymbol{\Lambda}_n^i + \mathrm{RR}(\mathbf{s}_{1:n}^i, \mathbf{s}_{1:n}^i)\big)^{-1}\big(\mathbf{f}_{1:n}^i - \mathbf{m}_0^f(\mathbf{s}_{1:n}^i)\big), \tag{4.10}$$

$$\mathcal{C}_n^i(t, \tilde{t}) = \mathcal{C}_N^{i-1}(s_1^i, s_1^i) + \mathrm{QQ}(t, \tilde{t}) - \mathrm{QR}(t, \mathbf{s}_{1:n}^i)\big(\boldsymbol{\Lambda}_n^i + \mathrm{RR}(\mathbf{s}_{1:n}^i, \mathbf{s}_{1:n}^i)\big)^{-1}\mathrm{RQ}(\mathbf{s}_{1:n}^i, \tilde{t}), \tag{4.11}$$

$$\mathcal{C}_n^{fi}(t,\tilde{t}) = \mathcal{C}_N^{f(i-1)}(s_1^i, s_1^i) + \mathrm{RR}(t,\tilde{t}) - \mathrm{RR}(t,\mathbf{s}_{1:n}^i)\big(\mathbf{\Lambda}_n^i + \mathrm{RR}(\mathbf{s}_{1:n}^i,\mathbf{s}_{1:n}^i)\big)^{-1}\mathrm{RR}(\mathbf{s}_{1:n}^i,\tilde{t}), \tag{4.12}$$

$$\mathbf{\Lambda}_n^i = \mathrm{diag}\big(\mathcal{C}_0^{fi}(s_1^i,s_1^i),\cdots,\mathcal{C}_{n-1}^{fi}(s_n^i,s_n^i)\big). \tag{4.13}$$

This process is repeated for each of the $I = \lceil (b-a)/\tau \rceil$ intervals and one additional update is performed over the entire domain of integration,

$$\mathbf{u}(\cdot,\boldsymbol{\theta}) \mid \mathbf{f}_{1:NI}, \boldsymbol{\phi}, \Psi_{NI} \sim \mathcal{N}\big(\mathbf{m}_{NI}, \mathcal{C}_{NI}\big)$$

where $\Psi_{NI} = [\alpha, \lambda, R, \mathbf{s}]$, $\mathbf{f}_{NI} = \big[\mathbf{f}_{1:N}^1, \ldots, \mathbf{f}_{1:N}^I\big]^\mathsf{T}$, and $\mathbf{m}_{NI}, \mathcal{C}_{NI}$ are defined in (3.6), (3.7). in order to ensure continuity of the solution between intervals.

As before, the smoothness of the solution depends on the choice of the covariance structure. Therefore, we must account for second or higher derivative discontinuities by selecting a derivative covariance function whose eigenbases span a space of differentiable functions (e.g. the uniform kernel in Chapter 6 has this property).

Probabilistic solution of the oscillatory decay model with uncertain initial function

We illustrated in Chapter 2 that even in very simple cases, uncertainty in the initial function can have a substantial effect on the numerical solution. Now we illustrate our probabilistic approach, which quantification of both the uncertainty incurred in the discretization and any additional uncertainty associated with the input.

The first row of Figure 4.4 shows the analytical, numerical, and mean probabilistic solutions to problem (2.9) with fully known history $\phi(t) = 1,\ t \in [-1, 0]$. The probabilistic solution was obtained using a total of $N = 500$ equally spaced solver knots on $I = 10$ intervals $[(i-1)\tau, i\tau]$, $i = 1, \ldots, 10$.

Let us consider a modified version of problem (2.9) with history $\phi(t) = \sin(4\pi t)/4+1$ that is only partially specified, without error, over a set of six nodes. The second row of Figure 4.4 illustrates this case. The first step to solving such a problem approximately is to infer the initial function over the entire initial interval. For this we use an interpolating Gaussian process with square exponential covariance structure. The uncertainty expressed by its posterior distribution given the six nodes is accounted for in the probabilistic algorithm. Although in this case the numerical and probabilistic mean solutions give similar results, the

Algorithm 4 Sample a probabilistic DDE solution from $p\big(\mathbf{u}(\mathbf{t},\boldsymbol{\theta}),\mathbf{f}_{1:NI}\big|\boldsymbol{\theta},\boldsymbol{\phi},\Psi_{NI}\big)$

Initialize $\mathcal{C}_0^1(s_1^1,s_1^1),\mathcal{C}_0^{f1}(s_1^1,s_1^1)$ from (4.8-4.9), and set,

$$\mathbf{u}^0(\mathbf{s}_{1:N}^1-\tau,\boldsymbol{\theta})=\tilde{\boldsymbol{\phi}}(\mathbf{s}_{1:N}^1-\tau)$$

$$\mathbf{f}_1^1=f_{\boldsymbol{\theta}}\big(s_1^1,\tilde{\boldsymbol{\phi}}(s_1^1),\tilde{\boldsymbol{\phi}}(s_1^1-\tau)\big)$$

for interval $I=1:I$ **do**

Conditionally simulate a probabilistic solution realization, $\mathbf{u}^i(\mathbf{s}^{i+1}-\tau,\boldsymbol{\theta})$, and derivative realizations, $\mathbf{f}_{1:N}^i$, from the density $p\big(\mathbf{u}^i(\cdot,\boldsymbol{\theta}),\mathbf{f}_{1:N}^i\,\big|\,\boldsymbol{\theta},\boldsymbol{\phi},\Psi_N^i\big)$ via Algorithm 1 with means and covariances defined in (4.10 - 4.13);

end for

for state $p=1:P$ **do**

Sample a realization of the solution, $\mathbf{u}^{(p)}(\mathbf{t})$, for state p from the conditional distribution at chosen points $\mathbf{t}\in[a,b]^T$,

$$\mathbf{u}^{(p)}(\mathbf{t},\boldsymbol{\theta})\sim p\big(\mathbf{u}^{(p)}(\mathbf{t},\boldsymbol{\theta})\big|\boldsymbol{\theta},\mathbf{f}_{1:NI}^{(p)},\boldsymbol{\phi},\Psi_{NI}\big)=\mathcal{N}\big(\mathbf{m}_{NI}(\mathbf{t}),\mathcal{C}_{NI}(\mathbf{t},\mathbf{t})\big);$$

end for

Return $\mathbf{u}(\mathbf{t},\boldsymbol{\theta}),\mathbf{f}_{1:NI}$.

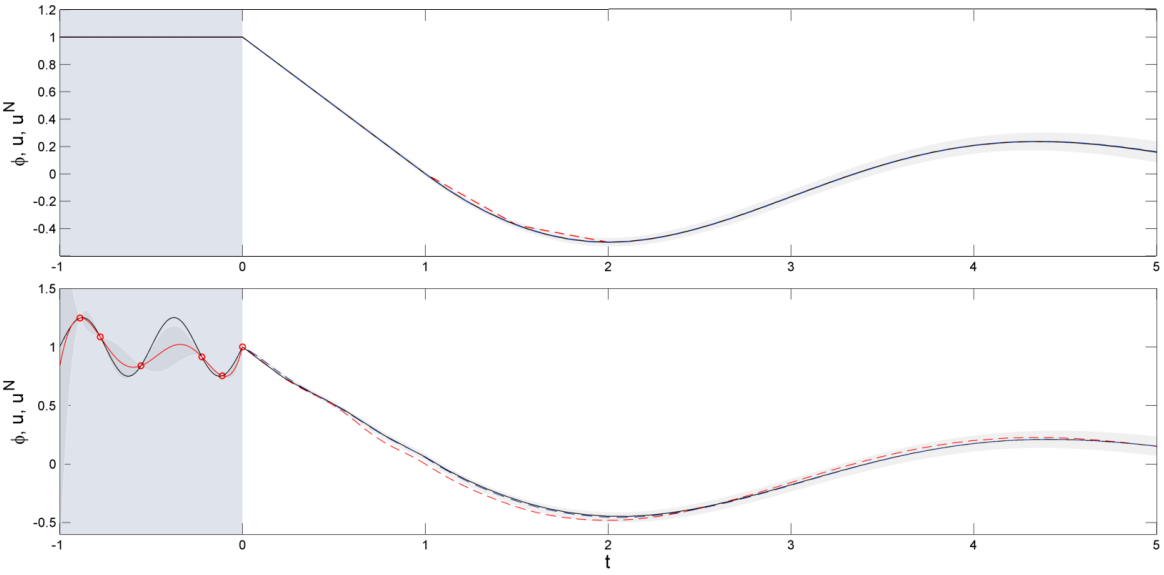

Figure 4.4: *Mean probabilistic solution (blue dashed line) constructed using 500 solver knots compared with numerical (red dashed line) and analytical (black solid line) solutions for the system (2.9) with initial function* $\phi(t) = 1,\ t \in [-1, 0]$ *fully specified (top), and* $\phi(t) = \sin(4\pi t)/4 + 1$ *(below) fully specified (black) and estimated (dotted red line) from six nodal points (red circles). The grey bands show* $\pm$ *100 standard deviations around the mean probabilistic solution for exposition.*

probabilistic solution provides information about how the additional functional uncertainty propagates through the estimated solution.

4.4 Solving PDE boundary value problems

In this section, we describe how to formulate probabilistic solutions to general PDE boundary value problems in two ways. The first, indirect method, models uncertainty along the temporal dimension of the domain using the probabilistic solution developed for ODE initial and boundary value problems, while the spatial discretization is achieved through spectral projection techniques. The second, direct method, is analogous to the finite-differencing approach and follows from the model developed in Section 3.2.2 for multivariate solutions, to produce a technique analogous to the numerical finite-differencing method, which is however limited for high dimensional domains.

4.4.1 Indirect probabilistic solution method

In Chapter 2 we introduced two nonlinear PDEs exhibiting temporal chaos, where interest lay in understanding the impact of temporal discretization on the system. Modeling the effect of discretization over the time domain can be achieved by using the framework developed in Section 4.1 for ODE initial value problems. The PDE boundary value problem is first discretized over the spatial domain and mapped to a finite-dimensional subspace of the solution space via spectral projection, yielding a system of coupled ODEs with initial constraints. We can then use Algorithm 1 to solve the system and reconstruct the estimated PDE solution.

Probabilistic solution of the Kuramoto-Sivashinsky nonlinear PDE

Following Kassam and Trefethen (2005), we considered the spatio-temporal domain $\mathscr{D} = [0, 32\pi] \times [0, 150]$ with initial function $u_B(x) = \cos(x/16)\left\{1 + \sin(x/16)\right\}$, and discretized the spatial domain via a Fourier spectral method, obtaining a high-dimensional (128 dimensions) system of stiff ODEs. The exponential time-differencing transformation was used to solve the linear part of each ODE exactly, while effectively dealing with the transformed nonlinear part via the probabilistic solver. The inverse transformation was then applied within each solver iteration. The probabilistic IVP solution was obtained via Algorithm 1 using $N = 2000$ equally-spaced mesh points. The squared exponential covariance was used with a length-scale of twice the step size and prior precision of 100 units.

Figure 4.5 shows fifteen realizations of the probabilistic posterior solution for the KS nonlinear PDE boundary value problem (2.11). The divergence between the solutions starting approximately around the middle of the temporal domain, illustrates the effect of temporal discretization error propagation on the solution of this stiff system.

Probabilistic solution of the Navier-Stokes equations on a torus

The Navier-Stokes model on a two-dimensional torus (2.12) was reduced to a set of 64×64 coupled ODEs with associated constraints through a pseudo-spectral projection in Fourier space. Once again, we used exponential time-differencing to solve the linear part of each ODE, alleviating problems with stiffness. The resulting probabilistic solution for this two-dimensional PDE in two spatial and one time dimensions is difficult to visualize. Figures

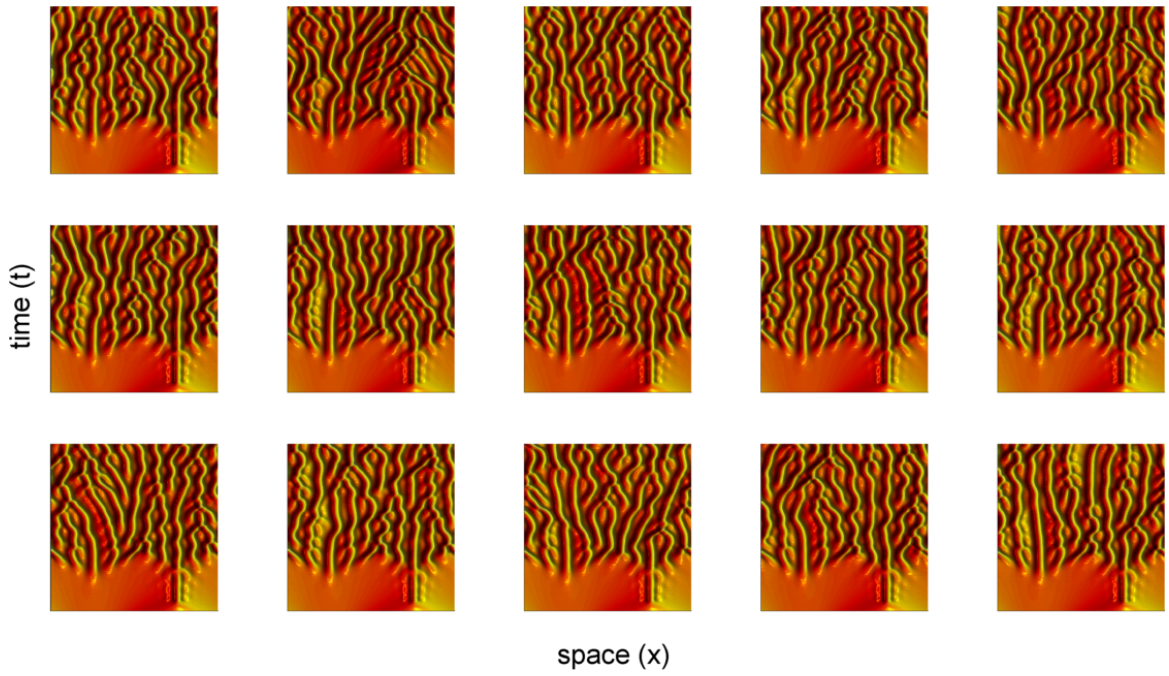

Figure 4.5: A sample of 100 realizations of the probabilistic solution of the Kuramoto-Sivashinsky PDE using a fixed initial function. The spatial and temporal dimensions are shown on the horizontal and vertical axes respectively. The solution is known to exhibit temporal chaos, as evidenced by the variety of dynamics observed due to uncertainty introduced in its estimation.

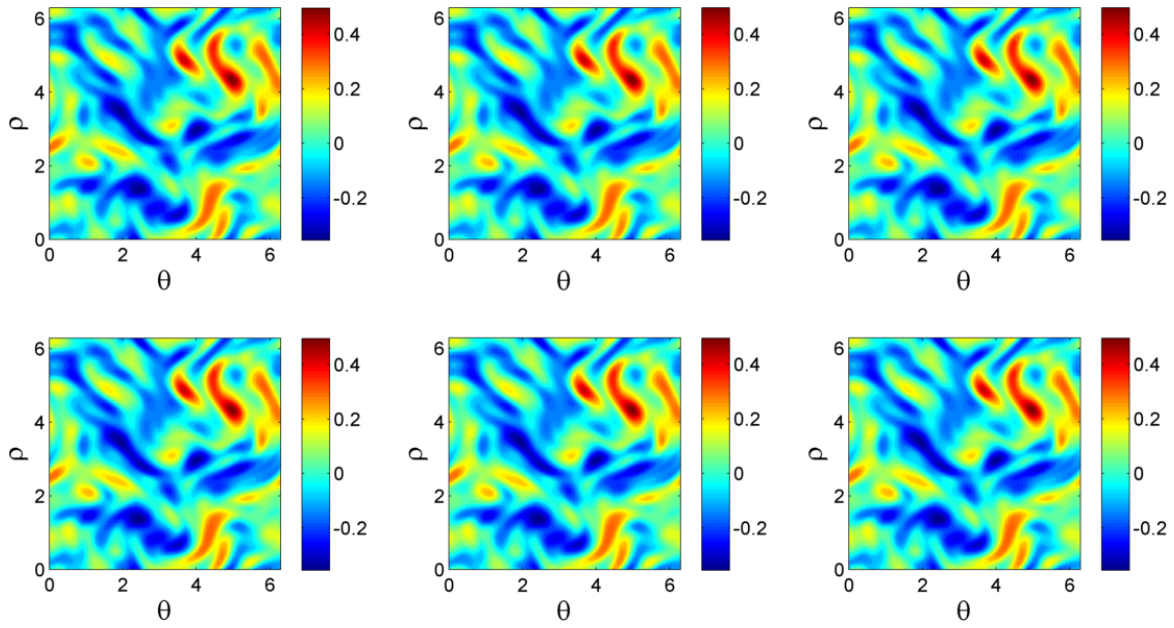

Figure 4.6: Vorticities for a sample of 6 realizations of the probabilistic solution of the Navier-Stokes equation on a two-dimensional torus at time $t = 30$ units, under a fixed initial field. Vorticity of the 6 realizations are very similar at this stage.

4.6 and 4.7, show vorticity, a function of the two components of velocity, on a torus parameterized in spherical coordinates by the angle of the inner ring, θ, on the horizontal axis and the angle of the cross-section of the ring, ρ, on the vertical axis. The probabilistic solution was computed using an equally spaced temporal discretization grid on the interval $[0, 100]$ with $N = 1000$ time steps. The length-scale was chosen to be twice the length of a time step, and the prior precision was set to the low value $\alpha = 0.5$ to reflect the fact that, under our choice of the viscosity parameter, the system lies in the turbulent regime.

Figure 4.6 corresponds to six realizations of the probabilistic solution for this system at time $t = 30$ units, where no difference between the samples can be detected. Figure 4.7 shows the same six realizations at time $t = 100$ units, where differences in vorticity can now clearly be seen. These differences are a result of the accumulation of discretization errors along the time domain and the chaotic nature of the system dynamics.

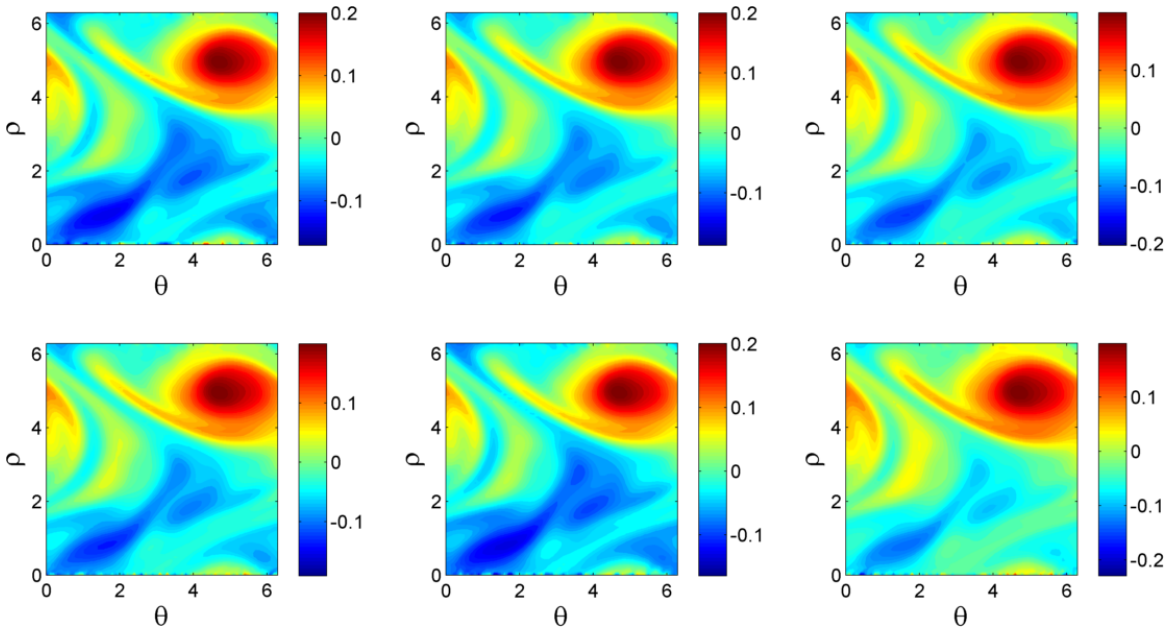

Figure 4.7: Vorticities for a sample of 6 realizations of the probabilistic solution of the Navier-Stokes equation on a two-dimensional torus at time $t = 100$ units, under a fixed initial field. Vorticity of the 6 realizations have begun to diverge from one another as a result of discretization error accumulation along the temporal domain.

4.4.2 Direct probabilistic solution method

If instead interest lies in quantifying discretization uncertainty along more than one dimension, we recommend constructing a spatio-temporal mesh and using a variant of Algorithm 1 based on the multivariate solution model presented in Section 3.2.2. An important consideration when solving PDEs in this way is how to enforce the spatio-temporal boundary condition, which is now a function instead of a single point. This turns out to be relatively straightforward once the domain is parameterized in a convenient way. In each dimension, the boundary condition may need to be enforced (i) at the lower bound of the domain, or (ii) at both endpoints, often within the same problem. In modelling dimensions of the type (i) any standard kernel function will automatically satisfy the boundary value at the lower limit of integration. In modelling dimensions of the type (ii) we recommend an asymmetrical kernel that takes on both positive and negative value and integrates to zero (such as the diagonal kernel constructed in Chapter 6), which ensures that the estimated solution in a particular dimension satisfies the model at both endpoints. As shown in Section 3.2.2 we may combine different kernels in each input dimension, which will allow us to enforce mixed boundary constraints or work with functions with different smoothness in different dimensions.

Finally, we note that this direct solution approach can be considered analogous to a finite-difference numerical method, and as such incurs the same problems related to dimensionality. Indeed, the number of vertices in the spatio-temporal mesh would need to increase exponentially in the number of dimensions to yield a reasonable solution as the number of dimensions increases.

Chapter 5

Incorporating Model Uncertainty in the Inverse Problem

This chapter examines the effect of model uncertainty on the *statistical inverse problem* of recovering information in the form of a probability distribution for variables[1] given data the y. In this chapter we consider the case where the data generating mechanism is governed by a differential equation model defined by unknown parameters $\boldsymbol{\theta} \in \Theta$. When the DE solution is known in closed form, the inverse problem can be approached via nonlinear regression. If the closed form solution is unavailable, we propose to incorporate model error resulting from discretization into the inverse problem by augmenting the unknown parameters by the solution $\mathbf{u}$ and related auxiliary variables.

The following sections show how our probabilistic model of discretization uncertainty for an unknown DE solution naturally fits into the Bayesian framework for solving inverse problems. We contrast our exact *fully probabilistic* approach with the conventional approximate inference method based on numerical DE solutions. Finally, we demonstrate our methodology on a delay initial function model of protein dynamics.

[1]Often in applications, the dimension of the unknown is greater than that of the observations y. Such *underdetermined* problems arise when we try to recover an infinite-dimensional function from finite-dimensional observations, as in the problem of inference on intractable differential equation models. This situation requires restricting attention to a finite-dimensional subspace, which is accomplished in the Bayesian approach by the choice of prior measure.

5.1 Statistical inverse problem

Statistical inversion is the problem of inferring ξ from data $y \in H^{\text{obs}}$, both elements of Hilbert spaces. The *error model* for the data depends on the often nonlinear operator G and a zero-mean stochastic process $\epsilon \in H^{\text{obs}}$ that is independent of ξ. For simplicity, we consider the additive error model,

$$y = G(\xi) + \epsilon. \tag{5.1}$$

5.1.1 Inference for differential equation models

Consider the problem of inference on parameters $\boldsymbol{\theta} \in \Theta$ defining a DE model given R-dimensional measurements $\mathbf{y}(\mathbf{t}) \in M^{T,R}\big(\mathbb{R}\big)$ taken at each of T time points, $\mathbf{t} \in \mathscr{D}^T$, and observed indirectly through the possibly nonlinear *observation function* $\mathcal{G} : M^{T,P}\big(\mathbb{R}\big) \to M^{T,R}\big(\mathbb{R}\big)$. Although this framework can be applied to general error models, for simplicity we shall hereafter consider the additive Gaussian model with error covariance $\Sigma^{(r)} \in M^{T}\big(\mathbb{R}\big)$ and R independent observation states:

$$\mathbf{y}^{(r)}(\mathbf{t}) = \mathcal{G}^{(r)}\big(\mathbf{u}(\mathbf{t},\boldsymbol{\theta})\big) + \epsilon^{(r)}(\mathbf{t}), \qquad \epsilon^{(r)}(\mathbf{t}) \sim \mathcal{N}_T(\mathbf{0}, \Sigma^{(r)}), \qquad 1 \le r \le R.$$

For $\boldsymbol{\Sigma} = \text{diag}\big(\Sigma^{(1)}, \ldots, \Sigma^{(R)}\big)$, the data likelihood follows as,

$$\mathcal{L}_{\mathbf{y}(\mathbf{t})}\big(\mathcal{G} \circ \mathbf{u}(\mathbf{t},\boldsymbol{\theta})\big) = \mathcal{N}_{T\times R}\big(\mathcal{G} \circ \mathbf{u}(\mathbf{t},\boldsymbol{\theta}), \boldsymbol{\Sigma}\big).$$

Therefore in (5.1), ξ typically represents any unknown model parameters, $\boldsymbol{\theta}$, indexing the DE:

$$\xi \equiv \boldsymbol{\theta} \in \Theta,$$

transformed via the nonlinear observation operator,

$$G \equiv \mathcal{G} \circ \mathbf{u}(\mathbf{t}, \cdot) : \Theta \to H^{\text{obs}}$$

which maps the parameters from Θ to the observation space H^{obs}. When the *true* or *exact* solution, $\mathbf{u} : \mathscr{D} \times \Theta \to \mathbb{R}^P$, is known in closed form, then G is known and the parameters $\boldsymbol{\theta}$ can typically be inferred via nonlinear regression.

When the exact solution is unknown, the observation operator $\mathcal{G} \circ \mathbf{u}(\mathbf{t}, \cdot)$ becomes uncertain, as only $\mathcal{G}$ is available. Therefore we propose to restate the inverse problem by considering the posterior probability distribution over the parameters $\boldsymbol{\theta}$ as well as the system states $\mathbf{u}$, by augmenting the ξ as follows:

$$\xi \equiv [\boldsymbol{\theta}, \mathbf{u}(\cdot, \boldsymbol{\theta}), \mathbf{u}_B, \mathbf{f}_{1:N}, \Psi_N] \in \Theta \times H \equiv \mathcal{H},$$

and rewriting the observation operator in terms of the observation transformation $\mathcal{G}$ only,

$$G \equiv \mathcal{G} : \mathcal{H} \to H^{\text{obs}}.$$

As a result, inference can now proceed via nonlinear regression as before.

5.1.2 Bayesian approach

In this section we will consider the standard Bayesian framework for statistical inverse problems, which consists of obtaining a posterior measure for the unknown $\xi \in \mathcal{H}$, where $\mathcal{H}$ is a general Hilbert space, and will be referred to as *inference* on ξ. Informally, this approach proceeds by applying Bayes' rule:

$$\xi \,|\, y \;\sim\; \frac{\mathrm{d}\nu^y}{\mathrm{d}\nu_0}(\xi) \;=\; \frac{\mathcal{L}_y\big(G(\xi)\big)}{\int_{\mathcal{H}} \mathcal{L}_y\big(G(\xi)\big)\,\mathrm{d}\nu_0(\xi)} \;\propto\; \mathcal{L}_y\big(G(\xi)\big), \tag{5.2}$$

where ν^y is the posterior measure of ξ conditioned on the data, and where $\mathrm{d}\nu^y/\mathrm{d}\nu_0$ denotes its Radon-Nikodym derivative with respect to the prior measure ν_0. As in Chapter 3, such an informal derivation is not typically sufficient to verify that the Radon-Nikodym derivative exists, particularly in the infinite-dimensional setting. The following theorem (see, for example, Stuart, 2010) sets out the conditions when this is the case.

Theorem 5.1.1. *Consider the error model (5.1). Suppose that $\mathcal{L}_y$ is defined on $\mathbb{R}^R$, and that $\nu_0(\mathcal{H}) = 1$. If the observation operator, $G : \mathcal{H} \to \mathbb{R}^R$, is continuous, then $\xi \,|\, y$ is distributed according to ν^y, which is absolutely continuous with respect ν_0, and has Radon-Nikodym derivative (5.2).*

From now on, we will work with distributions which are absolutely continuous with respect to the Lebesgue measure, and will therefore adopt a simpler notation by writing the

posterior density (5.2) as,

$$p(\xi \,|\, y) \;=\; \frac{\mathcal{L}_y\big(G(\xi)\big)\, p(\xi)}{\int_H \mathcal{L}_y\big(G(\xi)\big)\, p(\xi) \mathrm{d}\xi} \;\propto\; \mathcal{L}_y\big(G(\xi)\big)\, p(\xi).$$

5.1.3 Approximate inference under an unknown DE solution

When the DE solution is known, the likelihood $\mathcal{L}_{\mathbf{y(t)}}\big(\mathcal{G} \circ \mathbf{u}(\mathbf{t}, \boldsymbol{\theta})\big)$ can be evaulated, and thus functionals of the posterior distribution (5.2) may be obtained through standard techniques (see, for example, Gelman et al., 2004). In practice, however, the likelihood cannot be evaluated due to lack of a closed form solution for most nonlinear DE models (see, for example, discussion in Ramsay et al., 2007). Therefore, the conventional approach replaces the unknown analytical solution $\mathbf{u}(\mathbf{t}, \boldsymbol{\theta})$ by its finite-dimensional numerical approximation $\mathbf{u}^N(\mathbf{t}, \boldsymbol{\theta})$ obtained via numerical integration of the system equations over an N-dimensional spatio-temporal mesh, to obtain the likelihood approximation,

$$\mathcal{L}_{\mathbf{y(t)}}\big(\mathcal{G} \circ \mathbf{u}(\mathbf{t}, \boldsymbol{\theta})\big) \;\approx\; \mathcal{L}_{\mathbf{y(t)}}\big(\mathcal{G} \circ \mathbf{u}^N(\mathbf{t}, \boldsymbol{\theta})\big).$$

Under the conditions of Theorem 5.1.1, this approach yields the approximate posterior density,

$$p^N\big(\boldsymbol{\theta} \,|\, \mathbf{y(t)}\big) \quad \propto \quad \underbrace{\mathcal{L}_{\mathbf{y(t)}}\big(\mathcal{G} \circ \mathbf{u}^N(\mathbf{t}, \boldsymbol{\theta})\big)}_{\text{approximate likelihood of the data}} \quad \times \quad \underbrace{p(\boldsymbol{\theta}).}_{\text{prior density}} \tag{5.3}$$

The approximate observation operator $G^N \equiv \mathcal{G} \circ \mathbf{u}^N$ can differ substantially from $G \equiv \mathcal{G} \circ \mathbf{u}$ in practice, leading to estimation bias, as illustrated in the extreme cases of chaotic and ill-conditioned systems. Importantly, any systematic uncertainty associated with this approximation is ignored under the conventional framework. Our goal is to show that an alternative, exact model is not only feasible, but in many cases necessary.

5.2 A fully probabilistic approach

We propose to incorporate our probability model of discretization uncertainty into the inverse problem by introducing one additional layer in the posterior hierarchy, defined by the joint density $p\big(\mathbf{u}(\mathbf{t}, \boldsymbol{\theta}), \mathbf{f}_{1:N} \,|\, \boldsymbol{\theta}, \mathbf{u}_B, \Psi_N\big)$ over solutions $\mathbf{u}(\mathbf{t}, \boldsymbol{\theta})$ and derivative realizations

$\mathbf{f}_{1:N}$. This yields a fully probabilistic alternative to the approximate posterior density (5.3), by characterizing the uncertainty in the unknown system solution, $\mathbf{u}(\mathbf{t}, \boldsymbol{\theta})$.

5.2.1 Exact posterior density

First, define a prior measure ν_0 for the unknown vector $\xi = [\mathbf{u}(\cdot, \boldsymbol{\theta}), \mathbf{u}_B, \mathbf{f}_{1:N}, \Psi_N, \boldsymbol{\theta}] \in \mathcal{H}$ in such a way that $\nu_0(\mathcal{H}) = 1$. Intuitively this condition guarantees that the prior assigns positive probability to any function that satisfies the regularity conditions on the state space of possible solutions. If the observation operator $\mathcal{G} : M^{T,P}(\mathbb{R}) \to M^{T,R}(\mathbb{R})$ is continuous, then $\xi \,|\, \mathbf{y}$ is distributed according to the measure ν^y that is absolutely continuous with respect ν_0, by Theorem 5.1.1. Evaluating the solution at time points $\mathbf{t} \in \mathscr{D}^T$ ensures that the posterior distribution of the probabilistic solution is continuous with respect to the Lebesgue measure, with density (3.15). Thus, the posterior density of the solution and the model and auxiliary parameters is,

$$
\begin{aligned}
&p\left(\boldsymbol{\theta}, \mathbf{u}(\mathbf{t}, \boldsymbol{\theta}), \mathbf{u}_B, \mathbf{f}_{1:N}, \Psi_N \,|\, \mathbf{y}(\mathbf{t})\right) \\
&\quad \propto \underbrace{\mathcal{L}_{\mathbf{y}(\mathbf{t})}\big(\mathcal{G} \circ \mathbf{u}(\mathbf{t}, \boldsymbol{\theta})\big)}_{\text{likelihood of the data}} \times \underbrace{p\big(\mathbf{u}(\mathbf{t}, \boldsymbol{\theta}) \,|\, \boldsymbol{\theta}, \mathbf{u}_B, \mathbf{f}_{1:N}, \Psi_N\big)}_{\text{probabilistic solution}} \times \underbrace{p\big(\boldsymbol{\theta}, \mathbf{u}_B, \mathbf{f}_{1:N}, \Psi_N\big)}_{\text{prior density}}. \qquad (5.4)
\end{aligned}
$$

Marginalizing over the auxiliary variables, derivative realizations, and the solution, yields an exact posterior over model parameters, which explicitly takes into account the mismatch between the true solution and a finite-dimensional approximation.

5.3 Sampling from the posterior distribution over model parameters

Posterior functionals of (5.4) will not usually be analytically tractable, but can be obtained via Monte Carlo (e.g., Gelman et al., 2004). This requires a forward-simulation layer to address the fact that the density (5.4) is not available analytically for most DE models, due to the sequential nonlinear vector field transformation required to generate derivative realizations given $\boldsymbol{\theta}$.

We propose a specialized Monte Carlo procedure to generate a sample from the fully probabilistic posterior (5.4), which allows estimation of the model parameters and solution

while taking into account solver uncertainty. For each proposed value of $\boldsymbol{\theta}$, Algorithm 5 applies the observation transformation $\mathcal{G}$ to each probabilistic solution realization generated given initial conditions $\mathbf{u}_B$, and auxiliary parameters Ψ_N, avoiding explicitly calculating the intractable density of the observation states within the Metropolis-Hastings acceptance ratio. For clarity of exposition, Algorithm 5 targets the posterior distribution of model parameters $\boldsymbol{\theta}$ given boundary conditions $\mathbf{u}_B$, auxiliary parameters Ψ_N, and error covariances $\boldsymbol{\Sigma}$. However, the algorithm extends simply to accommodate sampling when $\mathbf{u}_B$, Ψ_N, and $\boldsymbol{\Sigma}$ are also unknown.

Algorithm 5 Draw K samples from $p\big(\boldsymbol{\theta}, \mathbf{u}(\mathbf{t},\boldsymbol{\theta}), \mathbf{f}_{1:N} \,|\, \mathbf{u}_B, \Psi_N, \mathbf{y}(\mathbf{t})\big)$

Initialize $\boldsymbol{\theta}$;

for $k = 1 : K$ **do**

Propose $\boldsymbol{\theta}^\star \sim q(\boldsymbol{\theta}^\star \,|\, \boldsymbol{\theta})$;

Conditionally simulate vector field realizations, $\mathbf{f}^\star_{1:N}$, and associated solution realization, $\mathbf{u}^\star(\mathbf{t},\boldsymbol{\theta}^\star)$, from $p\big(\mathbf{u}(\mathbf{t},\boldsymbol{\theta}^\star), \mathbf{f}_{1:N} \big| \boldsymbol{\theta}^\star, \mathbf{u}_B, \Psi_{1:N}\big)$ using one of Algorithms 1 through 4;

Compute:

$$\rho\big(\boldsymbol{\theta}, \mathbf{u}(\mathbf{t},\boldsymbol{\theta}), \mathbf{f}_{1:N} \to \boldsymbol{\theta}^\star, \mathbf{u}^\star(\mathbf{t},\boldsymbol{\theta}^\star), \mathbf{f}^\star_{1:N}\big) = \frac{q(\boldsymbol{\theta}^\star \,|\, \boldsymbol{\theta},)}{q(\boldsymbol{\theta} \,|\, \boldsymbol{\theta}^\star)} \, \frac{p(\boldsymbol{\theta}^\star)}{p(\boldsymbol{\theta})} \, \frac{p\big(\mathbf{y}(\mathbf{t}) | \mathcal{G}\big(\mathbf{u}^\star(\mathbf{t},\boldsymbol{\theta}^\star)\big), \boldsymbol{\Sigma}\big)}{p\big(\mathbf{y}(\mathbf{t}) | \mathcal{G}\big(\mathbf{u}(\mathbf{t},\boldsymbol{\theta})\big), \boldsymbol{\Sigma}\big)};$$

if $\min\{1, \rho\} > \mathrm{U}[0,1]$ **then**

Update $\boldsymbol{\theta} = \boldsymbol{\theta}^\star$;

Update $\mathbf{u}(\mathbf{t},\boldsymbol{\theta}) = \mathbf{u}^\star(\mathbf{t},\boldsymbol{\theta}^\star)$;

Update $\mathbf{f}_{1:N} = \mathbf{f}^\star_{1:N}$;

end if

Return $\boldsymbol{\theta}, \mathbf{u}(\mathbf{t},\boldsymbol{\theta}), \mathbf{f}_{1:N}$.

end for

5.3.1 Inference for the JAK-STAT protein network model

We demonstrate fully probabilistic state and parameter inference for a 4-state ODE delay initial function problem describing the dynamics of the JAK-STAT cellular signal transduction pathway (Raue et al., 2009). Features of this model which pose a challenge to conventional methods of parameter estimation include the presence of systematic model uncertainty inherent in numerical DIFP solutions, dependence of the model on an uncertain discretely specified input function, and possible model misspecification (Campbell and Chkrebtii, 2013).

This mechanism describes a series of reversible biochemical reactions of STAT-5 transcription factors in response to binding of Erythropoietin (Epo) hormone to cell surface receptors, Pellegrini and Dusanter-Fourt (1997). After gene activation occurs within the nucleus, the transcription factors revert to their initial state, returning to the cytoplasm to be used in the next activation cycle. This last stage is not well understood and is proxied in the model by the time delay τ. The model for this mechanism describes changes in 4 reaction states of STAT-5 through the DIFP,

$$\begin{cases} \dot{\mathbf{u}}^{(1)}(t,\boldsymbol{\theta}) &= -\theta_1\,\mathbf{u}^{(1)}(t,\boldsymbol{\theta})\,\mathrm{Epo}R_A(t) + 2\,\theta_4\,\mathbf{u}^{(4)}(t-\tau,\boldsymbol{\theta}), \\ \dot{\mathbf{u}}^{(2)}(t,\boldsymbol{\theta}) &= \theta_1\,\mathbf{u}^{(1)}(t,\boldsymbol{\theta})\,\mathrm{Epo}R_A(t) - \theta_2\,{\mathbf{u}^{(2)}}^2(t,\boldsymbol{\theta}), \\ \dot{\mathbf{u}}^{(3)}(t,\boldsymbol{\theta}) &= -\theta_3\,\mathbf{u}^{(3)}(t,\boldsymbol{\theta}) + 0.5\,\theta_2\,{\mathbf{u}^{(2)}}^2(t,\boldsymbol{\theta}), \\ \dot{\mathbf{u}}^{(4)}(t,\boldsymbol{\theta}) &= \theta_3\,\mathbf{u}^{(3)}(t,\boldsymbol{\theta}) - \theta_4\,\mathbf{u}^{(4)}(t-\tau,\boldsymbol{\theta}), \end{cases} \tag{5.5}$$

on $t \in [0, 60]$ time units, with known initial functions $\mathbf{u}^{(2)}(t,\boldsymbol{\theta}) = \mathbf{u}^{(3)}(t,\boldsymbol{\theta}) = \mathbf{u}^{(4)}(t,\boldsymbol{\theta}) = 0$ on $t \in [-\tau, 0]$. Constant initial function $\mathbf{u}^{(1)}(t,\boldsymbol{\theta})$ on $t \in [-\tau, 0]$, the time delay τ, and the reaction rates $\theta_1, \ldots, \theta_4$ are unknown variables parameterizing this model.

The states cannot be measured directly, but are observed through the nonlinear transformation $\mathcal{G} : \mathbb{R}^3 \times \Theta \to \mathbb{R}^4$

$$\mathcal{G}_1(\mathbf{u},\boldsymbol{\theta}) = \theta_5\left(\mathbf{u}^{(2)} + 2\mathbf{u}^{(3)}\right)$$
$$\mathcal{G}_2(\mathbf{u},\boldsymbol{\theta}) = \theta_6\left(\mathbf{u}^{(1)} + \mathbf{u}^{(2)} + 2\mathbf{u}^{(3)}\right)$$

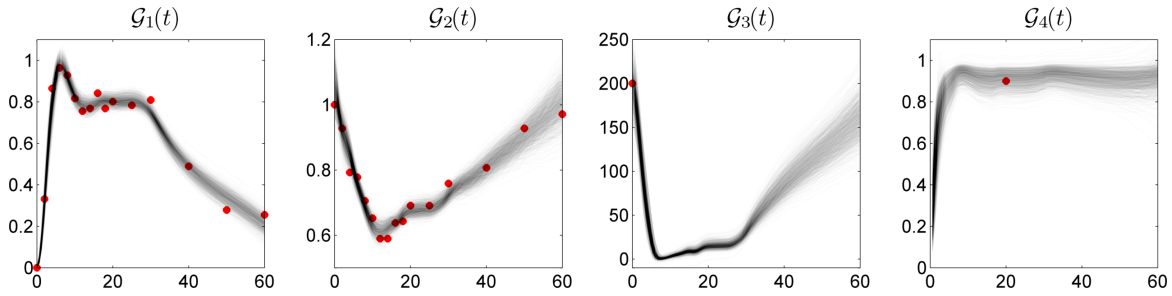

Figure 5.1: Experimental data (red circles) and sample paths (lines) of the observation processes. They are obtained by transforming a sample from the marginal posterior distribution of the states by the observation function (5.6).

$$\begin{aligned} \mathcal{G}_3(\mathbf{u}, \boldsymbol{\theta}) &= \mathbf{u}^{(1)} \\ \mathcal{G}_4(\mathbf{u}, \boldsymbol{\theta}) &= \mathbf{u}^{(3)} / \left(\mathbf{u}^{(2)} + \mathbf{u}^{(3)} \right), \end{aligned} \tag{5.6}$$

which is expressed in terms of unknown scaling factors θ_5 and θ_6. As per Raue et al. (2009), observations $\mathbf{y}(\mathbf{t}) = \mathcal{G}\big(\mathbf{u}(\mathbf{t}, \boldsymbol{\theta}), \boldsymbol{\theta}\big) + \epsilon(\mathbf{t})$ are assumed contaminated with additive zero-mean Gaussian noise with experimentally determined standard deviations.

Our analysis is based on experimental data from Swameye et al. (2003), which consists of 16 observations (illustrated by red circles in Figure 5.1) for the first two states of the observation process. Raue et al. (2009) further utilize an additional artificial data point for each of the third and fourth observation process states to deal with lack of parameter identifiability for this system. This assumption is also adopted in our analysis.

Prior distributions were defined on the unknown parameters as follows: $\theta_i \sim \text{Exp}\,(1)$, $i = 1, \ldots, 6$, $\tau \sim \chi^2_6$, and $\mathbf{u}^{(1)}(0) \sim \mathcal{N}_1\big(y^{(3)}(0), 40^2\big)$. We estimated functionals of the posterior distribution from a Monte Carlo sample of model parameters, $\boldsymbol{\theta} = [\theta_1, \ldots, \theta_6, \tau, u^{(1)}(0)]$, solution states, $\mathbf{u}(\mathbf{t}, \boldsymbol{\theta})$, and auxiliary variables, Ψ_N. In order to construct a Markov chain that would efficiently traverse the parameter space of this multimodal posterior distribution, we chose to use a parallel tempering sampler (Geyer, 1991) with 7 parallel chains along a uniformly spaced temperature profile over the interval $[0.4, 1]$. Parameters were sampled in three blocks. The first block consists of the four rate parameters, two scaling factors, the delay parameter and the initial value of the first state. The second and third blocks consist of the precisions and length-scales respectively, with priors $\alpha_i + 100 \sim \text{Log-}\mathcal{N}_1\,(10, 1)$ and $\lambda_i \sim \chi^2_1$, $i = 1, \ldots, 4$. Each probabilistic DIFP solution was generated using Algorithm 4

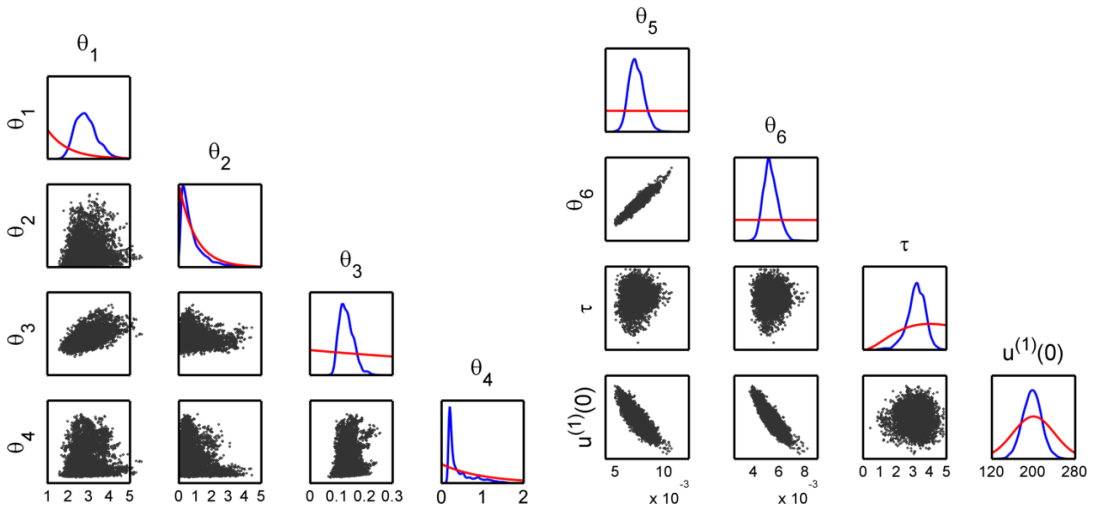

Figure 5.2: Marginal fully probabilistic posterior distribution in the model parameters based on a sample of size 100,000 generated by a parallel tempering algorithm utilizing seven chains, with the first 10,000 samples removed. Prior densities are shown in red.

using an equally spaced grid of size $N = 300$. The input function was estimated using a linear interpolator of the EpoR_A experimental data, following Swameye et al. (2003).

We obtained 100,000 posterior samples and removed the first 10,000 samples as burn-in. Convergence was monitored by examining the marginal empirical distributions visually, while ensuring that the acceptance rate fell roughly within the accepted range of 18%–28% for each of the three parameter blocks, and that the total swap rate between any two chains remained roughly within 5%-15%.

Marginal posterior samples of the observation states $\mathcal{G}\big(\mathbf{u}(\cdot,\boldsymbol{\theta}),\boldsymbol{\theta}\big)$ are shown in Figure 5.1, while marginal posterior samples of model parameters are illustrated using correlation plots in Figure 5.2. All rate and scaling parameters are found to be identifiable with the exception of θ_2, as noted also in the identifiability analysis of Raue et al. (2009). Scaling factors are correlated, positively with each other and inversely with the constant initial state $\mathbf{u}^{(1)}(0)$. Auxiliary parameters for the fully probabilistic model are found, for the most part, to be non-identifiable. Indeed the transformed probabilistic solution for this system does not appear to be overly sensitive to changes in the auxiliary parameters within a reasonable range.

Chapter 6

Choice of Covariance Structure

The covariance function describes how two elements of a space are related to one another. In the model for an unknown DE solution presented in Chapter 3, the prior covariance determines the regularity of the space of possible solutions, and thus its specification is an important consideration. In this chapter we discuss the construction of the covariance operator for the unknown solution and its derivative, examine its properties, and provide three examples of covariance structures that are used throughout this thesis.

6.1 Role and properties of prior covariances

In Chapter 3 we defined the following prior measures for the unknown DE solution state and its derivative:

$$\mu_0 = \mathcal{N}(\mathbf{m}_0, \mathcal{C}_0),$$
$$\mu_0^f = \mathcal{N}(\mathbf{m}_0^f, \mathcal{C}_0^f).$$

Covariance operators $\mathcal{C}_0^f = \mathrm{RR}(t, \tilde{t})$ and $\mathcal{C}_0 = \mathrm{QQ}(t, \tilde{t})$ follow a user-specified structure governed by the kernel function R_λ and its integrated version Q_λ.

6.1.1 Positive-definiteness

We have seen in Theorem 3.3.1 that a necessary condition for a well-defined probabilistic solution derivative (3.14) is that the cross-covariance operators, (3.18), between the derivative and n noisy realizations be positive definite. Let us show that this condition is satisfied

under the above prior covariance specification.

Recall that α denotes the prior precision defined in Section 3.2.1. Consider a kernel $R_\lambda \in L^2(\mathscr{D}^2)$, such that the integral transform $\mathrm{R}g$ of any nonzero function $g \in L^2(\mathscr{D})$ is not everywhere zero (this condition is simple to verify for a given kernel), then,

$$\begin{aligned}\langle g, RKR^*g\rangle &= \alpha^{-1}\int\int \mathrm{R}_\lambda(t,z)\,g\,(t)\,\mathrm{d}t\int \mathrm{R}_\lambda(\tilde{t},z)\,g\left(\tilde{t}\right)\mathrm{d}\tilde{t}\mathrm{d}z \\ &= \begin{cases} \alpha^{-1}\int\Big(\int \mathrm{R}_\lambda(t,z)g\,(t)\,\mathrm{d}t\Big)^2\mathrm{d}z = 0 & \text{if } g(t)=0 \ \ \forall t\in\mathscr{D} \\ \alpha^{-1}\int\Big(\int \mathrm{R}_\lambda(t,z)g\,(t)\,\mathrm{d}t\Big)^2\mathrm{d}z > 0 & \text{otherwise.}\end{cases}\end{aligned}$$

Therefore, the cross-covariance operators $\mathcal{C}_{11}, \mathcal{C}_{12}, \mathcal{C}_{21}$, defined in (3.18), are positive definite. Next, we consider the covariance operator $\mathcal{C}_{22}$, defined in (3.18). For any vector $g \in \mathbb{R}^n$ and positive semidefinite matrix Λ_N, we have,

$$\begin{aligned}\langle g, \big(RKR^* + \Lambda_n\big)g\rangle &= \sum_{i=1}^{n}\sum_{j=1}^{n}\big(\alpha^{-1}\textstyle\int_{\mathbb{R}}\mathrm{R}_\lambda(t_i,z)\mathrm{R}_\lambda(t_j,z)\mathrm{d}z + \Lambda_n(t_i,t_j)\big)g\,(t_i)\,g\,(t_j) \\ &= \begin{cases} \langle g, RKR^*g\rangle + \langle g, \Lambda_n\, g\rangle = 0 & \text{if } g(t)=0 \ \ \forall t\in\mathscr{D}, \\ \langle g, RKR^*g\rangle + \langle g, \Lambda_n\, g\rangle > 0 & \text{otherwise.}\end{cases}\end{aligned}$$

Therefore $\mathcal{C}_{22}$ is also positive definite. This argument simply extends to the case of the integrated covariances used for modelling the solution states.

6.1.2 Regularity

Theorem 4.1.3 requires that the mean-centered derivative of the true solution must be an element of the space H spanned by the eigenfunctions of the covariance operator $\mathcal{C}_0^f$. We give an intuitive justification for this requirement by showing that the prior Gaussian measure assigns positive probability to any function that is suitably regular, i.e. $\mu_0^f(H) = 1$. The following theorem shows how to obtain realizations of a Gaussian process on a Hilbert space, and relates the smoothness of the realizations to the covariance structure.

Theorem 6.1.1 (Karhunen–Loève theorem)**.** *Let $\mathcal{C}$ be a self-adjoint, positive semi-definite,*

trace class[1] *operator in a Hilbert space H with an orthonormal set of eigenfunctions and associated eigenvalues, $\{\phi_k, \gamma_k\}_{k=1}^{\infty}$, ordered so that $\gamma_1 \geq \gamma_2 \geq \cdots$. Let $\ell \in H$ and take $\{z_k\}_{k=1}^{\infty}$ to be a sequence of iid standard normal random variables. Then, the random function,*

$$u = \ell + \sum_{k=1}^{\infty} z_k \sqrt{\gamma_k} \phi_k$$

has distribution $\mu = \mathcal{N}(\ell, \mathcal{C})$.

From this theorem, follows a result (e.g. Stuart, 2010, pp. 539-540) which implies that samples from μ_0^f are almost surely in $L^2(\mathscr{D})$ under some relatively mild conditions on the covariance.

6.1.3 Role of kernel functions

Covariances for the unknown solution are constructed using the kernel R_λ and its integrated version Q_λ. Therefore, the choice of the kernel function should reflect our assumptions about the true unknown DE solution, such as smoothness and any fixed zero points. In general, imposing unrealistically strict smoothness assumptions on H by choice of covariance operator may introduce estimation bias if the true solution derivative is not an element of this space. Therefore, in cases where the solution smoothness is not known with certainty, we recommend to err on the side of less regular kernels which alleviate possible bias by allowing for the possibility of functions less smooth than the solution, at the cost of slower rate of convergence of the estimated solution to the true unknown solution.

6.2 Some useful covariances

The illustrative examples in this thesis employ one of three types of covariance structure constructed by the choice of kernel. In the following section, we provide closed form expressions of pairwise convolutions corresponding to each type of kernel.

[1] compact operator with finite trace that is independent of the choice of basis.

6.2.1 Squared exponential covariance

The *squared exponential* isotropic covariance function,

$$\mathcal{C}_0^f(t,\tilde{t}) = \sqrt{\pi}\,\alpha\,\lambda\,\exp\big(-\tfrac{1}{4}\left(\tfrac{t-\tilde{t}}{\lambda}\right)^2\big), \tag{6.1}$$

is popular in the Gaussian process literature (Rasmussen and Williams, 2006) for modelling analytic functions. Here, we will focus on the case that $\mathscr{D} = [a,b]$. We will show that this covariance is obtained by pairwise convolution of the *Gaussian kernel*,

$$R_\lambda(t,\tilde{t}) = \exp\big(-\tfrac{1}{2}\left(\tfrac{t-\tilde{t}}{\lambda}\right)^2\big),$$

and the integrated covariance is obtained by the pairwise convolution of the integrated kernel,

$$Q_\lambda(t,\tilde{t}) = \tfrac{1}{2}\,\mathrm{erf}\big(\tfrac{1}{\sqrt{2}}\left(\tfrac{t-\tilde{t}}{\lambda}\right)^2\big) - \tfrac{1}{2}\,\mathrm{erf}\big(\tfrac{1}{\sqrt{2}}\left(\tfrac{a-\tilde{t}}{\lambda}\right)^2\big).$$

The integrated kernel produces a non-stationary state covariance operator, $\mathcal{C}_0$, which allows us to constrain the solution state to zero at the initial boundary a of the domain.

Let us derive closed form expressions for the pairwise convolutions of the Gaussian kernel and its integrated version, which are required for updating the probabilistic solution as described in Chapter 4.

$$\alpha\mathrm{RR}(t,\tilde{t}) = \sqrt{\pi}\,\lambda\,\exp\big(-\tfrac{1}{4}\left(\tfrac{t-\tilde{t}}{\lambda}\right)^2\big), \qquad t,\tilde{t}\in[a,b]$$

$$\alpha\mathrm{QR}(t,\tilde{t}) = \pi\,\lambda^2\,\mathrm{erf}\big(\tfrac{1}{2\lambda}(t-\tilde{t})\big) + \pi\,\lambda^2\,\mathrm{erf}\big(\tfrac{1}{2\lambda}(\tilde{t}-a)\big), \qquad t,\tilde{t}\in[a,b]$$

$$\begin{aligned}\alpha\mathrm{QQ}(t,\tilde{t}) &= \pi\,\lambda^2(t-a)\,\mathrm{erf}\big(\tfrac{1}{2}\left(\tfrac{t-a}{\lambda}\right)\big) + 2\sqrt{\pi}\,\lambda^3\exp\big(-\tfrac{1}{4}\left(\tfrac{t-a}{\lambda}\right)^2\big)\\ &\quad -\pi\lambda^2(\tilde{t}-t)\,\mathrm{erf}\big(\tfrac{1}{2}\left(\tfrac{\tilde{t}-t}{\lambda}\right)\big) - 2\sqrt{\pi}\,\lambda^3\exp\big(-\tfrac{1}{4}\left(\tfrac{\tilde{t}-t}{\lambda}\right)^2\big)\\ &\quad +\pi\,\lambda^2(\tilde{t}-a)\,\mathrm{erf}\big(\tfrac{1}{2}\left(\tfrac{\tilde{t}-a}{\lambda}\right)\big) + 2\sqrt{\pi}\,\lambda^3\exp\big(-\tfrac{1}{4}\left(\tfrac{\tilde{t}-a}{\lambda}\right)^2\big) - 2\sqrt{\pi}\,\lambda^3, \qquad t,\tilde{t}\in[a,b]\end{aligned}$$

Importantly, the result $\mathrm{RR}(t,t), \mathrm{QQ}(t,t) < \infty$ for all $t \in \mathbb{R}$ implies that the kernel and its integrated version are square integrable. Also note that $\mathrm{RR}(t,\tilde{t})$ has the form of the squared exponential covariance (6.1). Contour plots of the kernel, its integrated version, and the state and derivative prior covariances are shown in Figure 6.1 on the domain $\mathscr{D} = [0,1]$ with prior precision $\alpha = 1$ and length-scale $\lambda = 0.1$.

The covariance operator, $\mathcal{C}_0^f$, is infinitely differentiable, so that the Gaussian process model for the derivative is mean-square differentiable. As such, this covariance is suited to modelling solution derivatives that are known a priori to be very smooth. In this thesis, we have used the squared exponential covariance for modelling the probabilistic solution of the Lorenz system, the Kuramoto-Sivashinsky initial boundary function problem, the Lane-Emden mixed boundary value problem, and the Navier-Stokes equations.

6.2.2 Uniform covariance

In some cases, one may wish to model the derivative by a function with first or higher derivative discontinuities. For this purpose we propose the following *uniform kernel* function and its integrated version:

$$
\begin{aligned}
R_\lambda(t,\tilde{t}) &= \mathbb{I}\big(\tilde{t} \in (t-\lambda, t+\lambda)\big), \\
Q_\lambda(t,\tilde{t}) &= \mathbb{I}\big(\tilde{t} \in (a+\lambda, t-\lambda)\big) + \tfrac{1}{2}\big(\tfrac{t-a}{\lambda}\big)\, \mathbb{I}\big(\tilde{t} \in (t-\lambda, a+\lambda)\big) \\
&\quad + \tfrac{1}{2}\big(\tfrac{\tilde{t}+\lambda-a}{\lambda}\big)\, \mathbb{I}\big(\tilde{t} \in (a-\lambda, \min(a+\lambda, t-\lambda))\big) \\
&\quad + \tfrac{1}{2}\big(\tfrac{t-\tilde{t}+\lambda}{\lambda}\big)\, \mathbb{I}\big(\tilde{t} \in (\max(a+\lambda, t-\lambda), t+\lambda)\big).
\end{aligned}
$$

Next, we derive the closed form expressions for the pairwise convolutions for the uniform kernel.

$$
\alpha\mathrm{RR}(t,\tilde{t}) = \big(\min(t,\tilde{t}) - \max(t,\tilde{t}) + 2\lambda\big)\, \mathbb{I}\big(\min(t,\tilde{t}) - \max(t,\tilde{t}) > -2\lambda\big), \qquad t,\tilde{t} \in [a,b],
$$

$$
\begin{aligned}
\alpha\mathrm{QR}(t,\tilde{t}) &= 2\lambda x\, \mathbb{I}\big(\min(t-\lambda, \tilde{t}+\lambda) > \max(a+\lambda, \tilde{t}-\lambda)\big)\big|_{\max(a+\lambda,\tilde{t}-\lambda)}^{\min(t-\lambda,\tilde{t}+\lambda)} \\
&\quad + \big(\tfrac{1}{2}x^2 + (\lambda - a)x\big)\, \mathbb{I}\big(\min(a+\lambda, t-\lambda, \tilde{t}+\lambda) > \tilde{t}-\lambda\big)\big|_{\tilde{t}-\lambda}^{\min(a+\lambda,t-\lambda,\tilde{t}+\lambda)} \\
&\quad + \big((t+\lambda)x - \tfrac{1}{2}x^2\big)\, \mathbb{I}\big(\min(t,\tilde{t}) + \lambda > \max(a+\lambda, t-\lambda, \tilde{t}-\lambda)\big)\big|_{\max(a+\lambda,t-\lambda,\tilde{t}-\lambda)}^{\min(t,\tilde{t})+\lambda} \\
&\quad + (t-a)\big(\max(t,\tilde{t}) - a - 2\lambda\big)\, \mathbb{I}\big(a - \max(t,\tilde{t}) > -2\lambda\big), \qquad t,\tilde{t} \in [a,b],
\end{aligned}
$$

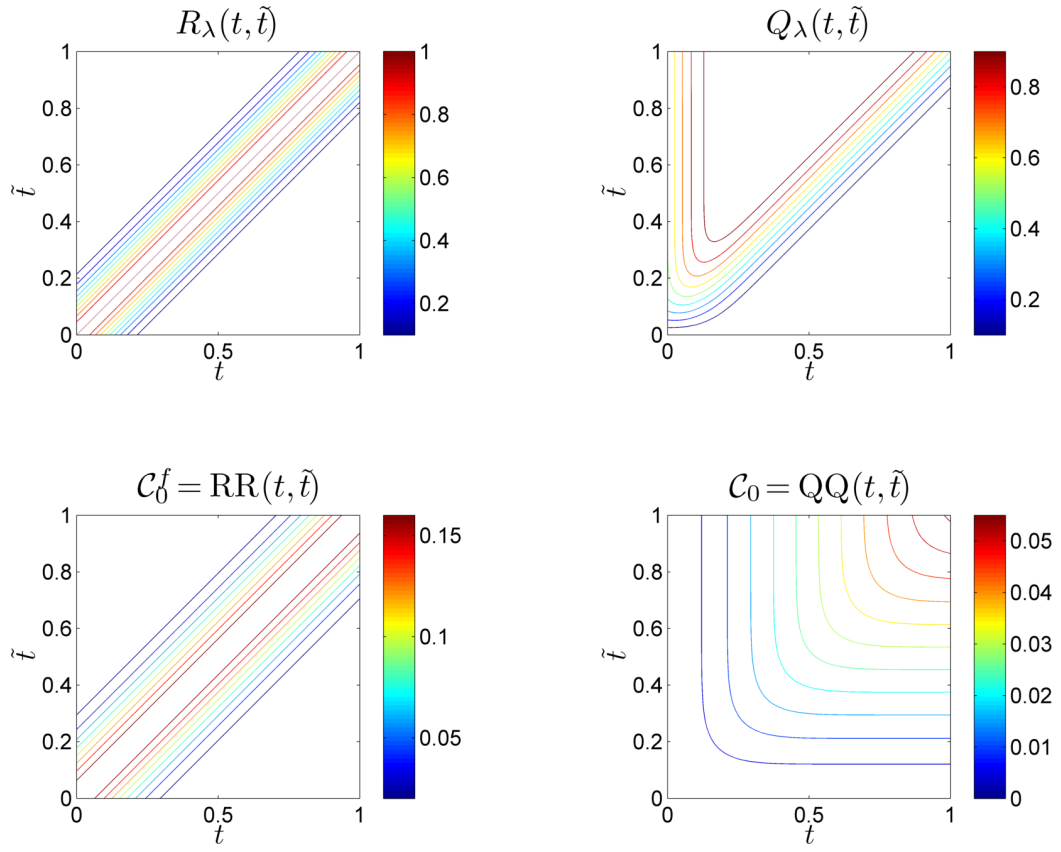

Figure 6.1: Top row: contour plots of Gaussian kernel (left), and its integrated version (right). Bottom row: contour plots of squared exponential derivative covariance (left) and associated state covariance (right). Functions are evaluated over $t, \tilde{t} \in [0, 1]$, with $(\alpha, \lambda) = (1, 0.1)$.

$$
\begin{aligned}
\alpha\mathrm{QQ}(t,\tilde{t}) = {} & 4\lambda^2\left(\min(t,\tilde{t}) - a - 2\lambda\right)\mathbb{I}\big(\min(t,\tilde{t}) > a + 2\lambda\big) \\
& +2\lambda\left((\tilde{t}+\lambda)x - \tfrac{1}{2}x^2\right)\mathbb{I}\big(\min(t-\lambda,\tilde{t}+\lambda) > \max(a+\lambda,\tilde{t}-\lambda)\big)\Big|_{\max(a+\lambda,\tilde{t}-\lambda)}^{\min(t-\lambda,\tilde{t}+\lambda)} \\
& +\left(\tfrac{1}{3}x^3 + (\lambda-a)x^2 + (\lambda-a)^2x\right)\mathbb{I}\big(\min(a+\lambda,t-\lambda,\tilde{t}-\lambda) > a-\lambda\big)\Big|_{a-\lambda}^{\min(a+\lambda,t-\lambda,\tilde{t}-\lambda)} \\
& +(\tilde{t}-a)\left(\tfrac{1}{2}x^2 + (\lambda-a)x\right)\mathbb{I}\big(\min(a+\lambda,t-\lambda) > \tilde{t}-\lambda\big)\Big|_{\tilde{t}-\lambda}^{\min(a+\lambda,t-\lambda)} \\
& +2\lambda\big((t+\lambda)x - \tfrac{1}{2}x^2\big)\mathbb{I}\big(\min(t+\lambda,\tilde{t}-\lambda) > \max(a+\lambda,t-\lambda)\big)\Big|_{\max(a+\lambda,t-\lambda)}^{\min(t+\lambda,\tilde{t}-\lambda)} \\
& +\big((t+\lambda)(\tilde{t}+\lambda)x - \tfrac{1}{2}(t+\tilde{t}+2\lambda)x^2 + \tfrac{1}{3}x^3\big) \\
& \qquad \mathbb{I}\big(\min(t,\tilde{t}) > \max(a,t-2\lambda,\tilde{t}-2\lambda)\big)\Big|_{\max(a+\lambda,t-\lambda,\tilde{t}-\lambda)}^{\min(t,\tilde{t})+\lambda} \\
& +(t-a)\left(\tfrac{1}{2}x^2 + (\lambda-a)x\right)\mathbb{I}\big(\min(a+\lambda,\tilde{t}-\lambda) > t-\lambda\big)\Big|_{t-\lambda}^{\min(a+\lambda,\tilde{t}-\lambda)} \\
& +(t-a)(\tilde{t}-a)\big(a+2\lambda-\max(t,\tilde{t})\big)\,\mathbb{I}\big(a+2\lambda > \max(t,\tilde{t})\big), \qquad\qquad t,\tilde{t} \in [a,b].
\end{aligned}
$$

The result $\mathrm{RR}(t,t), \mathrm{QQ}(t,t) < \infty$ implies that R_λ and Q_λ are square integrable. Contour plots of the resulting covariance functions $\mathcal{C}_0^f(t,\tilde{t}) = \mathrm{RR}(t,\tilde{t})$ and $\mathcal{C}_0(t,\tilde{t}) = \mathrm{QQ}(t,\tilde{t})$, as well as kernels R_λ, Q_λ are shown in Figure 6.2 on the domain $\mathscr{D} = [0,1]$ with prior precision $\alpha = 1$ and length-scale $\lambda = 0.1$.

The *uniform covariance* C_0^f is not everywhere differentiable, allowing discontinuities in the first derivative of the solution. First derivative-discontinuous solutions typically arise for delay initial function problems, where derivative discontinuities are often present at the lag locations. Examples include the JAK-STAT system considered in Chapter 5.

6.2.3 Diagonal boundary covariance

Smoothness is not the only property of the solution that may be modelled by appropriate choice of covariance. Indeed, we have seen that the use of integrated covariances in the previous sections guarantees that the solution state always takes a zero or baseline value, $\ell(a)$, at the initial boundary a. This is a very useful property for the ODE problems examined in this thesis, but is not always suitable for modelling multivariate PDE BVP solutions directly, where additional constraints may be required at the boundaries along some of the spatio-temporal dimensions.

In order to constrain solutions at both boundaries of a component of the domain, we propose a *diagonal kernel*, which takes on both positive and negative values in such a way that its integral over the full domain, $[a,b]$, is zero, and that still satisfies the necessary

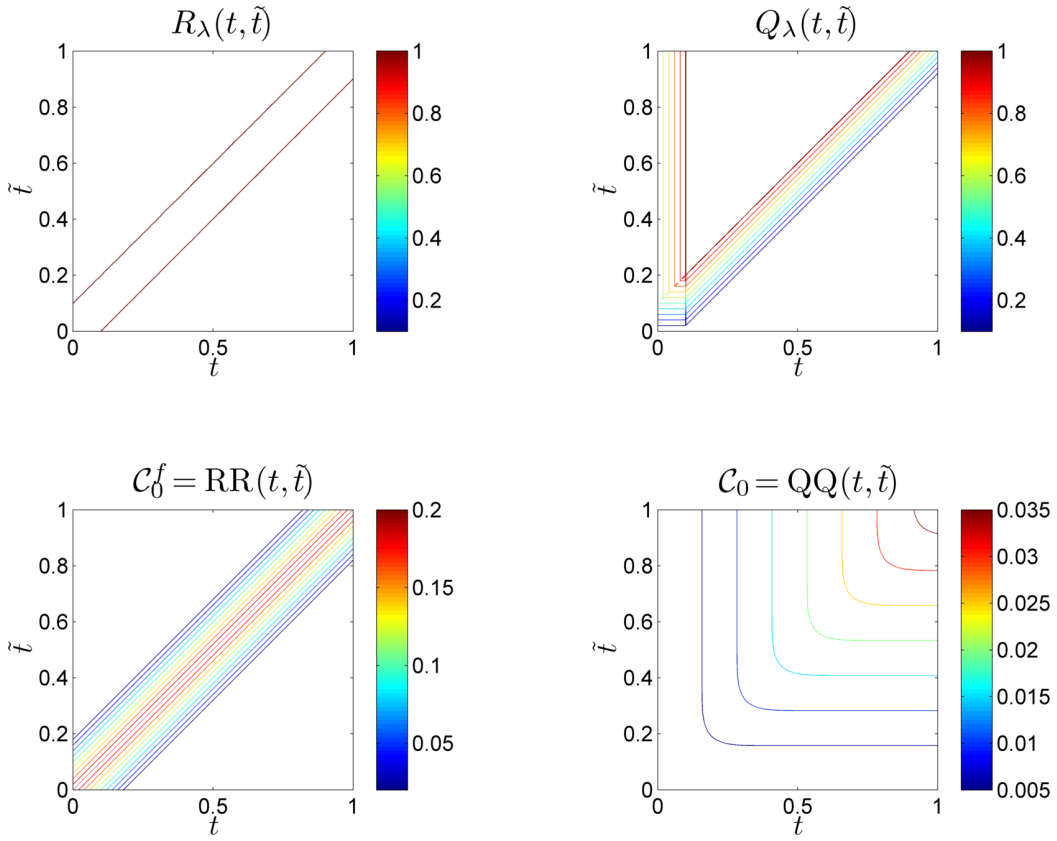

Figure 6.2: Top row: contour plots of uniform kernel (left), and its integrated version (right). Bottom row: contour plots of derivative covariance (left) and state covariance (right). Functions are evaluated over $t, \tilde{t} \in [0, 1]$, with $(\alpha, \lambda) = (1, 0.1)$.

condition for the resulting covariance to be positive definite (i.e. that Rg is not everywhere zero for all non-zero functions $g \in L^2(\mathscr{D})$). This has the effect of setting the solution state to zero at both ends of a one-dimensional domain. The proposed diagonal kernel function and its integrated version are given by,

$$\begin{aligned}
R_\lambda(t,\tilde{t}) = &\left(\tilde{t}-t\right)\ \mathbb{I}\big(t\in(\tilde{t}-\lambda,\tilde{t}+\lambda),\tilde{t}\in[a+\lambda,b-\lambda]\big)\\
&+\tfrac{1}{2}\left(a+\tilde{t}+\lambda-2t\right)\ \mathbb{I}\big(t\in(a,\tilde{t}+\lambda),\tilde{t}\in[a,\min(a+\lambda,b-\lambda))\big)\\
&+\tfrac{1}{2}\left(b+\tilde{t}-\lambda-2t\right)\ \mathbb{I}\big(t\in(\tilde{t}-\lambda,b),\tilde{t}\in(\max(a+\lambda,b-\lambda),b]\big)\\
&+\tfrac{1}{2}\left(a+b-2t\right)\ \mathbb{I}\big(t\in(a,b),\tilde{t}\in[b-\lambda,a+\lambda]\big),
\end{aligned}$$

$$\begin{aligned}
Q_\lambda(t,\tilde{t}) = &\tfrac{1}{2}\left(2\tilde{t}t-t^2-\tilde{t}^2+\lambda^2\right)\ \mathbb{I}\big(\tilde{t}\in[\max(t-\lambda,a+\lambda),\min(t+\lambda,b-\lambda)]\big)\\
&+\tfrac{1}{2}\left((a+\tilde{t}+\lambda)t-t^2-(\tilde{t}+\lambda)a\right)\ \mathbb{I}\big(\tilde{t}\in[\max(t-\lambda,a),\min(a+\lambda,b-\lambda))\big)\\
&+\tfrac{1}{2}\left((b+\tilde{t}-\lambda)t-t^2-(\tilde{t}-\lambda)b\right)\ \mathbb{I}\big(\tilde{t}\in(\max(a+\lambda,b-\lambda),\min(t+\lambda,b)]\big)\\
&+\tfrac{1}{2}\left((a+b)t-t^2-ab\right)\ \mathbb{I}\big(\tilde{t}\in[b-\lambda,a+\lambda]\big).
\end{aligned}$$

Below we derive the closed form convolutions required for function estimation under a diagonal kernel.

$$\begin{aligned}
\alpha\mathrm{RR}(t,\tilde{t}) = &\tfrac{1}{6}x\big(6t\tilde{t}-3(t+\tilde{t})x+2x^2\big)\ \Big|_{\max(t-\lambda,\tilde{t}-\lambda,a+\lambda)}^{\min(t+\lambda,\tilde{t}+\lambda,b-\lambda)}\\
&+\tfrac{1}{4}\left((a-2t+\lambda)(a-2\tilde{t}+\lambda)x+(a-t-\tilde{t}+\lambda)x^2+\tfrac{1}{3}x^3\right)\ \Big|_{\max(t-\lambda,\tilde{t}-\lambda,a)}^{\min(a+\lambda,b-\lambda)}\\
&+\tfrac{1}{4}\left((b-2t-\lambda)(b-2\tilde{t}-\lambda)x+(b-t-\tilde{t}-\lambda)x^2+\tfrac{1}{3}x^3\right)\ \Big|_{\max(a+\lambda,b-\lambda)}^{\min(t+\lambda,\tilde{t}+\lambda,b)}\\
&+\tfrac{1}{4}(a+b-2t)(a+b-2\tilde{t})x\ \Big|_{b-\lambda}^{a+\lambda}, \qquad t,\tilde{t}\in[a,b],
\end{aligned}$$

$$\begin{aligned}
\alpha\mathrm{RQ}(t,\tilde{t}) = &\tfrac{1}{24}x\left((-6\tilde{t}^2+6\lambda^2+8\tilde{t}x-3x^2)x+4t(3\tilde{t}^2-3\lambda^2-3\tilde{t}x+x^2)\right)\ \Big|_{\max\{t-\lambda,\tilde{t}-\lambda,a+\lambda\}}^{\min\{t+\lambda,\tilde{t}+\lambda,b-\lambda\}}\\
&+\tfrac{1}{4}(a-\tilde{t})\left((\tilde{t}-\lambda)(a-2t+\lambda)x+\tfrac{1}{2}(-a+2t+\tilde{t}-2\lambda)x^2-\tfrac{1}{3}x^3\right)\Big|_{\max(t-\lambda,\tilde{t}-\lambda,a)}^{\min(a+\lambda,b-\lambda)}\\
&+\tfrac{1}{4}(b-\tilde{t})\left((b-2t-\lambda)(\tilde{t}+\lambda)x+\tfrac{1}{2}(-b+2t+\tilde{t}+2\lambda)x^2-\tfrac{1}{3}x^3\right)\Big|_{\max(a+\lambda,b-\lambda)}^{\min(t+\lambda,\tilde{t}+\lambda,b)}\\
&-\tfrac{1}{4}(a+b-2t)(a-\tilde{t})(b-\tilde{t})x\Big|_{b-\lambda}^{a+\lambda}, \qquad t,\tilde{t}\in[a,b],
\end{aligned}$$

$$\alpha\mathrm{QQ}(t,\tilde{t}) = \tfrac{1}{4}\left(-(t^2-\lambda^2)(-\tilde{t}^2+\lambda^2)x-(t+\tilde{t})(t\tilde{t}-\lambda^2)x^2+\tfrac{1}{3}(t^2+4t\tilde{t}+\tilde{t}^2-2\lambda^2)x^3\right.$$

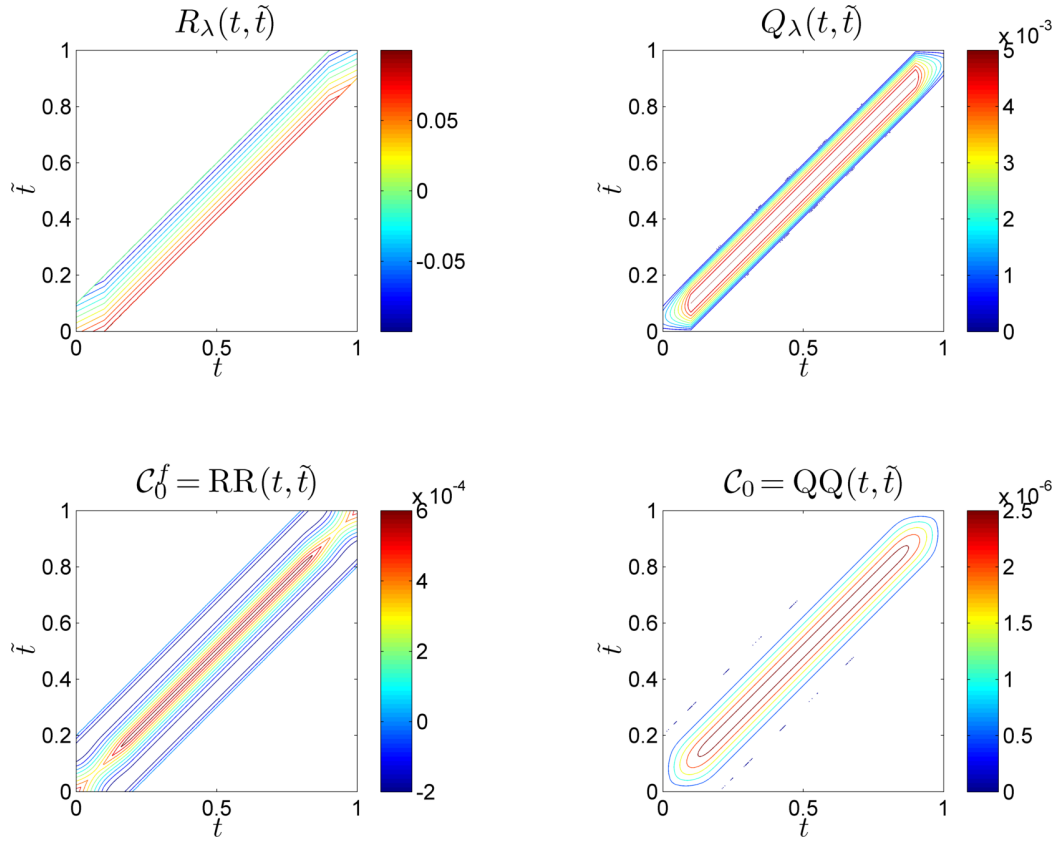

Figure 6.3: Top row: contour plots of diagonal kernel (left), and its integrated version (right). Bottom row: contour plots of derivative covariance (left) and state covariance (right). Functions are evaluated over $t, \tilde{t} \in [0,1]$, with $(\alpha, \lambda) = (1, 0.1)$.

$$
\begin{aligned}
&-\tfrac{1}{2}(t+\tilde{t})x^4 + \tfrac{1}{5}x^5\big)\ \mathbb{I}\big(t,\tilde{t} \in (x-\lambda, x+\lambda)\big)\big|_{a+\lambda}^{b-\lambda} \\
&+\tfrac{1}{24}x(a-t)(a-\tilde{t})(-6(t-\lambda)(-\tilde{t}+\lambda) - 3(t+\tilde{t}-2\lambda)x + 2x^2)\ \mathbb{I}\big(t,\tilde{t} \in (a, x+\lambda)\big)\big|_{a-\lambda}^{\min(a+\lambda,b-\lambda)} \\
&+\tfrac{1}{24}(b-t)(b-\tilde{t})(6(t+\lambda)(\tilde{t}+\lambda) - 3(t+\tilde{t}+2\lambda)x + 2x^2)\ \mathbb{I}\big(t,\tilde{t} \in (x-\lambda, b)\big)\big|_{\max(a+\lambda,b-\lambda)}^{b+\lambda} \\
&+\tfrac{1}{4}x(a-t)(b-t)(a-\tilde{t})(b-\tilde{t})\big|_{b-\lambda}^{a+\lambda}, \qquad\qquad t,\tilde{t} \in [a,b].
\end{aligned}
$$

Here again, we have $\mathrm{RR}(t,t), \mathrm{QQ}(t,t) < \infty$, so that R_λ and Q_λ are square integrable. Contour plots of the resulting diagonal covariance function $\mathcal{C}_0^f(t,\tilde{t}) = \mathrm{RR}(t,\tilde{t})$ and its integrated version $\mathcal{C}_0(t,\tilde{t}) = \mathrm{QQ}(t,\tilde{t})$, as well as kernels R_λ, Q_λ are shown in Figure 6.3 on the domain $\mathscr{D} = [0,1]$ with prior precision $\alpha = 1$ and length-scale $\lambda = 0.1$.

Chapter 7

Sequential Design for Probabilistic Mesh Selection

For many DE systems, such as those with fast-changing derivatives, small local errors in the solution approximation can propagate into large deviations from the true solution along the domain. We have seen that for a numerical or probabilistic DE solution approximation to be acceptable, it must converge in some sense to the true solution defined by the DE. Rates of convergence depend on many factors, such as the smoothness of the true function, and given these, are typically directly related to the size, N, of the discrete grid subdividing the domain. As N cannot be made arbitrarily large due to computational limitations, its choice presents a trade-off between accuracy of the estimated solution and computational resources. Therefore, given N, a natural question is how we can arrange the grid on the domain in such a way that the resulting approximation is as good as possible?

Most commercially available numerical DE solvers select the step length of the discretization grid sequentially. Below we discuss how this is done, and relate this method to a sequential design problem in the probabilistic setting.

7.1 Preliminaries

We propose to adaptively select the step length in each dimension for use in the probabilistic solution by optimizing a measure theoretic criterion. We then examine the modelling requirements for incorporating a variable step length into the probabilistic solvers presented

in Chapter 4.

7.2 Numerical step length selection

Local truncation error bounds for numerical methods at a given step n are usually proportional to the distance between the estimated solutions evaluated at subsequent knot locations, $|\tilde{\mathbf{u}}(s_n) - \tilde{\mathbf{u}}(s_{n-1})|$. This quantity is related to the linearized first derivative so that, when the derivative changes quickly, local truncation error increases proportionally. Controlling the local error by choice of the step length $s_n - s_{n-1}$ is called *adaptive step size selection* in the numerical analysis literature. In the simplest cases, this is accomplished by evaluating the local truncation error at each step and halving the step size if this exceeds an error tolerance that is pre-specified by the user (the process may be repeated several times per step until an appropriate local truncation error is achieved).

7.2.1 Kullback-Leibler divergence criterion

The *relative entropy* or *Kullback-Leibler (KL) entropy* (Kullback and Leibler, 1951) is a non-symmetric metric for the divergence between two probability distributions.

Definition 18 (Kullback and Leibler (1951))**.** *Let $\mu_i, i = 1, 2$ be two probability measures defined on the same measure space $(H, \mathcal{A})$, and absolutely continuous with respect to μ_0. Also let $f_i = d\mu_i/d\mu_0, i = 1, 2$ represent the corresponding densities. The Kullback-Leibler divergence is given by,*

$$D\big(f_1||f_2\big) = \int \log\left(\frac{f_1(u)}{f_2(u)}\right) d\mu_1(u) = \int f_1(u)\, \log\left(\frac{f_1(u)}{f_2(u)}\right) d\mu_0(u).$$

For example, the KL divergence between two K-variate Gaussian probability distributions, $\mu_i = \mathcal{N}_K(m_i, C_i), i = 1, 2$, defined on $(\mathbb{R}^K, \mathcal{B})$ is given by,

$$\begin{aligned} D\big(f_1||f_2\big) &= \int \frac{1}{2}\left(\log\left(\frac{|C_2|}{|C_1|}\right) + (u-m_2)^{\mathsf{T}} C_2^{-1}(u-m_2) - (u-m_1)^{\mathsf{T}} C_1^{-1}(u-m_1)\right) \mathrm{d}\mu_1 \\ &= \frac{1}{2}\left(\log\left(\frac{|C_2|}{|C_1|}\right) + \int (u-m_2)^{\mathsf{T}} C_2^{-1}(u-m_2)\mathrm{d}\mu_1 - \int (u-m_1)^{\mathsf{T}} C_1^{-1}(u-m_1)\mathrm{d}\mu_1\right) \\ &= \frac{1}{2}\left(\log\left(\frac{|C_2|}{|C_1|}\right) + (m_1-m_2)^{\mathsf{T}} C_2^{-1}(m_1-m_2) + \mathrm{tr}\big(C_2^{-1}C_1\big) - K\right), \end{aligned} \tag{7.1}$$

where we have used properties of expectations with respect to a multivariate Gaussian measure. Note that the divergence between the two distributions is directly proportional to the scaled distance between the means, inversely proportional to the number of dimensions, K, and depends nonlinearly on $C_2^{-1}C_1$. In particular, the direct dependence on scaled distance between the means is reminiscent of the form of the local truncation error objective function used for numerical step size selection.

7.3 Probabilistic sequential step length selection

Consider an ordered partition $\mathbf{s} = [s_1, \cdots, s_n] \in [a, s_n]^N, s_1 = a, s_n < b$, of the one-dimensional interval $[a, s_n]$. In this section we derive the KL divergence criterion between the latest estimated probabilistic solution state $\mathbf{u}_n(t, \boldsymbol{\theta})$ constructed using derivative realizations at $s_1, \ldots, s_n$, and the corresponding solution $\mathbf{u}_{n+1}(t, \boldsymbol{\theta})$ obtained by placing one additional knot at a new location $s^* \in (s_n, \min\{s_n + \varepsilon, b\}], \varepsilon > 0$.

7.3.1 KL divergence between current and step-ahead estimated solution

Finite-dimensional evaluations of both $\mathbf{u}_n(\cdot, \boldsymbol{\theta})$ and $\mathbf{u}_{n+1}(\cdot, \boldsymbol{\theta})$ are jointly Gaussian with mean vector and covariance matrix defined in (3.13) and (3.15). Therefore, we can obtain the integrated KL divergence from (7.1):

$$\begin{aligned}
&\int_a^b D\left(\mathbf{u}_{n+1}(t) \,||\, \mathbf{u}_n(t)\right) \mathrm{d}\lambda(t) \\
&= \int_a^b \frac{1}{2}\left[\frac{\mathcal{C}_{n+1}(t,t)}{\mathcal{C}_n(t,t)} + \frac{\{\mathbf{m}_n(t) - \mathbf{m}_{n+1}(t)\}^2}{\mathcal{C}_n(t,t)} - 1 - \log\frac{\mathcal{C}_{n+1}(t,t)}{\mathcal{C}_n(t,t)}\right] \mathrm{d}t.
\end{aligned}$$

Calculating this criterion becomes effectively computationally infeasible, due to the inversion of the matrix $RR([s_{1:n}; s^*], [s_{1:n}; s^*]) + \Lambda$ required to evaluate $\mathbf{m}_{n+1}(t)$ and $\mathcal{C}_{n+1}(t,t)$ for every proposed value of $s^* \in (s_n, \min\{s_n + \varepsilon, b\}], \varepsilon > 0$ at each step. However, this inversion can be easily avoided by using the recursive formulation from Lemma 4.1.1 to rewrite the criterion as,

$$\begin{aligned}
&\int_a^b D\left(\mathbf{u}_{n+1}(t) \,||\, \mathbf{u}_n(t)\right) \mathrm{d}\lambda(t) \\
&= \int_a^b \frac{1}{2}\left[\frac{\mathcal{C}_n(t,t) - \mathcal{C}_n^2(t,s^*)/2\mathcal{C}_n^f(s^*,s^*)}{\mathcal{C}_n(t,t)} + \frac{\{(\mathbf{m}_n^f(s^*) - f_\theta(s^*))\int_a^t \mathcal{C}_n^f(x,s^*)\mathrm{d}x/2\mathcal{C}_n^f(s^*,s^*)\}^2}{\mathcal{C}_n(t,t)}\right.
\end{aligned}$$

$$
\begin{aligned}
&\quad -1 - \log \frac{\mathcal{C}_n(t,t) - \mathcal{C}_n^2(t,s^*)/2\mathcal{C}_n^f(s^*,s^*)}{\mathcal{C}_n(t,t)} \Bigg] \mathrm{d}t \\
&= \int_a^b \frac{1}{2} \left[\frac{\{f_\theta(s^*) - \mathbf{m}_n^f(s^*)\}^2 \left(\int_a^t \mathcal{C}_n^f(x,s^*)\mathrm{d}x \right)^2}{4\mathcal{C}_n^{f2}(s^*,s^*)\mathcal{C}_n(t,t)} - \frac{\mathcal{C}_n^2(t,s^*)}{2\mathcal{C}_n^f(s^*,s^*)\mathcal{C}_n(t,t)} \right. \\
&\quad \left. - \log \left\{ 1 - \frac{\mathcal{C}_n^2(t,s^*)}{2\mathcal{C}_n^f(s^*,s^*)\mathcal{C}_n(t,t)} \right\} \right] \mathrm{d}t, \qquad (7.2)
\end{aligned}
$$

where now the expression is written solely in terms of the nth estimated derivative mean $\mathbf{m}_n^f$, state covariance $\mathcal{C}_n$, and cross-covariance $\int_a^t \mathcal{C}_n^f(x,\cdot)\mathrm{d}x$, which were already obtained at the nth iteration. It is important to note the integrand of criterion (7.2) is always non-negative and equal to zero iff $\mathbf{u}_{n+1}(t) = \mathbf{u}_n(t)$ almost everywhere (this holds in general for the KL divergence, see for example Cover and Thomas, 2006).

To our knowledge, the integral (7.2) cannot be evaluated in closed form. Thus, somewhat ironically, we must resort to numerical integration to evaluate this criterion. However, we note that this is a rather straightforward one-dimensional integration problem relative to the one of solving the DE itself, and is not sensitive to properties of the solution trajectory. Therefore, in practice we approximate the integral numerically with respect to t using the trapezoidal rule.

7.3.2 Implementation

Using the KL divergence to inform the step size requires a number of practical considerations. We suggest first specifying the maximum computationally feasible number of equidistant mesh points N^* for solving the DE, and allocating these to a temporary equidistant fixed design over $[a,b]$ with step size $h^* = (b-a)/N^*$. We may now define solver step sizes in terms of these smallest unit steps. In particular, we fix an integer $G > 1$ so that h^*G is the maximum allowable step length for the problem. The length-scale is typically defined in terms of step sizes, so we must be careful to specify a length-scale that is at least twice the maximum step size h^*G. In this way, information from nearby derivative realizations is included even when taking the largest allowed steps[1].

The algorithm must begin by iterating through the first G unit steps of length h^*. At iteration $n > G$ we may begin to adjust the step size. Define the candidate nodes

[1] for this purpose, adaptive selection of length-scales would be a useful extension.

$s_g^* = s_n + gh^*$ for $g = 1 \ldots, G$. We will choose the node s_g^* that maximizes the discrepancy between the posterior solution derivatives $\mathbf{u}_n = \left[\mathbf{u}(\cdot, \boldsymbol{\theta}) \,|\, \boldsymbol{\theta}, \mathbf{f}_{1:n}, \mathbf{u}_a, \Psi_n\right]$, and $\mathbf{u}_{n+1} = \left[\mathbf{u}(\cdot, \boldsymbol{\theta}) \,|\, \boldsymbol{\theta}, [\mathbf{f}_{1:n}; f_\theta(s_g^*)], \mathbf{u}_a, \Psi_n\right]$, the latter being computed using one additional derivative realization, i.e. $\mathbf{f}_{1:n+1} = [\mathbf{f}_{1:n}; f_\theta(s_g^*)]$. Thus the next node is selected as,

$$s_{n+1} = \arg\max_{s_g^*} \max_p \int_a^b D\left(\mathbf{u}_{n+1}^{(p)}(t) \,||\, \mathbf{u}_n^{(p)}(t)\right) \mathrm{d}\lambda(t).$$

Due to the recursion employed in the derivation of the criterion, the computational cost of step size selection is negligible relative to the rest of the algorithm. Thus, we recommend to adaptively select step sizes whenever possible. A computational issue arises when dealing with chaotic systems. After the onset of chaotic dynamics, the sample paths begin to differ substantially from one another, and have different associated optimal mesh designs. In theory, optimizing the design for each draw is certainly feasible. In reality this requirement introduces large computational costs associated with matrix operations, since covariances can no longer be recycled as suggested in Section 4.1.3. In comparison multiple draws from the probabilistic solution can be obtained almost instantaneously when the mesh is identical for each draw, as was shown.

Figure 7.1 shows a single realization of the probabilistic solution for the Lorenz system before the onset of chaos, obtained using adaptive step sizes with a maximum possible mesh size of $N^* = 2000$ and selection region defined by $G = 4$. The actual grid size obtained adaptively was only $N = 740$, as in practice the smallest step size was rarely selected by the algorithm.

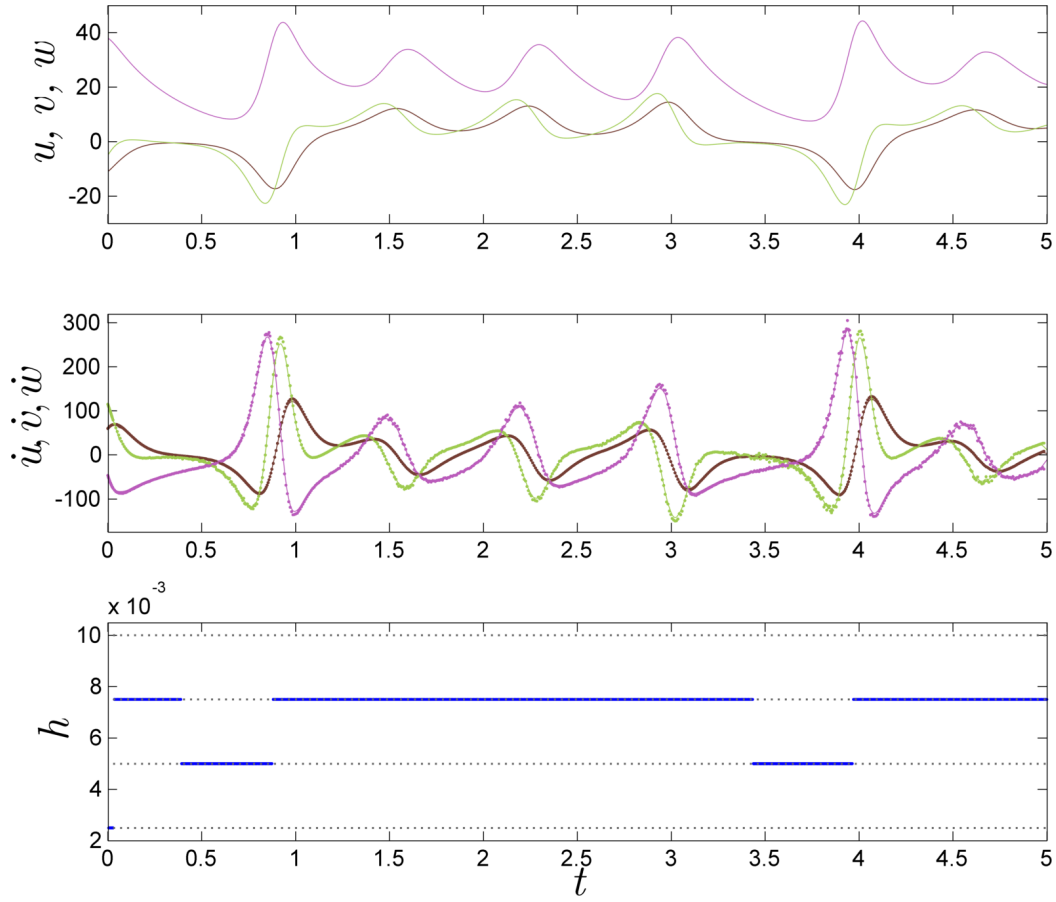

Figure 7.1: Realizations of the states (top, solid lines) and derivatives (middle, solid lines) of a single draw from the probabilistic solution of the Lorenz system on the interval $[0, 5]$. State and derivative realizations obtained at each step are shown as dots. The mesh was selected adaptively, and the resulting step lengths are shown in the lower panel in dark blue. Light blue dotted lines represent the possible step lengths $\{gh^*\}_{g=1\ldots,4}$.

Chapter 8

Conclusion

This thesis describes a new probabilistic formalism for studying the structure of solution uncertainty for general systems of differential equations. Rather than providing a single deterministic solution that approximately satisfies the model dynamics, our approach provides a probability statement over the space of suitably regular functions. This allows the explicit study of the error structure and propagation of functional uncertainty through the statistical inference process, which had been until now an open problem.

Specifically, we develop a Bayesian probability model first suggested in Skilling (1991) for the unknown deterministic solution of general intractable differential equation problems given a finite discretization mesh defined on the domain of integration. We show how such a model can (i) provide a probability statement about the dynamics of the unknown DE solution given a finite number of derivative evaluations, or (ii) define a level of uncertainty in a hierarchical model for any unknown model parameters. This allows us to characterize the systematic model uncertainty introduced into the inference problem by discretization and to further distinguish it from other sources of uncertainty.

8.1 Impact and Recommendations

The framework described in this thesis is a first step in a promising new avenue for research. Broadly, our work has potential for impact in three areas: uncertainty quantification for inverse problems, analysis of computer experiments, and the study of differential equation dynamics.

Uncertainty quantification is the study of the impact and propagation of variability

through complex dynamical systems. However, until now a coherent probabilistic framework for characterizing uncertainty resulting from discretization of infinite-dimensional DE solutions has been unavailable (DeVolder et al., 2002). This thesis demonstrates that such an approach is feasible and can be incorporated naturally into the inverse problem.

Large-scale models are often encoded in computer simulators, consisting of complex systems of differential equations and numerical algorithms to solve them approximately given unknown parameters or initial values of interest. Currently numerical uncertainty in the model is largely ignored, although it is incorporated heuristically through a covariance nugget when constructing the emulator (see, for example, Gramacy and Lee, 2012). Adopting our probabilistic approach on a large scale will have practical implications in this research area by allowing relaxation of the error-free assumption used for computer codes, resulting in more realistic and flexible emulators. We particularly recommend such an approach for models of turbulent systems, such as those found in local weather models or hydrodynamics. The inherent sensitivity of such models to perturbations highlights the need to characterize the impact of numerical uncertainty.

Further potential applications of the probabilistic approach include the extension to Stochastic Differential Equation (SDE) systems, for which closed form solutions are typically unavailable, and existing inference methods are largely simulation-based. In this context, probabilistic solutions could be useful in determining a set of probable sample paths. We demonstrated that our approach provides a functional probabilistic alternative to numerical solution and error analysis, which is particularly useful for systems that are sensitive to perturbations. This approach can be further extended to integration on complex domains, via finite element methods (FEMs). Indeed, we believe that a probabilistic approach has the potential to provide a general framework for error analysis of FEMs. Other useful extensions of our methodology include the area of numerical bifurcation analysis, used to study behaviours of analytically intractable systems over different regimes. Not only would fully probabilistic solutions yield credible intervals on estimated bifurcation boundaries, but they would also detect possible multiplicity of solutions when systems are ill-conditioned.

Bibliography

Afraimovich, V. S., V. V. Bykov, and L. P. Shil'nikov (1977). On the appearance and structure of the Lorenz attractor. *Proceedings of the USSR Academy of Sciences 234*, 336–339. 12

Baker, G. and J. Gollub (1996). *Chaotic Dynamics: an Introduction*. Cambridge University Press. 11

Bellen, A. and M. Zennaro (2003). *Numerical Methods for Delay Differential Equations*. Clarendon Press. 17

Berliner, L. M. and S. N. MacEachern (1993). Examples of inconsistent Bayes procedures based on observations on dynamical systems. *Statistics & Probability Letters 17*(5), 355–360.

Bernard, S., B. Čajavec, L. Pujo-Menjouet, M. C. Mackey, and H. Herzel (2006). Modelling transcriptional feedback loops: the role of Gro/TLE1 in Hes1 oscillations. *Philosophical Transactions: Mathematical, Physical and Engineering Sciences 364*(1842), 1155–1170. 16

Billingsley, P. (1968). *Convergence of Probability Measures*. Wiley. 26

Boyle, P. and M. Frean (2005). Dependent Gaussian processes. *Advances in Neural Information Processing Systems 17*, 217–224. 30

Busenberg, S. and B. Tang (1994). Mathematical models of the early embryonic cell cycle: the role of MPF activation and cyclin degradation. *Journal of Mathematical Biology 32*, 573–596. 16

Butcher, J. (2008). *Numerical Methods for Ordinary Differential Equations*. John Wiley and Sons Ltd. 2, 8, 47

Campbell, D. A. and O. Chkrebtii (2013). Maximum profile likelihood estimation of differential equation parameters through model based smoothing state estimates. *Mathematical Biosciences (in press)*. 69

Cover, T. M. and J. A. Thomas (2006). *Elements of Information Theory (Wiley Series in Telecommunications and Signal Processing)*. Wiley-Interscience. 85

DeVolder, B., J. Glimm, J. Grove, Y. Kang, Y. Lee, K. Pao, D. H. Sharp, and K. Ye (2002). Uncertainty quantification for multiscale simulations. *Journal of Fluids Engineering 124*, 29–41. 89

Diaconis, P. (1988). *Bayesian Numerical Analysis*. Springer-Verlag. 3

Doucet, A., A. M. Johansen, and V. B. Tadic (2010). On solving integral equations using Markov chain Monte Carlo methods. *Applied Mathematics and Computation 216*, 2869–2880. 4

Foias, C., R. R. M. O. and R. Temam (2001). *Navier-Stokes equations and turbulence*. Encyclopedia of Mathematics and Its Applications, Cambridge University Press. 12

Gelman, A., J. B. Carlin, H. S. Stern, and D. B. Rubin (2004). *Bayesian Data Analysis*. Chapman and Hall/CRC. 66, 67

Geyer, C. (1991). Markov chain Monte Carlo maximum likelihood. In *Computing Science and Statistics, Proceedings of the 23rd Symposium on the Interface, 156*. American Statistical Association. 49, 70

Gramacy, R. and H. Lee (2012). Cases for the nugget in modeling computer experiments. *Statistics and Computing 22*, 713–722. 89

Guckenheimer, J. and R. F. Williams (1979). Structural stability of Lorenz attractors. *Publications mathématiques de l'IHÉS 50*, 59–72. 12

Hastings, W. (1970). Monte Carlo sampling methods using Markov chains and their application. *Biometrika 57*, 97–109. 4

Jost, J. (2012). *Partial Differential Equations*. Graduate texts in mathematics. Springer. 20

Kassam, A. and L. Trefethen (2005). Fourth-order time-stepping for stiff PDEs. *SIAM Journal on Scientific Computing 26*(4), 1214–1233. 21, 58

Keller, H. B. (1968). *Numerical Methods for Two-point Boundary-value Problems*. Blaisdell Publishing Company. 14, 15

Kullback, S. and R. A. Leibler (1951). On information and sufficiency. *Annals of Mathematical Statistics 22*, 49–86. 83

Kuo, H. (1975). *Gaussian Measures in Banach Spaces*. Lecture Notes in Mathematics. Springer-Verlag. 26

Kuramoto, Y. and T. Tsuzuki (1976). Persistent propagation of concentration waves in dissipative media far from thermal equilibrium. *Progress of Theoretical Physics 55*, 356–369. 21

Lange, K. (1999). *Numerical Analysis for Statisticians*. Statistics and computing. New York, NY: Springer. 3

Leone, F. C., L. S. Nelson, and R. B. Nottingham (1961). The folded normal distribution. *Technometrics 3*, 543–550. 46

Lewis, J. (2003). Autoinhibition with transcriptional delay: a simple mechanism for the zebrafish somitogenesis oscillator. *Current Biology 13*(16), 1398 – 1408. 16

Lifshits, A. (1995). *Gaussian Random Functions*. Mathematics and Its Applications. Kluwer Academic Publishers. 25, 26

Lorenz, E. N. (1963). Deterministic nonperiodic flow. *Journal of the Atmospheric Sciences 20*, 130–141. 11

Megginson, R. (1998). *An Introduction to Banach Space Theory*. Graduate texts in mathematics. Plenum Press. 25

Metropolis, N. and S. Ulam (1949). The Monte Carlo method. *Journal of the American Statistical Association 44*, 335–341. 4

Mischaikow, K. and M. Mrozek (1995). Chaos in the Lorenz equations: a computer-assisted proof. *Bulletin of the American Mathematical Society 32*(1), 66–72. 13

Mrozek, M. and R. Srzednicki (2010). Topological approach to rigorous numerics of chaotic dynamical systems with strong expansion of error bounds. *Foundations of Computational Mathematics 10*(2), 191–220. 13

Neal, R. M. (2011). MCMC using ensembles of states for problems with fast and slow variables such as Gaussian process regression. 45

O'Hagan, A. O. (1992). Some Bayesian numerical analysis. *Bayesian Statistics 4*, 345–363. 4

Pellegrini, S. and I. Dusanter-Fourt (1997). The structure, regulation and function of the Janus kinases (JAKs) and the signal transducers and activators of transcription (STATs). *European Journal of Biochemistry 248*(3), 615–633. 69

Poincaré, H. (1896). *Calcul des Probabilities*. Georges Carré. 3

Poincaré, H. (1913). *The Foundation of Science: Science and Method, English translation*. Lancaster, PA: The Science Press. 11

Ramsay, J., G. Hooker, and J. Cao (2007). Parameter estimation for differential equations: a generalized smoothing approach. *Journal of the Royal Statistical Society B 69*, 741–796. 66

Rasmussen, C. E. and C. K. I. Williams (2006). *Gaussian Processes for Machine Learning*. Cambridge, Massachusetts: MIT Press. 4, 31, 54, 75

Raue, A., C. Kreutz, T. Maiwald, J. Bachmann, M. Schilling, U. Klingmller, and J. Timmer (2009). Structural and practical identifiability analysis of partially observed dynamical models by exploiting the profile likelihood. *Bioinformatics 25*, 1923–1929. 69, 70, 71

Robinson, J. (2001). *Infinite-Dimensional Dynamical Systems: An Introduction to Dissipative Parabolic PDEs and the Theory of Global Attractors*. Cambridge Texts in Applied Mathematics. Cambridge University Press. 12

Rohde, C. (1965). Generlized inverses of partitioned matrices. *Journal of the Society for Industrial and Applied Mathematics 13*(4), 1033–1035. 43

Sauer, T., C. Grebogi, and J. A. Yorke (1997). How long do numerical chaotic solutions remain valid? *Physical Review Letters 79*, 59–62. 12

Shampine, L. (2003). Singular boundary value problems for ODEs. *Applied Mathematics and Computation 138*, 99 – 112. 15

Shu, C., H. Ding, and K. Yeo (2003). Local radial basis function-based differential quadrature method and its application to solve two-dimensional incompressible Navier-Stokes equations. *Computer Methods in Applied Mechanics and Engineering 192*, 941 – 954. 10

Sivashinsky, G. I. and D. M. Michelson (1980). On irregular wavy flow of a liquid film down a vertical plane. *Progress of Theoretical Physics 63*(6), 2112–2114. 21

Skilling, J. (1991). *Bayesian Solution of Ordinary Differential Equations*, pp. 23–37. Seattle: Kluwer Academic Publishers. 4, 24, 88

Stuart, A. M. (2010). Inverse problems: a Bayesian perspective. *Acta Numerica 19*, 451–559. 25, 28, 65, 74

Swameye, I., T. Muller, J. Timmer, O. Sandra, and U. Klingmuller (2003). Identification of nucleocytoplasmic cycling as a remote sensor in cellular signaling by databased modeling. *Proceedings of the National Academy of Sciences 100*, 1028–1033. 16, 70, 71

Tucker, W. (1999). The Lorenz attractor exists. *Comptes Rendus de l'Acadeḿie des Sciences - Series I - Mathematics 328*(12), 1197 – 1202. 13

Williams, R. F. (1979). The structure of the Lorenz attractor. *Publications mathématiques de l'IHÉS 50*, 73–99. 12